UNIVERSITY of OTAGO

Te Whare Wānanga o Otāgo

NEW ZEALAND

Inactivation of a Thiol-Dependent Enzyme by Urate Hydroperoxide

A Bachelor of Biomedical Science Honours Thesis

Melanie Hamzah

27/10/15

Abstract

There are links between high serum urate (hyperuricemia) and many inflammatory diseases, yet the mechanism is obscure. Urate, the product of purine and ATP break down, builds up in plasma because humans lack the enzyme uricase to convert it to allantoin, which is freely excreted. Urate may benefit health by acting as an antioxidant that scavenges reactive oxygen species. However, hyperuricemia is associated with gout, metabolic syndrome and cardiovascular disease. Oxidative stress is also associated with all these inflammatory diseases.

During oxidative stress urate is converted to several reactive electrophiles, including urate hydroperoxide. This novel oxidant could contribute to the adverse effects of urate. Urate hydroperoxide is formed when urate is oxidized to a radical that subsequently combines with superoxide. Activated white blood cells called neutrophils, and xanthine oxidase along with myeloperoxidase/lactoperoxidase, can produce urate hydroperoxide. Previous studies characterized the formation of urate hydroperoxide and its oxidation of small biomolecules. In this investigation, I explored oxidation of thiols and the thiol-dependent enzyme glyceraldehyde-3-phosphate dehydrogenase (GAPDH) by urate hydroperoxide. The effectiveness of urate hydroperoxide as a thiol oxidant was compared with taurine chloramine.

Ellman's assay for reduced thiols was used to measure depletion of cysteine residues on GAPDH by urate hydroperoxide and taurine chloramine. GAPDH was exposed to oxidants in a dose-dependent manner, then assayed by measuring its ability to catalyse the production of NADH. Mass spectrometry was used to identify specific modifications of GAPDH.

Urate hydroperoxide oxidized exposed thiols on GAPDH and fully inactivated the enzyme at a ratio of about 5:1. Half of its activity was recovered by reduction with DTT. In comparison, taurine chloramine inactivated GAPDH at approximately 10:1 and DTT reduction recovered all activity. Hence, urate hydroperoxide inactivates GAPDH by reversible and irreversible routes. GAPDH increased in molecular mass by 132 Da with exposure to urate hydroperoxide, indicating the formation of a GAPDH-urate adduct. However, I could not identify which residue was modified with a tryptic digest. Formation of urate hydroperoxide during inflammation and its subsequent oxidative reactions may explain some of the adverse effects of hyperuricemia.

Preface

Dedications

I wish the best for my fellow BBiomedSci Honours students: Anishah Mandani, Mark Brinsden, Millie Taylor, Morgan Jones, Sarah Drake and Rebekah Crake.

Thank you lab mates and friends: Annika Seddon, Andrew Das, Bee Banish, Harry Hua, Masuma Zawari, Shufuka Nazari, Simone Bayer and Teagan Hoskin.

Thank you Alexander Peskin, Heather Parker, Louisa Forbes, Markus Dagnell, Paul Pace and Rufus Turner for your help in the lab.

Thank you everyone from the University of Otago Christchurch Centre for Free Radical Research and Pathology department for welcoming me with open arms.

Thank you Louise Paton for performing mass spectrometry on my samples.

To my wonderful supervisors, Tony Kettle and Mark Hampton, thank you for the advice and setting me down this path.

To my oldest and dearest friend Renee O'Halloran, thanks to being my sounding board and support beam.

Finally, I owe everything to my family. Mum, Dad, Sarah, Emilie and Adam; thank you for always being there.

Table of Contents

Abstract....2
Preface....3
Dedications....3
List of Tables....6
List of Illustrations and Figures....7
List of Abbreviations....8
Chapter 1. Literature Review....10
1.1 Introduction....10
1.2 Urate and Cardiovascular Disease....12
1.3 Urate and Inflammation....15
1.3.1 NLRP3 Inflammasome....15
1.3.2 Nitric Oxide....16
1.3.3 Proinflammatory Cytokines....16
1.4 Urate as an Antioxidant....17
1.4.1 Singlet Oxygen, Peroxyl and Hydroxyl Radicals....18
1.4.2 Peroxynitrite....18
1.4.3 Oxo-Heme Oxidants....19
1.4.4 Metal Ion Coordination....19
1.5 Urate as a Pro-oxidant....19
1.5.1 Low Density Lipoprotein....20
1.5.2 NADPH Oxidase....21
1.5.3 Inactivation of Enzymes....22
1.5.4 Urate Hydroperoxide....23
1.6 Conclusion....25
1.7 Summary....26
Chapter 2. Optimising the Formation of Urate Hydroperoxide....27
2.1 Introduction....27
2.2 Materials and Methods....30
2.2.1 Materials....30
2.2.2 Cytochrome C Assay of Superoxide Production by Xanthine Oxidase....31
2.2.3 Xanthine Oxidase/Lactoperoxidase System Photometry....31
2.2.4 Modified Ferrous Oxidation Xylenol Orange Assay for Hydroperoxides....32
2.2.5 Statistical Analysis....34
2.2.6 Graphs....34

2.3 Results 35
2.3.1 Superoxide Production by Xanthine Oxidase 35
2.3.2 Xanthine Oxidase/Lactoperoxidase System Photometry 36
2.3.3 FOX Assay of Urate Hydroperoxide 38
2.4 Discussion 42
Chapter 3. Urate Hydroperoxide and Reduced Thiols 43
3.1 Introduction 43
3.2 Materials and Methods 45
3.2.1 Materials 45
3.2.2 TMB Measurement of Taurine Chloramine 46
3.2.3 DTNB Assay for Reduced Thiols 46
3.3 Results 48
3.3.1 DTNB Assay 48
3.4 Discussion 52
Chapter 4. Urate Hydroperoxide and Glyceraldehyde-3-Phosphate Dehydrogenase 54
4.1 Introduction 54
4.2 Materials and Methods 57
4.2.1 Materials 57
4.2.2 GAPDH Assay 58
4.2.3 NAD^+ and NADH Photometry 59
4.2.4 Continuous Inactivation of GAPDH by Urate Hydroperoxide 60
4.2.5 Discontinuous Inactivation of GAPDH by Oxidants 61
4.2.6 Inactivation Kinetics for GAPDH 62
4.2.7 Reactivation of GAPDH Following Dose-Dependent Inactivation by Oxidants 62
4.2.8 DTNB Measurement of Cysteine Residues on GAPDH 63
4.2.9 Polyacrylamide Gel Electrophoresis 64
4.2.10 GAPDH Mass Spectrometry 65
4.3 Results 66
4.3.1 Optimising the GAPDH Assay 66
4.3.2 GAPDH Inactivation by Continuous Urate Hydroperoxide Formation 67
4.3.3 Discontinuous Inactivation of GAPDH 69
4.3.4 Inactivation Kinetics for GAPDH 71
4.3.5 Reactivation of GAPDH with DTT 73
4.3.6 Depletion of Cysteine Residues on GAPDH by Oxidants 74
4.3.7 Polyacrylamide Gel Electrophoresis of GAPDH 75
4.3.8 Mass Spectrometry of GAPDH 78

4.4 Discussion 79
Chapter 5. Conclusions 81
5.1 Summary of Findings 81
5.2 Strengths and Limitations 83
5.3 Recommendation for Future Work 84
References 86
Appendix 1: Supplementary Figures 96
Appendix 2: Supplementary Methods and Materials 105
5.1 Chapter 2 105
5.2 Chapter 3 106
5.3 Chapter 4 108
5.3.1 Mass Spectrometry 110

List of Tables

Table 1: Studies that explored the clinical association between serum urate and cardiovascular disease. 14
Table 2: Description of substances and solutions used to perform the cytochrome c assay, ferrous oxidation-xylenol orange assay (FOX) and the xanthine oxidase/lactoperoxidase system. 30
Table 3: Description of substances and solutions used to perform the DTNB assay and prepare taurine chloramine and thiols. 45
Table 4: Description of substances and solutions used to perform the GAPDH assay, gel electrophoresis and mass spectrometry. 57
Table 5: Species found during whole protein mass spectrometry of GAPDH treated with a low concentration of urate hydroperoxide. 78
Table 6*:* Volumes of substances used for the FOX assay of urate hydroperoxide formation. 105
Table 7: Samples made for the xanthine oxidase/lactoperoxidase system which was subsequently used to treat 70 µM cysteine or 30 µM glutathione. 106
Table 8: Samples made for dose-dependent treatment of cysteine and glutathione with taurine chloramine. 107
Table 9: Samples made for dose-dependent exposure of glutathione to urate hydroperoxide. 108
Table 10: Xanthine oxidase/lactoperoxidase system in the quartz cuvette during continuous inactivation of GAPDH. 108
Table 11: Xanthine oxidase/lactoperoxidase system samples used to treat GAPDH. 109
Table 12: Sample composition for GAPDH reactivation experiment following inactivation by taurine chloramine. 109
Table 13: Sample composition for the GAPDH reactivation experiment following inactivation by urate hydroperoxide. 110

List of Illustrations and Figures

Figure 1: Oxidation of urate to allantoin in human serum. 11
Figure 2: High serum urate due to a western diet can lead to inflammatory disease. 13
Figure 3: Urate has an antioxidant cycle with ascorbate. 17
Figure 4: Urate's pro-oxidant effects have physiological repercussions for inflammatory disease. 20
Figure 5: Pathways for urate hydroperoxide formation *in vitro* and *in vivo* (theoretically) by photooxidation or inflammatory processes. 24
Figure 6: A healthy human body balances pro-oxidant formation with the antioxidant defence system. 26
Figure 7: Riboflavin undergoes a photooxidation cycle to oxidise urate to urate hydroperoxide. 27
Figure 8: The xanthine oxidase/lactoperoxidase system to form urate hydroperoxide *in vitro*. 29
Figure 9: Optimised superoxide production by xanthine oxidase. 35
Figure 10: Urate hydroperoxide absorption at 310 nm over time. 36
Figure 11: Absorbance of the xanthine oxidase/lactoperoxidase system. 37
Figure 12: Urate hydroperoxide formed by the xanthine oxidase/lactoperoxidase system. 39
Figure 13: Optimising urate hydroperoxide formation (10 min reaction) by quadrupling urate and doubling xanthine oxidase. 40
Figure 14: Kinetics of urate hydroperoxide formation measured with the FOX assay. 41
Figure 15: Consequences of glutathione depletion for a cell. 44
Figure 16: Depletion of free thiols by urate hydroperoxide. 49
Figure 17: Exposure of free thiols to dose-dependent taurine chloramine. 51
Figure 18: Dose-dependent depletion of glutathione by urate hydroperoxide. 52
Figure 19: Crystal structure and active site configuration of rabbit muscle GAPDH. 55
Figure 20: Modifications of the GAPDH essential thiol formed during inactivation by oxidants. 56
Figure 21: Optimising the GAPDH assay. 66
Figure 22: GAPDH inactivation during continuous formation of urate hydroperoxide. 68
Figure 23: Inactivation of GAPDH by urate hydroperoxide. 69
Figure 24: Dose-dependent inactivation of GAPDH by taurine chloramine or urate hydroperoxide. 71
Figure 25: Kinetics of GAPDH inactivation by oxidants. 72
Figure 26: Reactivation of GAPDH following inactivation with taurine chloramine. 73
Figure 27: Reactivation of GAPDH following inactivation with urate hydroperoxide. 74
Figure 28: Dose-dependent depletion of cysteine residues on GAPDH by oxidants. 75
Figure 29: Non-reducing gel for the inactivation of GAPDH by urate hydroperoxide. 76
Figure 30: Reducing gel for the inactivation of GAPDH by urate hydroperoxide. 77
Figure 31: Neutrophil activity at inflammatory sites, during hyperuricemia, could produce urate hydroperoxide. 82
Figure 32: Standard curve for the FOX assay based on H_2O_2 absorbance at 560 nm. 96
Figure 33: FOX assay of each substance required to form urate hydroperoxide. 96
Figure 34: Thiol standard curve and xanthine oxidase/lactoperoxidase system controls with the DTNB assay. 97
Figure 35: Depletion of free thiols by urate hydroperoxide controls. 98
Figure 36: Standard curve for GAPDH concentration vs. initial activity. 98
Figure 37: GAPDH concentration and activity during spin column preparation. 99

Figure 38: NAD standard curves for absorbance at 260 and 340 nm. 99
Figure 39: Dose-dependent exposure of NAD to taurine chloramine. 100
Figure 40: Dose-dependent exposure of NAD to urate hydroperoxide. 100
Figure 41: GAPDH activity following exposure to the substances of the xanthine oxidase/lactoperoxidase system. 101
Figure 42: Standard curve of GAPDH concentration vs. reduced thiol concentration during the DTNB assay in a quartz cuvette. 101
Figure 43: Depletion of cysteine residues on GAPDH by the xanthine oxidase/lactoperoxidase system. 102
Figure 44: Mass Spectrum for the GAPDH and urate hydroperoxide experiment treated with urate hydroperoxide (1:1 ratio). 104

List of Abbreviations

Abbreviation	Explanation
A1AT	α1-antitrypsin
AAPH	2,2'-Azobis(2-amidinopropane) dihydrochloride
AMVN	2,2'-Azobis (2,4-dimethylvaleronitrile)
ANOVA	Analysis of variance
APS	Ammonium persulfate
BPG	1,3-Bisphosphoglycerate
Cata	Catalase
CRP	C-reactive protein
Cys	Cysteine
Cys-Cys	Cystine
DAMP	Damage-associated molecular patterns
DMF	Dimethylformamide
DTPA	Diethylene triamine pentaacetic acid
DTNB	5,5'-dithiobis-(2-nitrobenzoic acid)
DTT	Dithiothreitol
FOX	Ferrous oxidation-xylenol orange
GAP	Glyceraldehyde-3-phosphate
GAPDH	Glyceraldehyde-3-phosphate dehydrogenase
Gly	Glycine
GSH	Reduced glutathione
GSSH	Glutathione disulfide/oxidized glutathione
His	Histidine
HPLC	High performance liquid chromatography
HX	Hypoxanthine
IL	Interleukin
LDL	Low density lipoprotein
LPO	Lactoperoxidase
MCP-1	Monocyte chemoattractant protein-1
m/z	Mass-to-charge ratio
NAD	Nicotinamide adenine dinucleotide
NAD+	Oxidized nicotinamide adenine dinucleotide

NADH	Reduced nicotinamide adenine dinucleotide
NADPH	Reduced nicotinamide adenine dinucleotide phosphate
NF-κB	Nuclear factor kappa-light-chain-enhancer of activated B cells
NLRP3	NACHT, LRR and PYD domains-containing protein 3
NOX	NADPH oxidase
Ox-LDL	Oxidized low density lipoprotein
PAGE	Polyacrylamide gel electrophoresis
PB	Phosphate buffer
ROS	Reactive oxygen species
SDS	Sodium dodecyl sulfate
SOD	Superoxide dismutase
Tau-Cl	Taurine Chloramine
TEA	Triethanolamine
TEMED	Tetramethylethylenediamine
TMB	3,3',5,5'-Tetramethylbenzidine
TNB	Thionitrobenzoate
Tris	Tris(hydroxymethyl)aminomethane
UHP	Urate hydroperoxide
XO	Xanthine oxidase
YALDH	Yeast alcohol dehydrogenase

Chapter 1. Literature Review

1.1 Introduction

High levels of uric acid in our blood stream are associated with inflammatory disease, yet the pathological mechanism eludes us (1, 2). Uric acid (7,9-di-hydro-1H-purine-2,6,8(3H)-trione) is the product of purine and ATP break down and circulates the plasma as the monoanion urate, pK_a 5.4 (2, 3). Mammals produce the enzyme uricase to convert urate to allantoin, enabling its excretion. However, humans cannot produce this enzyme because the uricase gene lost functionality during primate evolution (2, 4). Thus, we have a high concentration of urate in our blood serum, the normal range is 240 – 360 µM (2, 5). Elevated serum urate may have evolved to prevent dehydration, promote serum antioxidant activity, fat storage and bipedal locomotion by increasing blood pressure (3, 6, 7). Urate has antioxidant activity and is potentially the most abundant antioxidant in our bloodstream (3, 8). This antioxidant scavenges a number of oxidant species, thus protecting other biomolecules from damage (3, 9, 10). Ascorbate, a serum antioxidant, reduces urate back to its antioxidant state hence promoting its activity (9, 10).

Yet, urate has a number of adverse effects on human health. Abnormally high serum urate, hyperuricemia, is associated with inflammatory diseases, including cardiovascular disease (1, 11). Hyperuricemia is characterised by inflammation and oxidative stress (5, 12). Under these conditions, urate acts as an endogenous signal molecule to initiate a number of inflammatory pathways (13-15). Urate promotes the oxidation of biomolecules, thus acting as a pro-oxidant, during oxidative stress and in lipid environments (16-18). This molecule forms a number of electrophilic intermediates on the oxidative pathway to allantoin (figure 1). Electrophilic oxidants damage biomolecules (19). In particular, oxidative conditions at an inflammatory site may produce the novel oxidant urate hydroperoxide. This species is stable enough to diffuse to biomolecules and cause oxidative damage (17, 19, 20). Formation of urate hydroperoxide during hyperuricemia may explain the pro-oxidant effects of urate.

In this literature review, I explain why this thesis focuses on the reactivity of urate hydropeorxide. A target of urate hydroperoxide oxidation could be biomolecules with thiol functional groups, such as cysteine and glutathione, due to their vulnerability to electrophiles (21, 22). In particular, urate hydroperoxide might inactivate thiol-dependent enzymes, which rely on a cysteine residue for activity (23-25). I hypothesize that urate

hydroperoxide oxidises thiol-dependent biomolecules, such as cysteine, glutathione and glycolytic enzyme GAPDH (26, 27). GAPDH uses an essential cysteine residue to covalently bind substrate glyceraldehyde-3-phosphate (GAP) (28). Oxidation of this residue reversibly or irreversibly inactivates GAPDH, which has repercussions for cell metabolism of glucose for energy (29). I aim to determine whether urate hydroperoxide inactivates this enzyme and the reversibility of inactivation. Mass spectrometry will be used to identify the structural change responsible for inactivation.

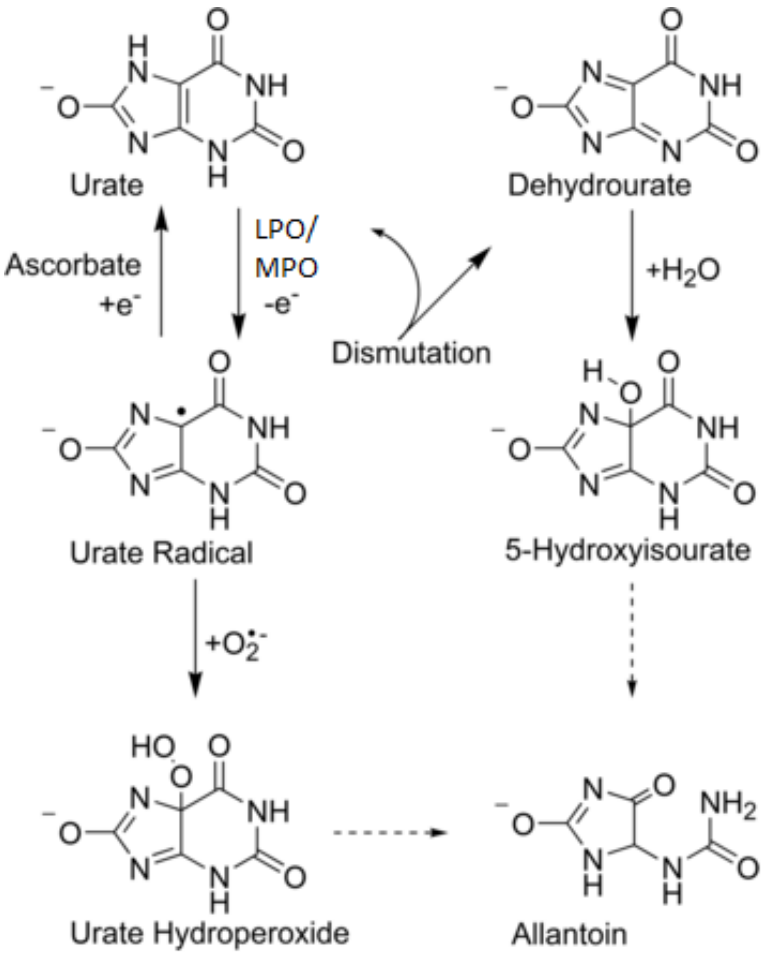

Figure 1: **Oxidation of urate to allantoin in human serum**. Urate is oxidized to a radical with the lone electron delocalised over the purine ring. The radical can dismutate to urate and dehydrourate. Dehydrourate is hydrolysed to 5-hydroxyisourate, which breaks down to allantoin. Alternatively, the urate radical can combine with superoxide to form urate hydroperoxide, this also degrades to allantoin. Figure adapted from (19).

1.2 Urate and Cardiovascular Disease

Urate is associated with cardiovascular disease (11), gout (5), renal disease (30), rheumatoid arthritis (12), hypertension (15), diabetes (2), metabolic syndrome (31) and cancer (32-34) (figure 2). The association between hyperuricemia and cardiovascular disease is debated. The literature has two positions: hyperuricemia is independently causative of cardiovascular disease or is a negative side effect of the disease. The association between hyperuricemia and cardiovascular disease in the general population is weak (11, 35-40). However, the association becomes stronger for patients with a high risk of cardiovascular disease. This includes patients with diabetes (41), hypertension (42, 43) and survivors of myocardial infarction or stroke (44-46) (table 1). For example, the GISSI-Prevenzione trial examined over 10,000 patients with myocardial infarction over 3.5 years. All-cause and cardiovascular disease mortality is significantly higher for patients with hyperuricemia. However, Levantesi et al. (46) did not have a balanced gender ratio, where 9,247 men and 1,593 women were examined, and did not compare to a healthy cohort. Studies on a specific population are not generalizable to other populations. The National Health and Nutrition Examination Survey (NHANES) III presented opposing evidence. Zalawadiya et al. (40) surveyed 11,009 healthy US participants and did not find an independent association between hyperuricemia and cardiovascular disease or coronary heart disease mortality (40). This study examined multiple ethnicities and could be a good representation of the US population. To verify hyperuricemia is associated with cardiovascular disease, a large and multicultural, cross-population study is required to examine individuals with high cardiovascular risk.

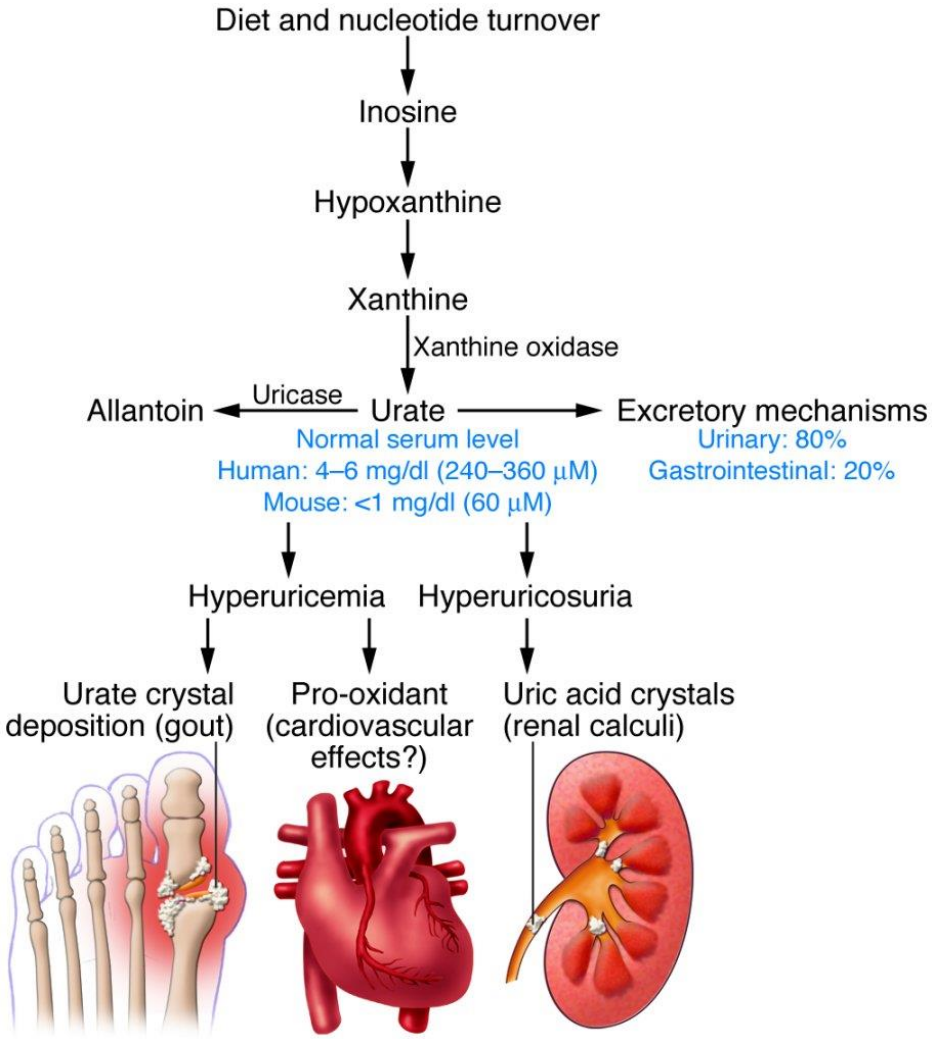

Figure 2: **High serum urate due to a western diet can lead to inflammatory disease**. Urate enters our body through diet and the consumption of purines. Purine breaks down to inosine, hypoxanthine, xanthine and urate. Urate enters the blood serum and is excreted through urine or the bile. The loss of uricase during human evolution led to build up of urate in human serum. Overconsumption of purine leads to hyperuricemia. Urate crystals form in the joints, causing gout. Pro-oxidant effects of urate aggravate oxidative stress and may explain the association between hyperuricemia and cardiovascular disease. Excess urate in urine (hyperuricosuria) leads to the formation of urate crystals in the kidneys. Figure adapted from (2)

Table 1: Studies that explored the clinical association between serum urate and cardiovascular disease.

The association is stronger for patients with a high risk of cardiovascular disease. All examples used multivariate analysis. Table adapted from (47).

Study	References	N	Urate (μM)	Major findings	Independent association
Studies in samples of general population					
Austrian Elderly Women 2007	Strasak, AM (39)	28,613 F	> 370	Serum urate is an independent predictor for all-cause death cardiovascular disease and stroke in elderly women.	Yes Women
MJ Health Screening 2009	Chen, J-H (38)	90,393 M/F	> 380	Serum urate is associated with cardiovascular disease and ischemic stroke.	Yes
Taiwanese Cohort Study 2010	Wen, CP (11)	484,568 M/F	> 380	High serum urate is a risk marker for cardiovascular disease mortality and all-cause mortality, but the association is not independent.	No
Large Chinese Cohort 2012	Chuang, S-Y(36)	2,049 M/F	> 380	Serum urate is associated with development of ischemic heart disease.	Yes
Healthy Israeli Adults 2013	Kivity S (37)	9,139 M/F		Serum urate is associated with cardiovascular events. The association is stronger for women than men.	Yes
Middle-Aged and Elderly Chinese 2014	Qin, L (35)	8,510 M/F	> 340	Serum urate is associated with cardiovascular disease. This is independent of risk factors and metabolic syndrome.	Yes
NHANES III 2015	Zalawadiya, SK (40)	11,009 M/F	> 340	Serum urate is not independently associated with cardiovascular disease or coronary heart disease mortality.	No
Studies involving selected groups of patients at high cardiovascular risk					
PreCIS Study 2008	Ioachimescu, AG (48)	3,098 M/F	> 450	Serum urate is associated with cardiovascular disease in patients with high risk of cardiovascular disease.	Yes
Chinese Cohort High CVD Risk 2008	Wu, Y (11)	3,648 M/F	> 380	Serum urate is independently associated with cardiovascular disease risk and all-cause mortality in patient with high cardiovascular disease risk.	Yes
JCARE-CARD 2011	Hamaguchi, S (45)	1,869 M/F	> 410	Serum urate in patients with heart failure is associated with all-cause and cardiac mortality.	Yes
LURIC 2011	Silbernagel, G (44)	3,245 M/F	> 410	Serum urate is independently associated with cardiovascular disease risk and all-cause mortality in subjects referred for coronary angiography.	Yes
Japanese Hypertension Patients 2011	Ito, H (41)	1,213 M/F	> 330	Serum urate is associated with coronary heart disease in patient with type 2 diabetes.	Yes
Japanese Hypertension Patients 2012	Kawai, T (43)	669 M/F	> 500	Serum urate is associated with cardiovascular disease, stroke event and mortality, and all-cause mortality in hypertension patients.	Yes
GISSI-Prevenzione Trial 2013	Levantesi, G (46)	10,840 M/F	> 380	Serum urate is a risk factor cardiovascular disease event and all-cause mortality in patients with recent myocardial infarction.	Yes
Chinese Hypertension Patients 2015	Wang, J (42)	2,725 M/F	> 420	Serum urate independently predicts all-cause and cardiovascular disease mortality in hypertension patients.	Yes

1.3 Urate and Inflammation

Inflammatory disease is caused by an immune response in the absence of pathogenic threat, or sterile conditions. Immune cells are recruited by damage-associated molecular patterns (DAMP), which are endogenous molecules secreted by dying cells (49). Necrotic, or dying cells also produce reactive oxygen species (ROS), which are harmful oxygen and peroxide radicals (50). Immune cells respond by releasing hydrolase, which cleave proteins, thus effecting an adjacent cell's ability to survive (51). Urate should be counted among the DAMP which exacerbate a sterile inflammatory response (13). Urate crystals upregulate the NACHT, LRR and PYD domains-containing protein 3 (NLRP3) inflammasome (14, 52, 53). The NLRP3 inflammasome activates factors responsible for promoting an inflammatory response (54). Urate also depletes nitric oxide (NO), which is an endogenous signalling molecule for inflammatory pathways (15, 55, 56). Urate activates proinflammatory cytokines. These factors recruit the inflammatory response (30, 57-60).

1.3.1 NLRP3 Inflammasome

Urate could aggravate inflammation by activating the NLRP3 inflammasome, a protein complex in the inflammation signalling pathway (14, 52, 53). When the inflammasome forms it activates proinflammatory cytokines interleukin-1 beta/8 (IL-1β, IL-18) (52, 53). Exposure of THP-1, a human leukaemia monocyte cell line, to urate activated IL-1β. Thus the inflammasome formed. Activation of these cytokines was lost when a preceding enzyme on the inflammasome pathway, caspase-1, was inhibited (14). Martinon et al. (14) presented strong evidence for the IL-1β activation in response to urate, yet inflammasome activity and formation was not directly measured. Injection of urate crystals into the inflamed lungs of mice led to IL-1β activation and recruitment of immune cells lymphocytes and neutrophils (53). Whereas injection of urate crystals into inflammasome-deficient mice did not recruit an inflammatory response (53). The applicability of these studies is limited by the use of urate crystals, which form in the synovial fluids during gout (5). Urate crystals do not form during most inflammatory disease, however are found in atherosclerotic plaques. Interestingly, urate crystals in an atherosclerotic plaque were colocalized with superoxide generating enzyme xanthine oxidase. Hence there may be a pro-oxidant element to the adverse effects of urate crystals in atherosclerotic plaques (61).

1.3.2 Nitric Oxide

Depletion of NO, an inflammatory signalling molecule and relaxant of the arteries, could be a mechanism by which urate promotes inflammation (15, 55, 56). NO reacts with urate to produce 6-aminouracil. This reaction occurred when NO was bubbled through buffer, human serum and human aortic endothelial cell lysate with urate (55). Gersch el al. (55) exposed urate to NO in anaerobic conditions, hence these results have limited relevance to oxygenated endothelium, though, hypoxia could occur during inflammation and atherosclerosis (62). Under aerobic conditions, NO added to urate to form nitrosylated urate. This molecule decayed at a half-life of 2.2 min and transferred the NO moiety to glutathione (63). Suzuki (63) did not explore whether nitrosylated urate or glutathione could release NO. NO could be depleted or carried by nitrosylated urate (63).

Alternatively, urate could deplete NO by activating quencher arginase. In endothelial cells NO is exclusively synthesised from L-arginine, which can be diverted to urea and ornithine by arginase. Porcine pulmonary arterial endothelial cells treated with urate had a lower concentration of NO and cGMP, the secondary signalling molecule for the NO pathway. Urate activated arginase by lowering its affinity constant (15). Zharikov et al.'s (15) cell model was appropriate for human endothelium, but the authors studied one of many quenchers of NO. Depletion of NO might lead to endothelial dysfunction, which is a key factor for cardiovascular disease (55, 64). NO may have pro- or anti-inflammatory effects (64-66).

1.3.3 Proinflammatory Cytokines

Proinflammatory cytokines are proteins secreted by cells to recruit an inflammatory response (67). A range of proinflammatory cytokines are upregulated by urate: cyclooxygenase-2, cytosolic phospholipases A2, IL-1α, IL-1β and monocyte chemoattractant protein-1 (MCP-1) (30, 57-60). Incubation of rat vascular smooth muscle cells with a physiological concentration of urate increased MCP-1 mRNA and protein expression. The addition of ROS inhibitors halved MCP-1 protein expression, hence urate upregulated this protein through a pro-oxidant pathway (58). In another paper, vascular smooth muscle cells exposure to urate increased cyclooxygenase-2 mRNA and protein expression. Cell proliferation was promoted (30). The strength of these papers was the use of rat vascular smooth muscle cells to model human blood vessels. In humans, vascular smooth muscle cell secrete cytokines to the intima to recruit macrophages, a type of white

blood cell (68). Urate's upregulation of these cytokines could promote cell proliferation and immune response during atherosclerotic plaque growth (68).

1.4 Urate as an Antioxidant

Antioxidants are preferentially oxidized to stable products by oxidants, hence preventing damage to biomolecules. Urate is a proven antioxidant and is responsible for > 60% of the antioxidant activity in blood serum (69). Urate depletes singlet oxygen (3), peroxyl and hydroxyl radicals (3, 70-72), peroxynitrite (73-75) and oxo-heme oxidants (3, 69). Transition metal ion coordination to urate hinders their reactivity (76). These oxidants are biologically relevant. Singlet oxygen is formed during photooxidation by photosensitisers such as riboflavin (67). Hydroxyl radicals are very powerful oxidants formed during radiolysis of water (3, 67). Oxo-heme oxidants form when the iron of hemoglobin binds oxygen and peroxide (3, 67). Transition metals generate hydroxyl radicals and superoxide (70). Peroxyl radicals are formed during the breakdown of organic peroxide (67). Peroxynitrite is a cytotoxic oxidant formed when NO adds to superoxide (73). Thus, urate's removal of these species is important for maintaining a balance between antioxidants and pro-oxidants in serum.

Urate's antioxidant activity yields a urate radical with an unpaired electron delocalised over the purine ring (77). Ascorbate recovers urate by reducing the radical, thus creating an antioxidant cycle (figure 3). Ascorbate extends urate's antioxidant activity (74, 78).

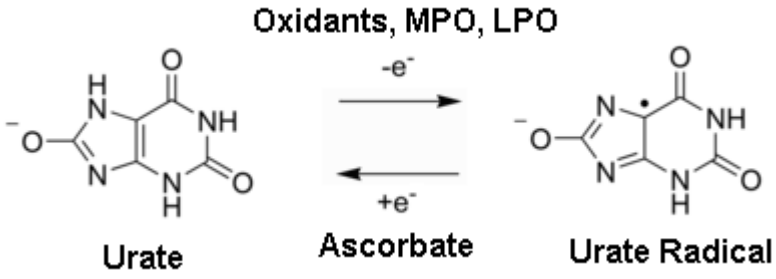

Figure 3: Urate has an antioxidant cycle with ascorbate. Urate scavenges singlet oxygen, oxo-heme oxidants, peroxynitrite, peroxyl and hydroxyl radicals to form the urate radical. The urate radical is also formed enzymatically by myeloperoxidase and lactoperoxidase. The radical electron of the urate radical is delocalised over the purine ring. Ascorbate is oxidized by the urate radical, thus regenerating urate. Figure adapted from (19).

1.4.1 Singlet Oxygen, Peroxyl and Hydroxyl Radicals

Ames et al. (3) heralded the antioxidant theory for urate by studying its depletion during gamma irradiation. Hydroxyl radicals and singlet oxygen depleted more than half of physiological urate (300 μM) in five minutes. These radicals consumed 20% of ascorbate in the same conditions (3). The results for hydroxyl radicals were not exclusive since gamma irradiation induces many ROS (67). Urate's ability to scavenge these oxidants might be vital for preventing damage to biomolecules during irradiation (3).

Urate's antioxidant activity with peroxyl radicals is debated in the literature (9, 10, 71, 72). Azo-initiators 2,2'-azobis(2-amidinopropane) dihydrochloride (AAPH) and 2,2'-Azobis (2,4-dimethylvaleronitrile) (AMVN) can be used to initiate organic peroxidation (67). Urate prevented inactivation of lysozyme, double-strand breaks in DNA plasmids and lipid peroxidation by AAPH-induced peroxyl radicals. Yet, urate had no effect on AMVN-induced peroxidation. The former oxidant is water-soluble while the latter is lipid-soluble, hence urate may not be able to scavenge across the lipid-water partition (71). Urate's antioxidant activity with lipid peroxyl radicals is prolonged and replenished by the presence of ascorbate (9, 10). Frei et al. (9, 10) found that urate and ascorbate were depleted sequentially by peroxyl radicals, indicating urate is the first line of antioxidant defence. Ascorbate reduced the urate radical back to urate to form an antioxidant cycle (9, 10). Urate scored poorly with the total oxidant scavenging assay compared to glutathione, when scavenging hydroxyl and peroxyl radicals (72). Thus, there are disagreements in the literature for urate's effectiveness with peroxyl radicals which may be explained by urate's inability to scavenge lipid environments (9, 10, 71).

1.4.2 Peroxynitrite

Urate's ability to scavenge peroxynitrite, an oxidant and nitrating agent, is supported in the literature (73-75). Tyrosine and guanine are common targets of this oxidant (73). Urate prevented peroxynitrite-induced tyrosine nitrosylation and inhibited guanine nitration (73). Yet, urate failed to scavenge peroxynitrite with the pyrogallol red assay and was the least effective scavenger of peroxynitrite compared to ascorbate and glutathione. This experiment was performed in the presence of bicarbonate to model physiological conditions (73). Peroxynitrite oxidises bicarbonate, forming a carbonate radical which propagates the effect of peroxynitrite (67). In a similar study, Kuzkaya et al. (74) measured urate's scavenging of peroxynitrite in the presence of physiological ascorbate and

bicarbonate. Urate's antioxidant activity yielded a carbon-centred radical, which ascorbate reduced to form an ascobyl radical. The presence of ascorbate or thiols tripled urate's antioxidant capacity (74) Urate's antioxidant activity therefore coexists with ascorbate, forming an antioxidant cycle (9, 10, 74). Urate's antioxidant activity was ineffective against superoxide (74).

1.4.3 Oxo-Heme Oxidants

Ames et al. (3) published the only paper to show that urate scavenges oxo-heme oxidants in metalloenzymes. Ames et al. (3) oxidized haematin, a Fe-porphyrin co-ordinated to a hydroxide; and methemoglobin, an alternative oxidation state of haemoglobin; with hydrogen peroxide. Half of urate (300 µM) was consumed in four minutes as it scavenged the oxo-heme adducts (3).

1.4.4 Metal Ion Coordination

Davies et al. (76) published the only paper to link urate coordination of metal ions to antioxidant activity. Urate completely prevented the oxidation of ascorbate in a solution of Fe^{3+}. Allantoin was not formed, hence urate coordinated the metal ion instead of scavenging oxidants. Thus, urate lowered the metal ion's reductive potential and reactivity as an oxidant (76). However, Davies et al. (76) used urate 1-10 µM; which is well below the physiological concentration of urate. Few papers describe urate's antioxidant activity in hyperuricemia. Other studies examined urate coordination to metal ions but did not measure the effect on oxidation (79, 80). Fe ions are abundant in blood serum but are always chelated to metalloenzymes (81). 'Free' Fe ions, due to the overconsumption of Fe, produce ROS which damage biomolecules (82). This antioxidant activity may be crucial in preventing mutagenesis and carcinogenesis during Fe poisoning.

1.5 Urate as a Pro-oxidant

Pro-oxidants are species that directly or indirectly promote oxidative stress (83). Many antioxidants can act as pro-oxidants under specific conditions. Ascorbate and phenolics promote copper-induced oxidation of oxidised low density lipoprotein (oxLDL), phenolics also oxidise DNA at low pH (83-85). Compelling evidence is emerging that urate

acts as an antioxidant or pro-oxidant depending on the microenvironment (figure 4). Urate is a conditional pro-oxidant of low density lipoprotein (LDL) (16, 75, 86, 87). Urate upregulates NADPH (reduced nicotinamide adenine dinucleotide phosphate) oxidase (NOX), which generates ROS (18, 88, 89). A urate peroxyl radical inactivates yeast alcohol dehydrogenase (YADH) (90) and α_1-antitrypsin (A1AT) (73, 91). Urate oxidation produces urate hydroperoxide, which could be a powerful oxidant of biomolecules (5, 12, 17, 19, 20).

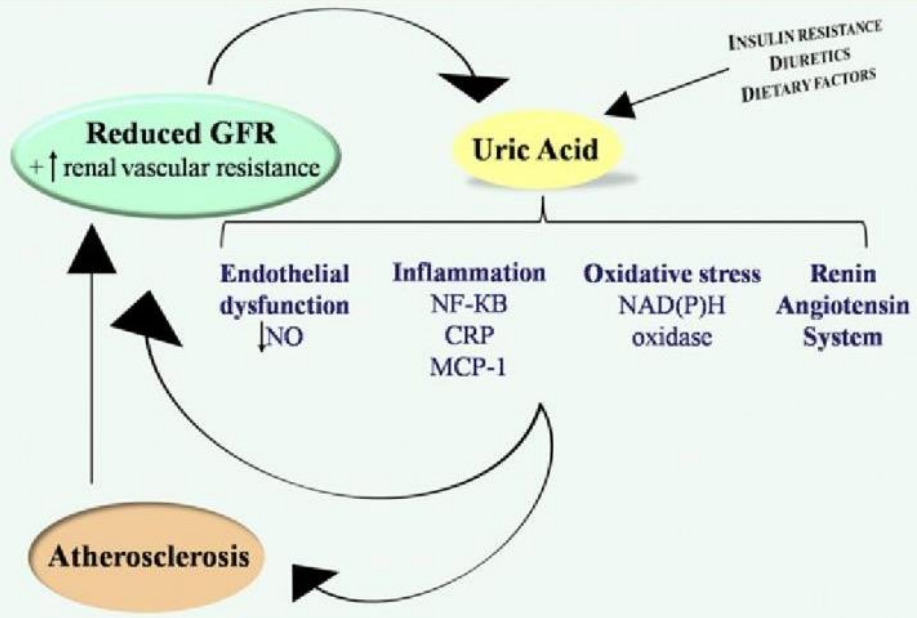

Figure 4: Urate's pro-oxidant effects have physiological repercussions for inflammatory disease. Depletion of NO could lead to endothelial dysfunction, the lack of ability to control vascular dilation in blood vessels. Activation of cytokines: nuclear factor kappa-light-chain-enhancer of activated B cells (NF-κB), C-reactive protein (CRP) and MCP-1 aggravate inflammation. Activation of NOX produces ROS, hence elevates oxidative stress. Urate directly affects the renin-angiotensin system, as evident in hyperuricemia's association with high blood pressure. These mechanisms feed the pathology of atherosclerosis and reduced glomerular filtration rate (GFR), a measure of kidney function. Reduced GFR, insulin resistance, diuretics and diet elevate serum urate. Figure adapted from (92).

1.5.1 Low Density Lipoprotein

Urate increases the oxidation of LDL, despite its well documented antioxidant capacity (16, 75, 86, 87). Urate acts as a pro-oxidant or antioxidant of LDL during copper-induced ($CuSO_4$) oxidation (16). Urate addition alongside the oxidant $CuSO_4$ extended the lag phase of lipid oxidation, hence acted as an antioxidant. On the contrary, when addition of urate followed $CuSO_4$ the rate and amount of lipid peroxides increased, hence urate acted as a pro-oxidant (16). Free metals are rare in serum, but there is growing evidence that transition metals are present in atherosclerotic plaques and facilitate its progress (93,

94). Urate's pro-oxidant activity with LDL is not limited to copper-induced oxidation. A urate concentration equivalent to hyperuricemia (500 µM) doubled oxLDL formation during peroxynitrite-induced oxidation (75). These results are pathologically relevant because oxLDL is linked to atherosclerosis (95-97). Urate is present in the muscular endothelium where LDL becomes trapped and oxidized (16). Urate may act as a pro-oxidant for LDL oxidation, hyperuricemia would promote these effects.

Urate's pro-oxidant effect was evident when copper-induced LDL oxidation was examined in human serum ultra-filtrate. Ultra-filtrate with 10 µM urate delayed peroxidation initiation. However, ultra-filtrate brought forward the propagation phase when it was added after initiation. Ultra-filtrate lost antioxidant and pro-oxidant activity when uricase removed urate, this is strong evidence that urate was responsible for enhancing oxidation of oxLDL (87). Urate's pro-oxidant and antioxidant activity for LDL is evident *ex vitro* and *in vitro* (16, 75, 86, 87). The discrepancies in the literature for urate's effect on oxLDL can be explained by the experimental method. Previous studies (9, 10, 98, 99) added urate prior to peroxidation initiation, hence did not account for the effect of oxidative stress on urate.

1.5.2 NADPH Oxidase

A number of studies have shown that urate upregulates neutrophil phagosomal and non-phagosomal NOX (18, 88, 89). The hydrophobic and oxidative nature of adipocytes provides the perfect microenvironment for urate to act as a pro-oxidant (18). Urate uptake by mouse 3T3-L1 differentiated adipocytes increased intracellular ROS. Urate increased uptake of NOX subunits $p67^{phox}$ and $p47^{phox}$ into membranes, enabling activation of non-phagocyte NOX. NOX transfers electrons from reduced nicotinamide adenine dinucleotide phosphate (NADPH) to oxygen to yield superoxide, hence generating ROS (18). This study is limited by the fact that the authors did not directly measure NOX, and many isoforms of NOX exist in adipocytes which may not require the subunits measured. The mechanisms of non-phagocyte NOX activation are elusive, however $p67^{phox}$ and $p47^{phox}$ are required for phagocyte NOX activation (100). Hence, this pro-oxidant effect could be significant for neutrophils at an inflammatory site (89). Also, 60 µM urate generated the most ROS; serum urate concentration is many times greater (230-360 µM) (2). A possibility unexplored by Sautin et al. (18) was that urate is acting as an oxidant in addition

to activating NOX. In support of this, NOX inhibitors did not completely remove ROS. Obesity accompanies hyperuricemia, hence these results are physiologically relevant (101).

Urate also activated the NOX of human aerotic smooth muscle cells (88). Treatment with urate promoted cell proliferation and the Endothelin-1, which signals the contraction of blood vessels (vasoconstrictor) and associated with cardiovascular disease (88, 102). The uptake of the $p47^{phox}$ subunit into microsomal membranes increased, thus urate activated NOX. It was apparent that urate acted through a pro-oxidant mechanism since pre-treatment of the cells with antioxidant N-acetylcysteine prevented cell proliferation (88). These results link the pro-oxidant effects of urate to damage vascular smooth muscle cells during atherosclerosis (30, 58, 88).

1.5.3 Inactivation of Enzymes

The literature for urate's redox interaction with enzymes is lacking. Physiological urate (240 µM) enhanced inactivation of gamma irradiated A1AT, an anti-inflammatory serpin for elastase (91). A urate peroxyl radical formed via ROS oxidation was thought to be responsible for inactivation of this enzyme. Addition of ascorbate recovered urate's antioxidant activity (91). The peroxyl radical could be a reactive intermediate to urate hydroperoxide which oxidises essential A1AT residues. Conflicting results were published more than a decade later by Whiteman et al. (73). Very high urate (1000 µM) offered a small but significant protection against peroxynitrite-induce A1AT inactivation. Urate's antioxidant activity increased in the presence of bicarbonate (73). The discrepancy between these papers is due to the oxidant used. Aruoma and Halliwell (91) used irradiation to generate ROS. Urate scavenged the ROS to form a radical, and then combined with oxygen or superoxide to form the peroxyl radical. Whereas Whiteman et al. (73) used peroxynitrite prepared from peroxide and nitrite. Superoxide was absent in the reaction system, hence the peroxyl radical was unlikely to form (73). A serum urate concentration of 1000 µM is not an unreasonable concentration to model serum urate for humans. During hyperuricemia and starvation serum urate can rise to > 1000 µM (103).

A similar mechanism was proposed for inactivation of Yeast alcohol dehydrogenase (YALDH) in a study by Kittridge and Wilson (90). Addition of a very high concentration of urate (1000 µM) to an irradiated solution of YALDH resulted in a sharp loss of enzyme activity. Similarly to Aruoma and Halliwell (91), a urate peroxyl radical was thought to oxidise this enzyme. YALDH retained its activity when the urate solution was purged with

nitrogen, hence superoxide is essential for peroxyl radical formation (90). A flaw in Kittridge and Wilson's (90) study is that they did not show inactivation for a physiologically relevant enzyme. YALDH is not found in humans and urate failed to inactive hog lactate dehydrogenase (LDH) (90). Kittridge and Wilson (90) and Aruoma and Halliwell (91) demonstrated a urate peroxyl radical, which could be analogous to urate hydroperoxide, can oxidise enzymes. The urate peroxyl likely oxidized catalytic residues. YALDH is a thiol-dependent enzyme, oxidation of the cysteine ligands to sulfinic or sulfonic acids results in loss of the catalytic Zn (104). The catalytic methionine residues of A1AT are oxidized to sulfoxide adducts, resulting in irreversible inactivation (105). Further research is required to elucidate the pro-oxidant effect of urate on enzymes.

1.5.4 Urate Hydroperoxide

The biological context of urate hydroperoxide formation can be understood when we recall that activated white blood cells called neutrophils have all the machinery to produce urate hydroperoxide. Neutrophils are recruited to inflammatory sites where they are trapped and spill their oxidative contents (106, 107). This includes myeloperoxidase, which oxidises urate to the radical and NOX, which generates superoxide (17, 20, 108). Superoxide adds very quickly to the urate radical, at rate constant $k = 8 \times 10^8\ M^{-1}s^{-1}$, to form urate hydroperoxide (17, 19, 109). During hyperuricemia, the concentration of urate overwhelms other antioxidants leading to oxidative stress. Therefore, urate hydroperoxide could be formed at an inflammatory site during neutrophil invasion and hyperuricemia (20). *In vitro* urate hydroperoxide can also be formed by riboflavin photooxidation (figure 5) (20, 77).

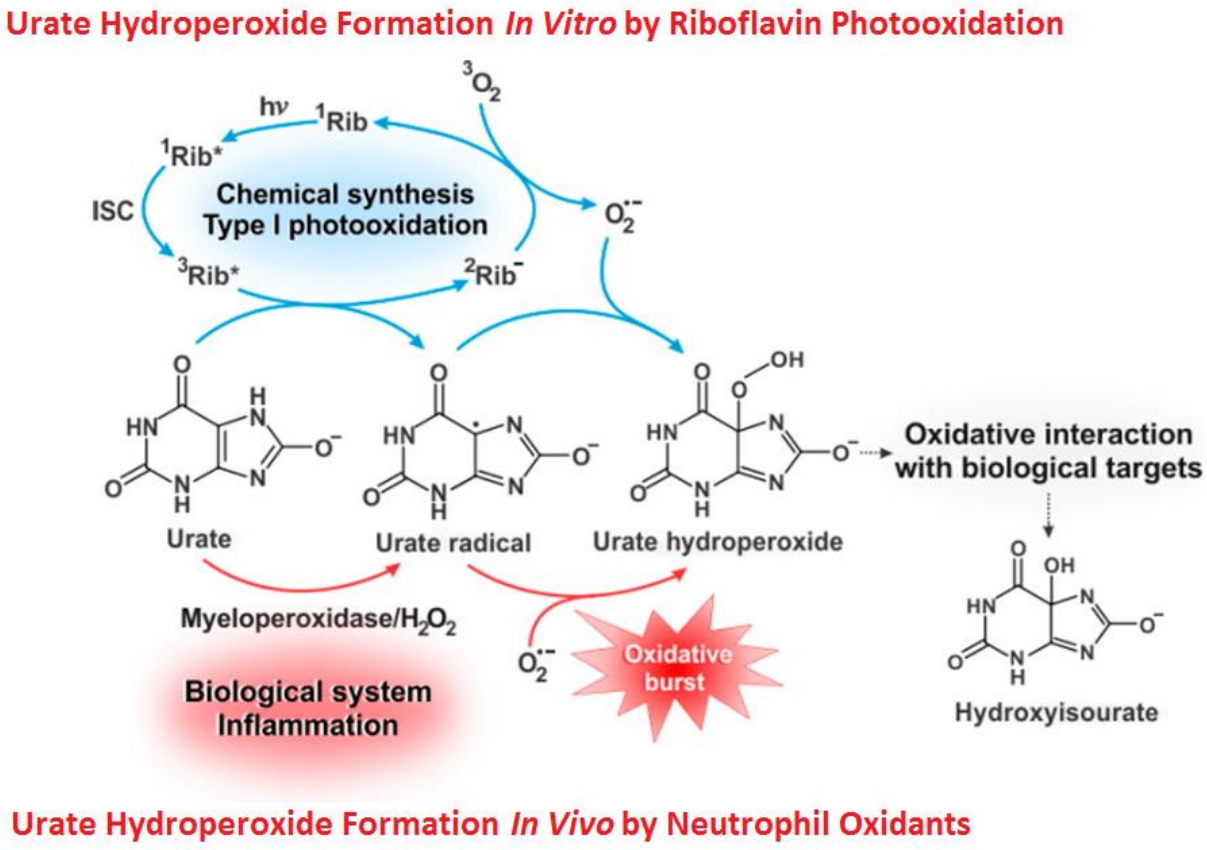

Figure 5: Pathways for urate hydroperoxide formation *in vitro* and *in vivo* (theoretically) by photooxidation or inflammatory processes. The basic process involves conversion of urate to a radical and combination of the radical with superoxide to form urate hydroperoxide. *In vitro* urate hydroperoxide can be formed at high concentration using the riboflavin photocycle. During this process superoxide is generated and urate is converted to a radical. The proposed *in vivo* system for urate hydroperoxide formation involves neutrophil oxidants myeloperoxidase and superoxide. Neutrophils spill myeloperoxidase and hydrogen peroxide into inflammatory site during inflammation. These can convert urate to a radical. Neutrophil oxidative bursts produce superoxide, which adds to the urate radical. These reactions are described further in the next chapter. Urate hydroperoxide oxidises several biomolecules forming electrophilic product hydroxyisourate. Figure adapted from (20).

A recent study by Patrício et al. (20) characterised urate hydroperoxide's reaction with small biomolecules. Urate hydroperoxide absorbs ultraviolet light at 308 nm: $\varepsilon_{(308)}$ = 6,540 ± 380 $M^{-1}cm^{-1}$, this can be visualised on a spectrophotometer. This molecule decays quickly at half-life 41 min at room temperature (20). Urate hydroperoxide oxidized methionine to methionine sulfoxide, cysteine to cystine and glutathione to glutathione disulfide, in a two-electron reaction. The urate oxidative product was hydroxyisourate. Urate hydroperoxide had no effect on histidine, lysine, taurine or tryptophan (20). Urate hydroperoxide has not been studied with enzymes or larger biomolecules. Theoretically, urate hydroperoxide could act like lipid hydroperoxides. These species are powerful oxidants and will induce DNA, protein and cell membrane damage (110). Urate

hydroperoxide formation could explain the pro-oxidant effects of urate during hyperuricemia (20).

1.6 Conclusion

The association between serum urate and gout was proposed 150 years ago (111), yet our understanding of the pathology of hyperuricemia and inflammatory diseases is incomplete. The literature shows evidence for urate acting as an antioxidant, pro-oxidant and having pro-inflammatory effects. Urate can deplete NO (15, 55, 56), activate the NLRP3 inflammasome (14, 52, 53) and upregulate cytokines (30, 57-60) to exacerbate inflammation. These mechanisms recruit a sterile inflammatory response leading to the formation of ROS and tissue damage. Urate's inflammation mechanisms are intertwined with its pro-oxidant effects.

Urate is an abundant antioxidant in humans and scavenges a range of oxidant species: singlet oxygen (3), peroxyl and hydroxyl radicals (3, 70-72), peroxynitrite (73-75) and oxo-heme oxidants (3, 69). Nonetheless there are flaws in urate's antioxidant activity. Urate cannot scavenge radicals into lipid environments, it must be regenerated by ascorbate and it cannot scavenge superoxide (74, 76, 78). Urate's antioxidant ability during hyperuricemia and the depletion of antioxidants is not well understood. High concentrations of urate should help not hinder inflammatory diseases by removing ROS that initiate and propagate inflammation (112). Yet, hyperuricemia is associated with many inflammatory diseases (5, 11, 12, 30).

Like other antioxidants, urate has pro-oxidant activities in specific microenvironments. Urate oxidises LDL (16, 75, 86, 87), upregulates NOX (18) and inactivates enzymes YALD (90) and A1AT (73, 91). Urate-induced oxidation of LDL has many supporting papers, but the evidence for NOX activation and enzyme inactivation is sparse. These mechanisms are insufficient to justify urate's association with cardiovascular disease. A new and convincing mechanism for urate's pro-oxidant effects involves formation of urate hydroperoxide by enzymes xanthine oxidase and peroxidise, or riboflavin photooxidation (5, 12, 17, 19, 20). This novel oxidant depletes methionine, cysteine and glutathione (20). Urate hydroperoxide's effect on enzymes has not been characterised. Whether urate hydroperoxide forms *in vivo* at inflammatory site remains to

be seen. However, neutrophils have all the mechanisms to produce urate hydroperoxide during the inflammatory response (17).

1.7 Summary

My literature search leads me to conclude that urate can be an antioxidant or pro-oxidant depending on its concentration and the oxidative state of blood serum. Basal urate undergoes an antioxidant cycle in which urate is oxidized by ROS, myeloperoxidase or lactoperoxidase, and is recovered by ascorbate. During hyperuricemia, depletion of antioxidants and in lipid environments; urate acts as a pro-oxidant to directly and indirectly produce oxidant species. Thus, urate ceases to provide antioxidant defence and tips the balance to oxidative stress, favouring the development of inflammatory disease (figure 6). Concentration and oxidative stress affects to urate's antioxidant capacity. Thus, urate as a pro-oxidant does not conflict with its roles an antioxidant *in vivo*. Urate follows Paracelsus' famous philosophy: "The dose makes…a poison" (113).

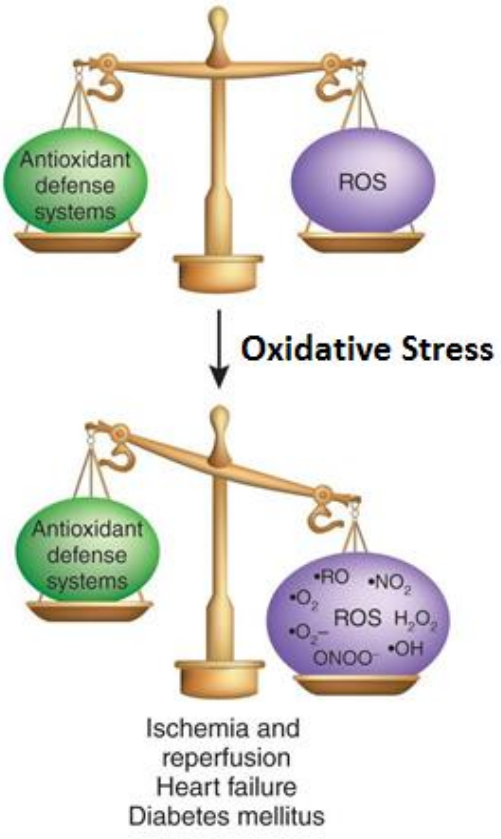

Figure 6: A healthy human body balances pro-oxidant formation with the antioxidant defence system (homeostasis). During oxidative stress the antioxidant defence system is overwhelmed by ROS. Oxidative stress characterises inflammatory disease, including cardiovascular disease, ischemia/reperfusion injury, heart failure and diabetes. Figure adapted from (114).

Chapter 2. Optimising the Formation of Urate Hydroperoxide

2.1 Introduction

Urate hydroperoxide is transient and highly reactive (19, 20). For this chapter I wanted to produce a high concentration of urate hydroperoxide to use in proceeding experiments and to study its formation. Urate hydroperoxide can be formed *in vitro* by riboflavin photooxidation or by enzymes xanthine oxidase and myeloperoxidase/lactoperoxidase (17, 19, 20, 77). These systems produce a urate hydroperoxide of the same structure (20).

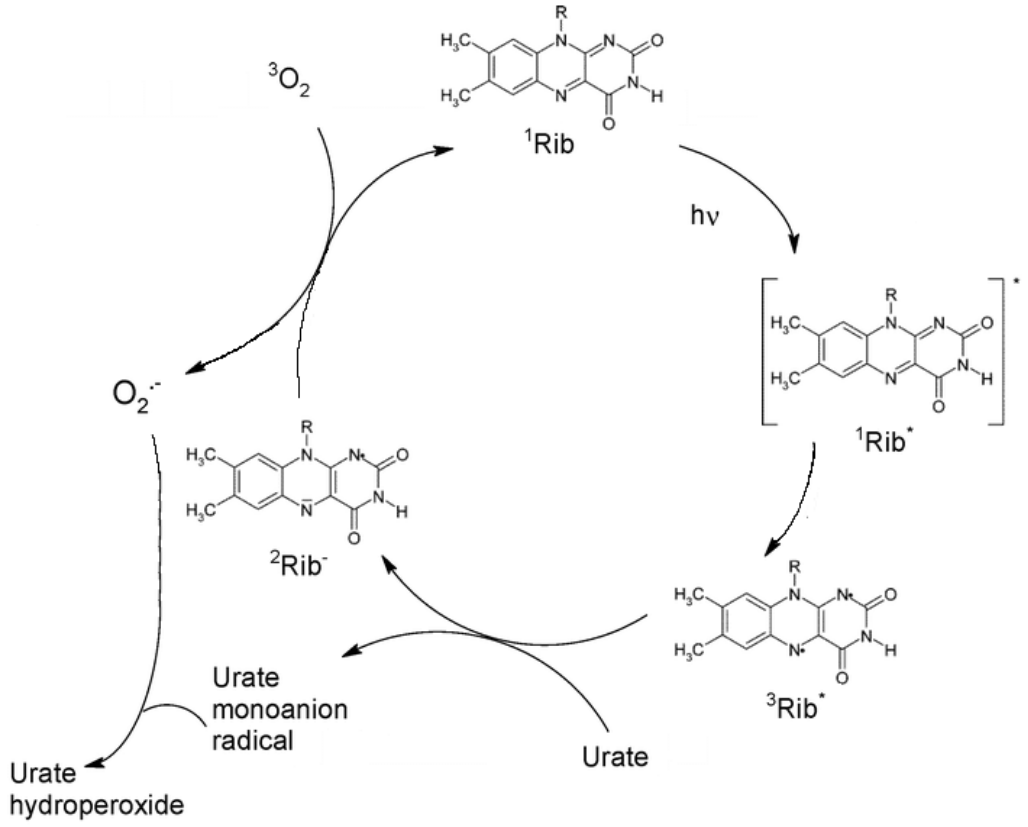

Figure 7: Riboflavin undergoes a photooxidation cycle to oxidise urate to urate hydroperoxide. Light promoted riboflavin (Rib) to a higher energy state (^{1}Rib*), this rearranges to form a radical (^{3}Rib*). The riboflavin radical is reduced by urate to form a riboflavin radical anion (^{2}Rib$^-$) and the urate radical. The riboflavin radical anion is oxidised by oxygen to form native riboflavin and superoxide. Thus, riboflavin receives an electron from urate and passes it to oxygen to act as a catalyst. The urate radical and superoxide combine to produce urate hydroperoxide. Figure adapted from (77).

Urate hydroperoxide can be formed at a high concentration with type I riboflavin photooxidation (20, 77). When riboflavin is illuminated with light at 440 nm it forms an excited state. The excited state rearranges to a radical with two extra electrons (115, 116). In this state riboflavin receives an electron from urate and passes it to oxygen. The

products, the urate radical and superoxide, combine to form urate hydroperoxide (figure 7) (77, 115, 116). The resulting hydroperoxide was catalase-resistant and quenched by superoxide dismutase, indicating formation of urate hydroperoxide (77). Patrício et al. (20) optimised the formation of urate hydroperoxide by exposing 600 μM urate to ultraviolet A light (365 nm) for 10 min. This method produced 300 μM urate hydroperoxide (20).

A compelling mechanism for the formation of urate hydroperoxide by myeloperoxidase was published by Meotti et al. (17). Myeloperoxidase typically catalyses the oxidation of chloride and hydrogen peroxide to hypochlorous acid (5, 12, 17). This peroxidase also performs a one-electron oxidation of urate to form a urate radical (17). Myeloperoxidase uses a peroxidase cycle, where the heme cycles through states compound I and II by redox reaction with substrates (117). Compound I catalyses the oxidation of urate with a first order rate constant $k = 4.6 \times 10^5\ M^{-1}s^{-1}$. This is significantly higher than the rate constant for chloride catalysis $k = 2.5 \times 10^4\ M^{-1}s^{-1}$. Compound II oxidises urate at second order rate constant $k = 1.7 \times 10^4\ M^{-1}s^{-1}$. In spite of the high rate constants, myeloperoxidase preferentially catalyses the production of hypochlorous acid (17). Myeloperoxidase's preference for chloride may be the result of high chloride concentration (100 μm) in neutrophil phagocytes (108). In vitro production of urate hydroperoxide involves use of xanthine oxidase to generate superoxide. Superoxide added to the urate radical to form approximately 20 μM urate hydroperoxide from > 100 μM urate (17).

Lactoperoxidase is antibacterial enzyme catalyses the two-electron oxidation of thiocyanate and hydrogen peroxide to hypothiocyanite. This peroxidase also converts urate to the urate radical. Urate was oxidized by compound I at a second-order rate constant $k = 1.1 \times 10^7\ M^{-1}s^{-1}$ (19). This rate is the highest of lactoperoxidase's substrates and > 20 times greater than catalysis by myeloperoxidase (17, 19). Compound II reduced urate in a second-order reaction with rate constant $k = 8.5 \times 10^3\ M^{-1}s^{-1}$ to produce another urate radical. An enzyme system of xanthine oxidase, lactoperoxidase and their substrates produced approximately 20 μM urate hydroperoxide from 200 μM urate (19).

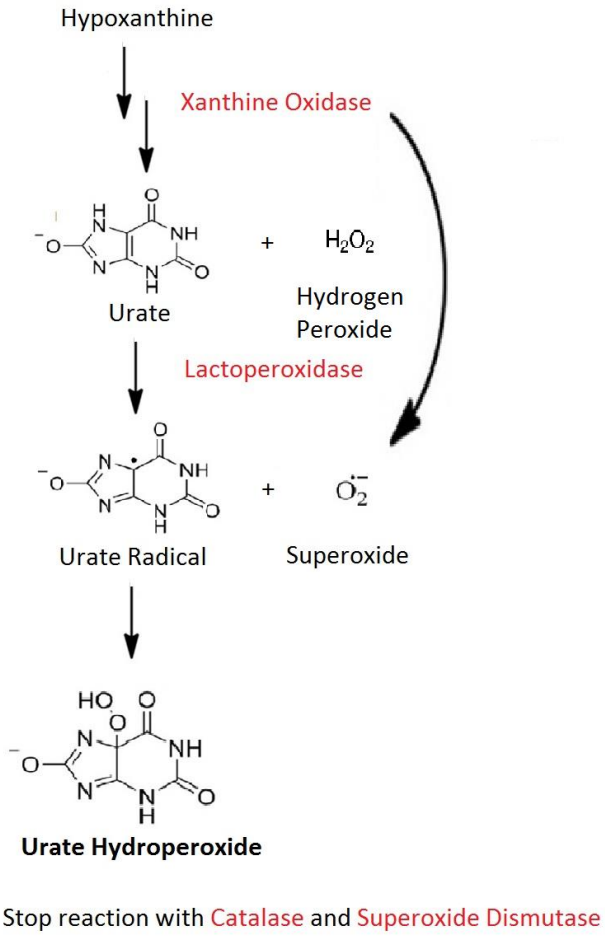

Figure 8: The xanthine oxidase/lactoperoxidase system to form urate hydroperoxide *in vitro*. The following substances combined in phosphate: hypoxanthine, urate, lactoperoxidase and xanthine oxidase (the initiator). Hypoxanthine is the substrate for xanthine oxidase, which generates superoxide, which dismutases to hydrogen peroxide. Lactoperoxidase converts urate and hydrogen peroxide to the urate radical. The urate radical and superoxide combine to form urate hydroperoxide. To stop the reaction, catalase and superoxide dismutase were added to deplete hydrogen peroxide and superoxide, hence quenching urate hydroperoxide formation. Figure adapted from (19).

The xanthine oxidase/lactoperoxidase system was chosen to produce urate hydroperoxide because I did not have the UV lamps required for riboflavin photooxidation. The use of enzymes to form urate hydroperoxide is quick and simple. However, enzymes create interference, their activity is variable and this system forms less urate hydroperoxide than riboflavin photooxidation. The goal of this chapter is to optimise the formation of urate hydroperoxide by a xanthine oxidase/lactoperoxidase system (figure 8).

2.2 Materials and Methods

2.2.1 Materials

Substances and solutions used throughout experimental work were put in table 2.

Table 2: Description of substances and solutions used to perform the cytochrome c assay, ferrous oxidation-xylenol orange assay (FOX) and the xanthine oxidase/lactoperoxidase system. The preparation and company sourced were described. Buffers were autoclaved before use.

Substance	Preparation	Company
Catalase from bovine liver	Stock of 2 mg/mL dissolved in phosphate buffer.	Sigma, C40
Cytochrome c from equine heart	Stock of 2 mg/mL dissolved in phosphate buffer.	Sigma, C2506
Diethylene triamine pentaacetic acid (DTPA)	Stock of 10 mM dissolved in phosphate buffer.	Sigma, D1133
Ferrous Ammonium Sulfate		Baker Reagents
FOX reagent (modified)	In 25 mL MilliQ: 400 µM xylenol orange, 1 mM ferrous ammonium sulfate, 400 mM sorbitol, 200 mM sulfuric acid.	
Hydrogen Peroxide	Stock of 30% solution diluted to 20 µM in MilliQ using molar extinction coefficient: ε(240) = 43.6 $M^{-1}cm^{-1}$ (118).	LabServ, BSPA5.500
Hypoxanthine	Stock of 10 mM in phosphate buffer, heated at 70 °C for 2 min to dissolve before use.	Sigma, H9377
Phosphate buffer	Approximately 80:20 of 50 mM NaH_2PO_4 and 50 mM K_2HPO_4 dissolved in MilliQ, pH 7.4.	
Potassium hydrogen orthophosphate (K_2HPO_4)		BHD, 102034B
Lactoperoxidase from bovine milk	Dissolved in phosphate buffer at 1mg/mL, concentration determined with molar extinction coefficient: ε(412) = 112.3 $mM^{-1}cm^{-1}$.	Sigma, L2005
MilliQ	Ultrapure water	Millipore Corporation
Sodium dihydrogen orthophosphate (NaH_2PO_4)		Anhydrous, Labserv, BSPSO766.500
D-Sorbitol		Sigma, S1876
Sulfuric acid	Concentrated stock 18.76 M.	AnalaR, 102761
Superoxide dismutase from bovine liver	Stock of 2 mg/mL dissolved in phosphate buffer and diluted 10 times.	Sigma, S7571
Uric acid	In 10 mL MilliQ: 1 mM was dissolved in 1 ml 0.1 mM sodium hydroxide.	Sigma, U2625
Xanthine oxidase from bovine milk	Diluted at 1:20 ratio in phosphate buffer. This dilution was equivalent to approximately 90 µM. The extinction coefficient of xanthine oxidase was ε(450) = 37,800 $M^{-1}cm^{-1}$ (119).	Sigma, X1875
Xylenol Orange tetrasodium salt		Fluka, 33825

2.2.2 Cytochrome C Assay of Superoxide Production by Xanthine Oxidase

The cytochrome c assay was used to determine superoxide production by xanthine oxidase. The cytochrome c assay involved reduction of ferric to ferrous cytochrome c by superoxide. The colour change in the cuvette was orange to pink. Ferrous cytochrome c absorbed light at 550 nm (120). The following substances were mixed in plastic cuvettes in 50 mM phosphate buffer: 240 µg/mL cytochrome c, 100 µM DTPA, 100 µM hypoxanthine. Superoxide dismutase (10 µg/mL) was added as a negative control. The final volume was 1 mL. The Hitachi spectrophotometer (UV solutions Application program no. 2J24311-04 (build556)) was set to time scan, six cell mode. The spectrophotometer measured absorbance (-0.1 – 1) at 550 nm for 300 sec. Other setting included: spectral band width = 0.5 nm and lamp change mode = auto for 325 nm. The spectrophotometer was blanked with all substances except xanthine oxidase, 450 nM of this enzyme was added to initiate the assay. The initial rate was calculated for the first 30 sec as $A.min^{-1}$ (ΔA). This value was used to calculate superoxide production by xanthine oxidase:

$$Rate\ of\ Superoxide\ Production\ (\mu M min^{-1}) = \frac{\Delta A}{0.0211}$$

Samples were made in triplicate. Firstly, the concentration of enzyme of interest, xanthine oxidase, was optimised. The volume of 90 µM xanthine oxidase injected into the cuvette was varied to achieve concentrations 0 – 1800 nM. Next, the concentration of xanthine oxidase's substrate, hypoxanthine, was varied by creating a dilution series in phosphate buffer. Each dilution was transferred (100 µL) into plastic to achieve concentrations 0 – 100 µM. Superoxide production was plotted against xanthine oxidase or hypoxanthine concentration.

2.2.3 Xanthine Oxidase/Lactoperoxidase System Photometry

The xanthine oxidase/lactoperoxidase system had unique absorbance spectrum between 240 – 340 nm due to the formation of purines (19). In particular, hypoxanthine, urate and urate hydroperoxide absorbed light at 250, 290 and 310 nm. The absorbance spectrum for urate hydroperoxide formation was monitored with kinetic mode on the 8453 Agilent spectrophotometer (UV visible chemstation Rev.A.10.01 [81]). The instrument was set to wavelength range 190 – 1100 nm, interval 1 nm and integration time 0.5 sec. Both the deuterium and tungsten lamps were used.

Samples were made in a 1 mL quartz cuvette. The final concentrations of substances were: 100 µM urate, 100 µM hypoxanthine, 100 µM DTPA, 200 nM lactoperoxidase and approximately 1.8 µM xanthine oxidase in 50 mM phosphate buffer. As controls, 100 µg/mL catalase and 10 µg/mL superoxide dismutase were added to quench the formation of urate hydroperoxide. A sample without additional urate was made to determine whether xanthine oxidase activity alone produced urate hydroperoxide. The spectrophotometer was set to measure the full spectrum (200 – 1000 nm) every 30 sec for 2000 sec. Measurements were made in triplicate. The absorbance spectrum was extracted for time points: 0, 120, 240, 360, 480 and 600 sec and plotted for 240 – 340 nm. The full system absorbance at 310 nm was extracted and plotted with time.

2.2.4 Modified Ferrous Oxidation Xylenol Orange Assay for Hydroperoxides

Hydroperoxide concentration was measured with the modified FOX assay. During this assay hydroperoxides oxidised ferrous to ferric iron, which formed a complex with xylenol orange (121). Formation of the ferric-xylenol orange complex changes the reagent colour from orange to brown and absorbed light at 560 nm. A modified FOX assay was used to measure urate hydroperoxide concentration (121). The assay samples were made with volume ratio 3:1 for the unknown hydroperoxide sample to FOX reagent. The samples were incubated for 45 min at room temperature then transferred into a 100 µL quartz cuvette. The Agilent spectrophotometer was set to standard mode with manual measurement at fixed wavelength 560 nm. The sample absorbance was compared with a standard curve for hydrogen peroxide to determine the hydroperoxide concentration. When the sample absorbance was outside the range of the linear standard curve the sample was diluted in phosphate buffer then reassayed. Hydroperoxide concentration was plotted against substance or concentration.

2.2.4.1 FOX Standard Curve with Hydrogen Peroxide

Since the concentration of urate hydroperoxide was unknown, a standard curve was made for the FOX assay against hydrogen peroxide. Hydrogen peroxide absorbed light at 240 nm, the Beer-Lambert law was used to calculate concentration its concentration:

$$A = \varepsilon c l$$

Where A = absorbance, ε = molar extinction coefficient in $M^{-1}cm^{-1}$, c = concentration in M, and l = path length, 1 cm. The molar extinction coefficient of hydrogen peroxide was: $\varepsilon_{(240)} = 43.6\ M^{-1}cm^{-1}$ (118). Measurement of hydrogen peroxide concentration was described in table 2. Hydrogen peroxide (20 µM) was diluted in 50 mM phosphate buffer to concentrations: 0 – 5 µM. The FOX assay was performed (2.2.4) and plotted absorbance at 560 nm against hydrogen peroxide stock concentration.

2.2.4.2 Initial Assay of Urate Hydroperoxide Formation

The FOX assay was performed on all the substances of the xanthine oxidase/lactoperoxidase system to determine their interferences for later experiments. The substances were diluted to 300 µL in 50 mM phosphate buffer: 100 µM hypoxanthine, 100 µM urate, 200 nM lactoperoxidase, 0.9 µM xanthine oxidase, 100 µg/mL catalase, 10 µg/mL superoxide dismutase and 50 mM phosphate buffer. FOX reagent (100 µL) was added to each sample (2.2.4).

Next, the FOX assay was performed on xanthine oxidase/lactoperoxidase system after a 10 min reaction period to form urate hydroperoxide. Samples were made to represent the full system, removal of each substance and addition of superoxide dismutase as control (Appendix 2, table 6). Hypoxanthine, urate, lactoperoxidase and xanthine oxidase (the initiator) were mixed in phosphate buffer. The final concentration of substances was the same as the previous paragraph. After 10 min incubation at room temperature, urate hydroperoxide production was quenched by adding 20 µg/mL catalase and 20 µg/mL superoxide dismutase. The samples were incubated for a further 10 min at room temperature. The FOX reagent (102 µL) was added and the assay was performed (2.2.4).

2.2.4.3 Optimising Urate Hydroperoxide Formation

This experiment optimised urate hydroperoxide formation detailed in 2.2.4.2, and measured the resulting hydroperoxide concentration with the FOX assay. The concentration of urate was increased from 100 to 400 µM, and xanthine oxidase from 0.9 to 1.8 µM. Samples (300 µL) were made to represent the old full system (2.2.4.2), quadruple urate, double xanthine oxidase and both (new full system). The final concentrations of the new full system were: 100 µM hypoxanthine, 400 µM urate, 200

nM lactoperoxidase and 1.8 µM xanthine oxidase in phosphate buffer. After 10 min incubation 100 µg/mL catalase and 10 µg/mL superoxide dismutase were added to stop the reaction. The FOX assay was performed as described in section 2.2.4.

2.2.4.4 Kinetics of Urate Hydroperoxide Formation

This experiment used the FOX assay to measure hydroperoxide concentration over time for the optimised xanthine oxidase/lactoperoxidase system (2.2.4.3). The reaction mixture was made up to 2 mL in phosphate buffer. A control solution was made with the addition of 10 µg/mL superoxide dismutase. Xanthine oxidase was added last and the stopwatch was immediately started. At time points 0, 2, 5, 10, 15, 20, 25 and 30 min, 220 µL of the urate hydroperoxide solution was transferred into an Eppendorf tube with 10 µL of 2 mg/mL catalase and 0.2 mg/mL superoxide dismutase. After 2 min incubation, 80 µL FOX reagent was added (2.2.4).

Hydroperoxide concentration was plotted vs. time. To calculate the initial rate of urate hydroperoxide formation, the data was converted into a linear graph. The first four points were squared and plotted them against time. The square-root of the gradient gave the rate in $\mu M min^{-1}$.

2.2.5 Statistical Analysis

The equation and regression statistics of linear graphs were added with Excel. Statistical analysis of column graphs was performed with SigmaPlot for Windows version 11.0 (Systat Systems Incorporated 2008).One-way analysis of variance (ANOVA) was performed to determine if the groups were significantly different. The Holm-Sidak test compared the significance found by ANOVA to a control. ANOVA was performed on replicates where the p value to reject was 0.05. Tests included the Shapiro-Wilk normality test (sample size 5000), Post HOC test (power, Alpha value 0.05) and the Holm-Sidak test vs. a control. The differences between replicates was considered significant when $p<0.05$.

2.2.6 Graphs

All graphs were plotted with Microsoft Excel 2013 © Microsoft Corporation 2013. Column graphs were made for datasets with multiple conditions/substance. Datasets where concentration was varied were plotted as scatter graphs with an appropriate trend line.

Error bars represented the standard deviation for multiple experiments or multiple readings. The number of repeat experiments performed was given in the legend.

2.3 Results

2.3.1 Superoxide Production by Xanthine Oxidase

For this experiment I sought to optimise the superoxide generation by xanthine oxidase. The substrate inhibition of xanthine oxidase by hypoxanthine was determined to optimise superoxide production. The concentration of xanthine oxidase and hypoxanthine were varied in the assay cuvette and the resulting superoxide production was measured with the cytochrome C assay.

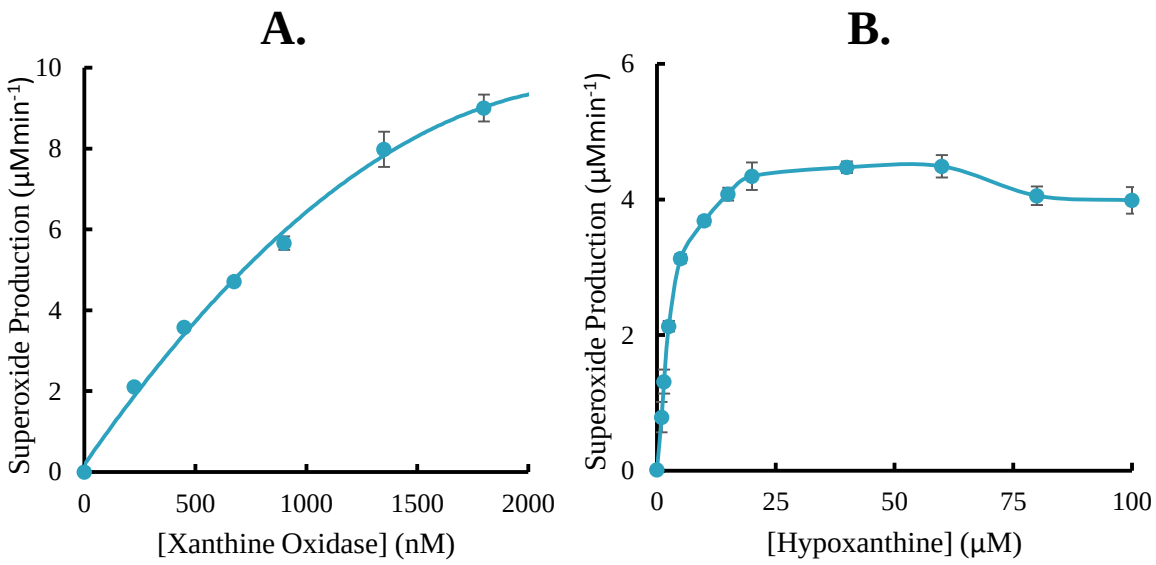

Figure 9: Optimised superoxide production by xanthine oxidase. The cytochrome c assay was used to measure superoxide production. **A.** Superoxide production by xanthine oxidase with varying concentration of enzyme. The concentration of hypoxanthine was 100 µM. **B**. Superoxide production by xanthine oxidase with varying concentration of hypoxanthine. These graphs were based on one experiment. The error bars represent triplicate readings.

Superoxide production increased with xanthine oxidase concentration and plateaued at approximately 10 $\mu Mmin^{-1}$ (figure 9 A). Approximately 0.2 $\mu Mmin^{-1}$ superoxide was produced per nM xanthine oxidase. When hypoxanthine was varied, the superoxide production reached a maximum of 4.5 $\mu Mmin^{-1}$ with 20 µM hypoxanthine (figure 9 B). Superoxide production ($\mu Mmin^{-1}$) was 0.9 per µM hypoxanthine. There was some loss of superoxide production with concentrations of hypoxanthine above 60 µM, however it was

minor. Thus, a high concentration of xanthine oxidase (1.8 µM) and hypoxanthine (100 µM) were used for proceeding experiments since the substrate inhibition was minimal.

2.3.2 Xanthine Oxidase/Lactoperoxidase System Photometry

In this experiment I sought to visualise the formation of urate hydroperoxide and other products of the xanthine oxidase/lactoperoxidase system. This was achieved by monitoring the absorbance spectrum for the xanthine oxidase/lactoperoxidase system on a spectrophotometer.

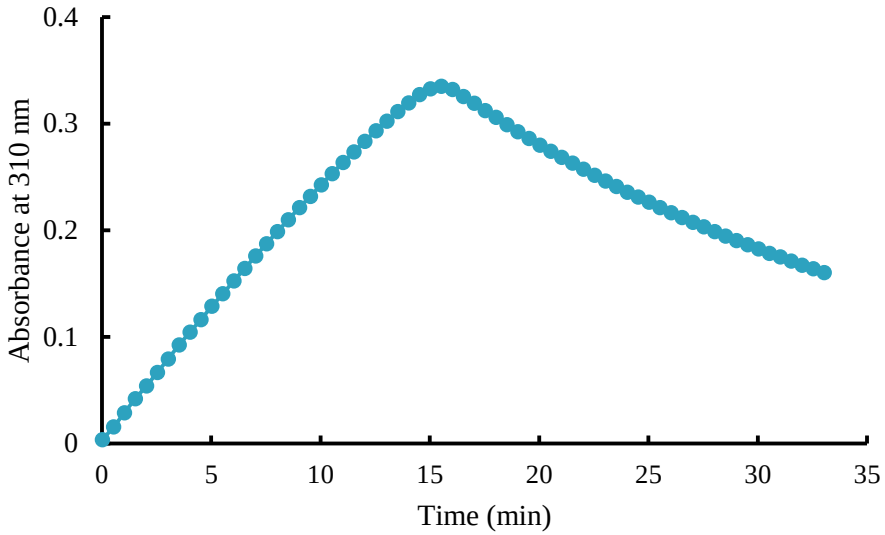

Figure 10: Urate hydroperoxide absorption at 310 nm over time. The absorbance at 310 nm was extracted from the full xanthine oxidase/lactoperoxidase system (figure 11 A). This graph was representative of two experiments.

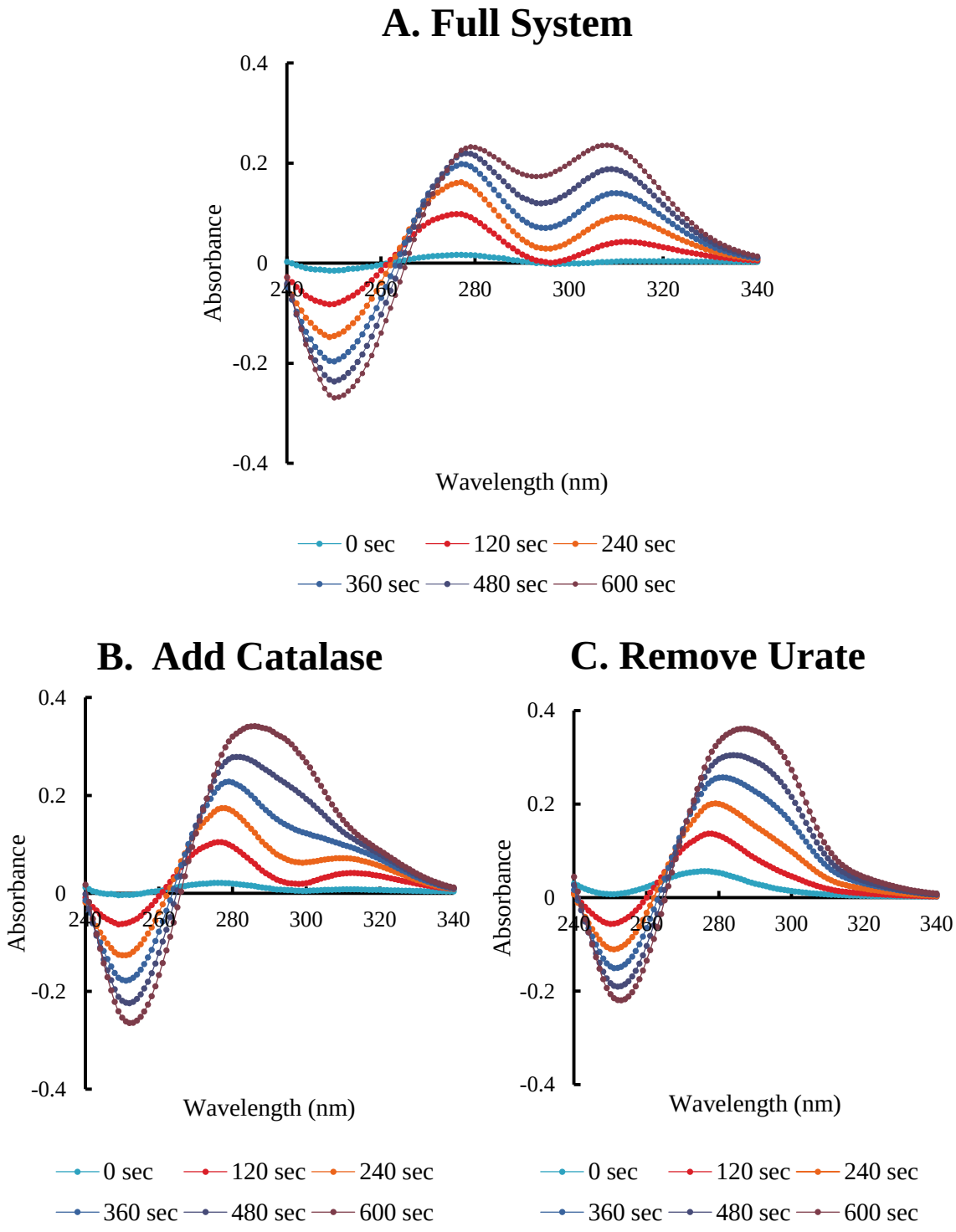

Figure 11: Absorbance of the xanthine oxidase/lactoperoxidase system. The valley at 290nm represented the depletion of hypoxanthine. The peaks at 290 and 310 nm was the formation of urate and urate hydroperoxide respectively. **A.** Urate hydroperoxide formation for the full enzyme system. **B**. Urate hydroperoxide formation plus catalase. **C.** Urate hydroperoxide formation in the absence of addition urate. These graphs were representative of two experiments.

Urate hydroperoxide formation by xanthine oxidase and lactoperoxidase was visualised by monitoring multiple wavelengths on a spectrophotometer (figure 11). Consumption of hypoxanthine by xanthine oxidase formed a trough at 250 nm, the product urate formed a peak at 290 nm. The full system (figure 11 A) had a peak at approximately 310 nm, which Patrício et al. (20) characterised to be urate hydroperoxide ($\varepsilon_{(308)}$ = 6,530 $M^{-1}cm^{-1}$). Urate hydroperoxide absorbance at 310 nm peaked at approximately 15 min, after which the absorbance declined as the molecule degraded (figure 10). Addition of catalase to the system eliminated the urate hydroperoxide peak (figure 11 B). The 310 nm peak was also lost when urate was removed from the system (figure 11 C). Thus, urate hydroperoxide formation was dependent on the presence of ROS and a high concentration of urate.

2.3.3 FOX Assay of Urate Hydroperoxide

For these experiments I sought to determine whether the FOX assay was appropriate for measurement of urate hydroperoxide formed by the xanthine oxidase/lactoperoxidase system. Since urate hydroperoxide was of an unknown concentration, a standard curve was made for the FOX assay of hydrogen peroxide as a comparison (figure 32). This standard curve was used as reference for the urate hydroperoxide concentration.

2.3.3.1 Initial Assay Urate Hydroperoxide Formation

The goal of this experiment was to measure the hydroperoxide concentration formed by the xanthine oxidase/lactoperoxidase system and whether optimisation was required. The FOX assay was used to measure hydroperoxide concentration through absorbance at 560 nm. The substances of the xanthine oxidase/lactoperoxidase system were also assayed to determine their interference (figure 33).

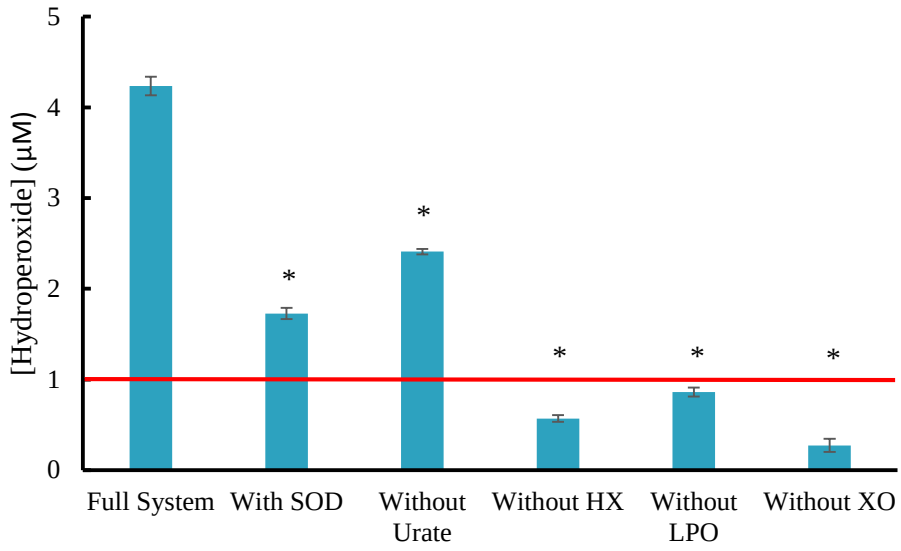

Figure 12: Urate hydroperoxide formed by the xanthine oxidase/lactoperoxidase system. The full system, removal of each substance or addition of superoxide dismutase as a quencher were assayed. The red line represented the baseline absorbance for the substances of the xanthine oxidase/lactoperoxidase system. This graph was representative of three experiments. The error bars represented the standard deviation for triplicate readings of one experiment. One-way ANOVA followed by Holm-Sidak multiple comparison on triplicate readings was used to identify samples that were significantly different from the full system (* $p < 0.05$).

The full xanthine oxidase/lactoperoxidase system formed approximately 4 µM hydroperoxide (figure 12). The addition of superoxide dismutase halved the hydroperoxide concentration. When urate was removed from the system, approximately 2.5 µM hydroperoxide was formed due to xanthine oxidase activity. The removal of hypoxanthine, lactoperoxidase and xanthine oxidase formed less than 1 µM hydroperoxide. No urate hydroperoxide was made in the absence of these substances (20); hence 1 µM hydroperoxide represented the baseline for the FOX assay. A hydroperoxide concentration above the baseline represented formation of urate hydroperoxide. The baseline was variable with repeat experiments. For succeeding experiments the spectrophotometer was blanked with the full system minus hypoxanthine, with FOX reagent. This method removed interference by substances that were not urate hydroperoxide. A urate hydroperoxide concentration of 3 µM was not useful, thus the system was optimised.

2.3.3.2 Optimising Urate Hydroperoxide Formation

I sought to optimise urate hydroperoxide formation by the xanthine oxidase/lactoperoxidase system by increasing the concentration of xanthine oxidase and urate. Samples were made to represent the old full system and new full system with double xanthine oxidase and quadruple the concentration of urate. The resulting hydroperoxide concentration was determined with the FOX assay.

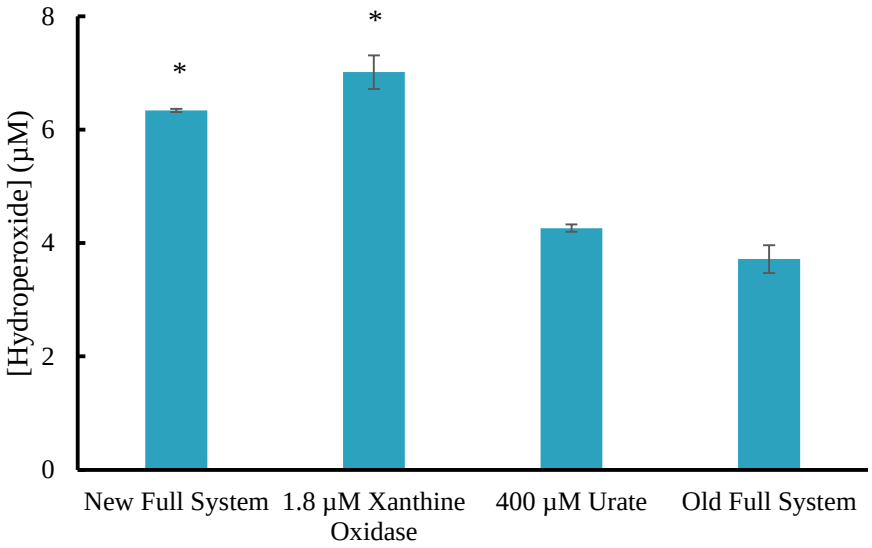

Figure 13: Optimising urate hydroperoxide formation (10 min reaction) by quadrupling urate and doubling xanthine oxidase. The new full system was composed of 100 µM hypoxanthine, 400 µM urate, 200 nM lactoperoxidase and 1.8 µM xanthine oxidase in 50 mM phosphate buffer. Urate hydroperoxide formation was measured with the FOX assay. This graph was for one experiment. The error bars represented the standard deviation for triplicate readings. One-way ANOVA followed by Holm-Sidak multiple comparison on triplicate readings was used to identify samples that were significantly different from the old full system (* $p < 0.05$).

Doubling the concentration of xanthine oxidase doubled the hydroperoxide concentration compared with the old full system (figure 13). Quadrupling the concentration of urate did not affect hydroperoxide concentration. The new reaction system produced approximately 6.5 µM urate hydroperoxide for a 10 min reaction. 400 µM urate was chosen for the optimised reaction system because it models the concentration of urate in serum during hyperuricemia. The concentration of lactoperoxidase and urate were varied with measurements of hydroperoxide concentration over time but there was no significant difference. The system was saturated by 100 µM urate and 100 nM lactoperoxidase.

2.3.3.3 Kinetics of Urate Hydroperoxide Formation

The purpose of this experiment was to measure the formation of urate hydroperoxide over time with and without the presence of superoxide dismutase. At five min intervals urate hydroperoxide solution was transferred into an Eppendorf with catalase and superoxide dismutase. The reaction stopped was stopped at the hydroperoxide concentration was measured with the FOX assay.

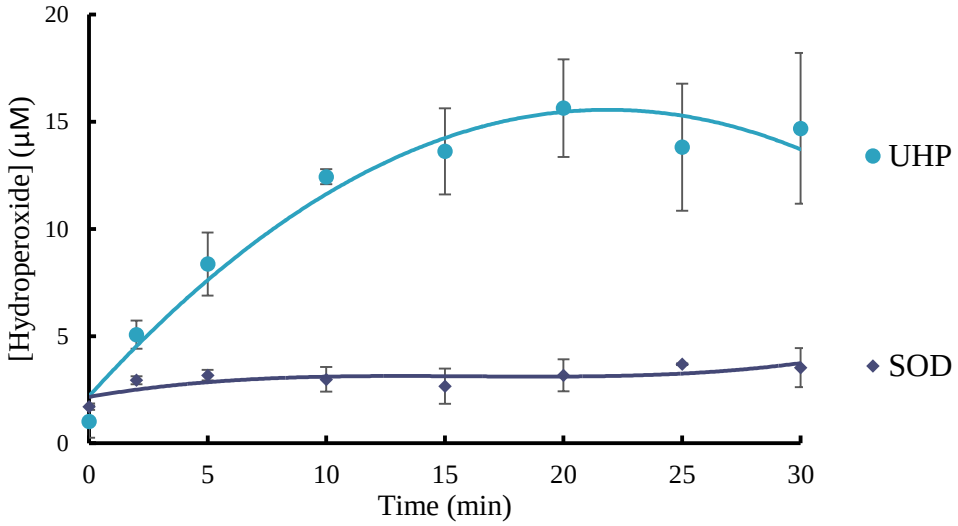

Figure 14: Kinetics of urate hydroperoxide formation measured with the FOX assay. At each time point, 220 µL of the reaction mixture was transferred into a cuvette with catalase and superoxide dismutase and performed the FOX assay. A reaction mixture with superoxide dismutase was also made and the same method was used to measure hydroperoxide concentration. This graph was the mean of three experiments. The error bars represented the standard deviation for three experiments.

The urate hydroperoxide concentration peaked at > 15 µM at 20 min (figure 14). The initial rate of urate hydroperoxide formation was approximately 3.2 $\mu M min^{-1}$. The maximum concentration of urate hydroperoxide formed and its subsequent degradation was variable between batches. When superoxide dismutase was added the hydroperoxide concentration remained constant at approximately 3 µM. This result supports that urate hydroperoxide was formed since it was superoxide-dependent. Future experiments used: 100 µM hypoxanthine, 400µM urate, 200 nM lactoperoxidase and 1.8 µM xanthine oxidase in 50 mM phosphate buffer with 20 min incubation. The reaction was stopped with 100 µg/mL catalase and 10 µg/mL superoxide dismutase.

2.4 Discussion

I successfully formed urate hydroperoxide with xanthine oxidase, lactoperoxidase and their substrates. Urate hydroperoxide formation was optimised by using a high concentration of hypoxanthine, xanthine oxidase and urate. I choose 100 µM hypoxanthine because the substrate inhibition of xanthine oxidase was minimal and this concentration had a high rate of superoxide. A high concentration of xanthine oxidase (1.8 µM) was used for the same reason. Increasing the concentration of urate > 100 µM did not affect urate hydroperoxide formation, but I choose to use 400 µM of this substance to match hyperuricemia. My optimised system formed > 15 µM urate hydroperoxide in 20 min.

The FOX assay was used to determine urate hydroperoxide concentration. I assumed that urate hydroperoxide oxidized Fe^{2+} at the same ratio as H_2O_2, and work by Patrício et al. (20) supports this assumption. The concentration of urate hydroperoxide was measured with iodine redox titration and the FOX assay and were found to be identical. Thus, the FOX assay accurately measures urate hydroperoxide concentration (20). Urate hydroperoxide concentration could not be measured photometrically because the xanthine oxidase/lactoperoxidase system produced many purine products, such as xanthine, urate and urate hydroperoxide, with overlapping spectrums at 310 nm (figure 11 A). Patrício et al. (20) calculated the extinction coefficient through riboflavin photooxidation, where the concentration of urate was constant and did not interfere.

Urate hydroperoxide was not an easy substance to form and use. The concentration of this oxidant was variable between batches and must be used immediately because it degrades quickly. Measurement of urate hydroperoxide with FOX assay, which requires 45 min to develop, hindered later experiments. The exact concentration of urate hydroperoxide was not known as I studied its reactivity. Thus, the concentration of urate hydroperoxide used to treat thiols in later chapters was not normalised. For future experiments, I hope to have the equipment to form urate hydroperoxide from photooxidation of riboflavin since it was shown to produce 300 µM urate hydroperoxide (20).

Chapter 3. Urate Hydroperoxide and Reduced Thiols

3.1 Introduction

Urate hydroperoxide depletion of thiols could be a secondary mechanism by which this oxidant promotes oxidative stress and inflammation. Thiols, also known as sulfhydryls, are essential functional groups for a range of reactions. The most important thiols in biology are cysteine and glutathione, which are responsible for building biomolecules and antioxidant protection (21, 24). Depletion or deficiency of these thiols is associated with cancer, sepsis, aging, impaired HIV survival, pulmonary and neurodegenerative disease (22, 122-125). In terms of inflammatory disease, lack of thiols exposes cells to oxidative stress and aggravates inflammation (126). This chapter explores the oxidation of cysteine and glutathione by urate hydroperoxide and discusses the implications for inflammation.

Cysteine, a thiol amino acid, is essential for protein structure and function. Two cysteine residues can form a disulfide bond to join secondary structure or monomers of proteins (24, 127). Cysteine is chemically diverse to enable enzyme catalysis. This thiol is capable of acting as a nucleophile and metal ion, proton, hydride and oxygen atom transfer (24). ATPase, protein tyrosine phosphatase and glycolytic enzymes use cysteine residues for catalysis (128). Cysteine is also a precursor for glutathione, coenzyme A and hydrogen sulfide synthesis (127). This thiol has antioxidant activity, though this is predominantly expressed through glutathione (129, 130). Depletion of cysteine will prevent synthesis of key biomolecules required for cell survival (127).

Glutathione, a thiol containing tripeptide, functions in protein and DNA synthesis, cell proliferation, reduction reactions, regulation of thiol-dependant enzymes, conjugation to toxins and antioxidant protection (21, 22). This thiol can scavenge hydroxyls, peroxyls and secondary radicals like hydroperoxides, dehydroascorbate and oxidized thiols (131). Glutathione's thiol bond is facile, thus it can donate a hydride to form a sulfur-centred radical, or a carbon-centred radical with hydroxyl radicals. The radicals dimerise via a disulfide bond to glutathione disulfide (21). Glutathione disulfide is only reduced by glutathione reductase, which poorly replenishes glutathione during oxidative stress (22). Loss of this antioxidant affects many metabolic pathways. Glutathione depletion promotes lipid peroxidation, DNA fragmentation, increased intracellular calcium and loss of antioxidant and conjugation capacity (21, 132-135). On a cellular scale, glutathione depletion leads to tissue damage and inflammatory recruitment (figure 15) (134, 136-139).

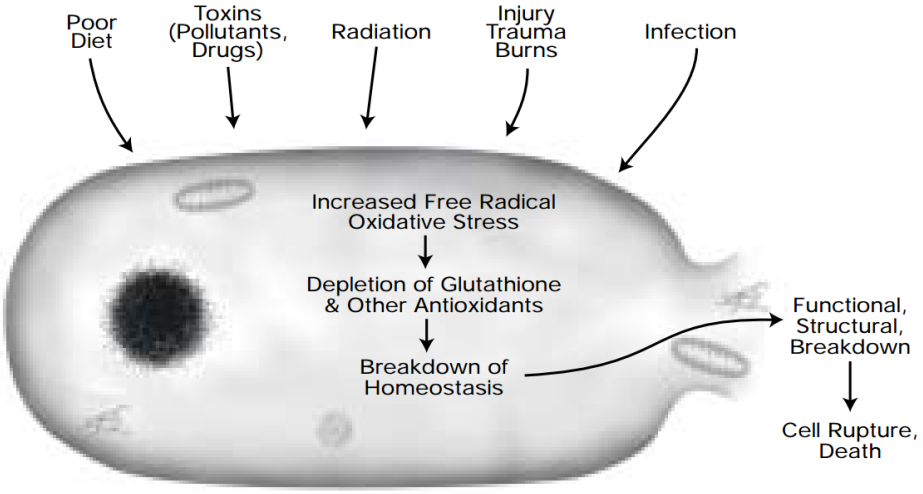

Figure 15: Consequences of glutathione depletion for a cell. Poor diet, toxins, radiation, traumatic burns and infection perpetuate oxidative stress. Oxidative stress depletes antioxidants like glutathione. Loss of antioxidant balance (homeostasis) leads to cell functional and structural breakdown and death. Figure adapted from: (136).

Patrício et al. (20) found that urate hydroperoxide oxidized glutathione at a 2:1 ratio with second order rate constant k = 13.7 ± 0.8 $M^{-1}s^{-1}$.Urate hydroperoxide did not form an adduct with either cysteine or glutathione. The aim of this chapter was to repeat these results for the oxidation of cysteine and glutathione. If urate hydroperoxide is formed at an inflammatory site, then I hypothesize it will oxidatively deplete cysteine and glutathione. The 5, 5'-dithiobis-(2-nitrobenzoic acid) (DTNB)/Ellman's assay will be used to quantify thiol oxidation by urate hydroperoxide and determine the stoichiometry. Depletion of cysteine and glutathione *in vivo* will have severe consequences for a cells antioxidant protection, enzyme catalysis and biomolecule synthesis (21, 24, 127). These implications could be a mechanism by which hyperuricemia leads to tissue damage during inflammatory disease.

I compared the effectiveness of urate hydroperoxide with fellow neutrophil oxidant taurine chloramine. Taurine chloramine is formed when hydrogen peroxide formed during neutrophil oxidative burst combines with amino acid taurine (140, 141). This oxidant is routinely used in our lab. Peskin and Winterbourn (142, 143) characterised taurine chloramine's oxidation of thiols and GAPDH.

3.2 Materials and Methods

3.2.1 Materials

Substances and solutions used throughout experimental work were put in table 3.

Table 3: Description of substances and solutions used to perform the DTNB assay and prepare taurine chloramine and thiols. The preparation and company sourced were described. Buffers were autoclaved before use.

Substance	Preparation	Company
Acetic acid	100% glacial	AnalaR, B10001-78
Bleach	The concentration was approximately 500 mM.	Janola premium bleach
Catalase-treated phosphate buffer	Phosphate buffer (50 mM) was treated with 10 µg/mL catalase.	
Cysteine hydrochloride	Stock of 1 mM dissolved fresh in phosphate buffer.	Sigma, 7477
L-Cystine	Stock of 1 mM dissolved fresh in phosphate buffer.	Sigma, C8755
Dimethylformamide (DMF)	Transfer of acid was made with glass pipette.	J.T. Baker, 9221-06
DTNB Reagent	DTNB was dissolved in phosphate buffer at 10 mM and ultrasonicated for 2 min. Stored in dark and made fresh. $\varepsilon(412) = 14{,}100\ M^{-1}cm^{-1}$ (144).	Sigma, D8130
Glutathione	Stock of 1 mM dissolved fresh in phosphate buffer	Sigma, G4251
Glutathione disulfide	Stock of 1 mM dissolved fresh in phosphate buffer	Sigma, G9027
Potassium iodide	Stock of 10 mM dissolved in MilliQ.	J.T. Baker, 3165
Sodium acetate	Stock of 400 mM dissolved in MilliQ, pH adjusted to 5.4 with acetic acid.	BHD, 102364Q
Taurine	10 mM dissolved in phosphate buffer, made fresh.	Sigma, T0625
Taurine Chloramine	Taurine (10 mM in phosphate buffer) and bleach were mixed at 10:1 molar ratio (142). Taurine chloramine was made fresh.	
3,3',5,5'-Tetramethylbenzidine (TMB)	Stock of 20 mM dissolved in 100% DMF.	Fluka, 87748
TMB Reagent	Stock of 2 mM TMB/DMF (row above) diluted in 100 µM potassium iodide and 400 mM sodium acetate buffer. This reagent was kept in the dark and made fresh every week.	
Urate hydroperoxide formed by the xanthine oxidase/lactoperoxidase system	In 50 mM phosphate buffer: 100 µM hypoxanthine, 400 µM urate, 200 nM lactoperoxidase and 1.8 µM xanthine oxidase. After 20 min the reaction was stopped with 100 µg/mL catalase and 10 µg/mL superoxide dismutase. This solution was used immediately quantified with the FOX assay and used for experiments.	
Urate hydroperoxide control solution	This was the xanthine oxidase/lactoperoxidase system without hypoxanthine. In phosphate buffer: 400 µM urate, 200 nM lactoperoxidase, 1.8 µM xanthine oxidase, 100 µg/mL catalase and 10 µg/mL superoxide dismutase.	

3.2.2 TMB Measurement of Taurine Chloramine

The TMB assay was used to quantify taurine chloramine (145). During this assay, chloramines oxidized colourless TMB to a blue product, which was photometrically measured at 645 nm. This reaction was catalysed by iodine. In a quartz cuvette, 20 µL of taurine chloramine solution (table 3) was diluted to 800 µL with phosphate buffer and was treated with 200 µL TMB reagent (table 3). The cuvette was incubated for 5 min then the absorbance was read at 645 nm on the Agilent spectrophotometer on standard mode. The concentration of taurine chloramine was determined with the Beer-Lambert law where: $\varepsilon_{(645)}$ = 30,000 $M^{-1}cm^{-1}$ (145). Taurine chloramine was diluted to 20 µM with phosphate buffer to be used experimentally.

3.2.3 DTNB Assay for Reduced Thiols

The DTNB assay was used to quantify reduced thiols. Colourless DTNB was reduced by reduced thiols to yellow thionitrobenzoate (TNB), which absorbs light at 412 nm (144). For the assay, 10 – 100 µM reduced thiol was transferred into a 1 mL plastic cuvette and was treated with 20 µM of 10 mM DTNB. Samples were made in triplicate. The cuvettes were incubated in the dark at room temperature for 10 min. The Agilent spectrophotometer was set to standard mode with manual measurement of fixed wavelength 412 nm. The spectrophotometer was blanked with 50 mM phosphate buffer and DTNB reagent before sample absorbance was read at 412 nm. The reduced thiol concentration was calculated with the DTNB extinction: $\varepsilon_{(412)}$ = 14,100 $M^{-1}cm^{-1}$ (144). Experiments with exposure of thiols to oxidants were performed with a discontinuous system, wherein the thiols and oxidants were prepared separately then combined. Thiols were diluted with phosphate buffer when the absorbance was above 1. Reduced thiol concentration was plotted against substance or concentration of oxidant.

3.2.3.1 Standard Curve and Controls

Standard curves were made for the DTNB assay of cysteine, glutathione, cystine and glutathione disulfide to determine the linearity and specificity of the assay for reduced thiols. A stock of 1 mM of the thiols was transferred into plastic cuvettes to achieve concentrations: 0 – 100 µM. The volume was made up to 980 µL with

phosphate buffer and the DTNB assay was performed (3.2.3). Absorbance at 412 nm was plotted vs. thiol concentration.

The DTNB assay was performed on the substances of the xanthine oxidase/lactoperoxidase system to determine their interference for later experiments. In plastic cuvettes, each substance was diluted to 980 µL with phosphate buffer. The final concentrations: 50 mM phosphate buffer, 78 µM hypoxanthine, 195 µM urate, 156 nM lactoperoxidase, 1.4 µM xanthine oxidase, 78 µg/mL catalase and 7.8 µg/mL superoxide dismutase. The substances of the xanthine oxidase/lactoperoxidase system were also transferred (780 µL) into plastic cuvettes with 200 µL of 350 µM cysteine or 150 µM glutathione. The DTNB assay was performed as previously described (3.2.3). The final concentration of substances was the same as section 3.2.3.2.

3.2.3.2 Depletion or Cysteine and Glutathione by Urate Hydroperoxide

Cysteine and glutathione were treated with urate hydroperoxide in a discontinuous system and the resulting reduced thiol concentration was measured with the DTNB assay. Samples were made for the xanthine oxidase/lactoperoxidase system with controls where each substance was removed or the addition of catalase and superoxide dismutase (Appendix 2, table 7). In these samples, urate hydroperoxide was allowed 20 min to form then catalase and superoxide dismutase were added to stop the reaction. Immediately after the reaction was stopped 780 µL of each sample was transferred into plastic cuvettes with 70 µM cysteine or 30 µM glutathione in triplicate. Cysteine and glutathione were diluted in 780 µL phosphate buffer to determine the untreated reduced thiol concentration. The DTNB assay was performed (3.2.3). The hydroperoxide concentrations of the xanthine oxidase/lactoperoxidase system samples were determined with FOX assay (2.2.4).

3.2.3.3 Dose-Dependent Depletion of Cysteine and Glutathione by Oxidants

The DTNB assay was performed on cysteine and glutathione treated with varying concentrations of taurine chloramine or urate hydroperoxide to determine the stoichiometry of reduced thiol depletion. Stock cysteine (125 µM) or glutathione (75 µM) were transferred into a plastic cuvette at 200 µL. The reduced thiols were then treated with varying volumes of 20 µM taurine chloramine (Appendix 2, table 8). This

experiment was also performed with urate hydroperoxide (2.3.3.3). Glutathione (200 µL of 150 µM) was dose-dependently treated with 12 µM urate hydroperoxide (Appendix 2, table 9). To account for interference by lactoperoxidase, a control solution was made with all the substances except hypoxanthine. The volume of the samples were equalled at 980 µL with phosphate buffer. The final concentrations of oxidants were 0 – 16 µM taurine chloramine and 0 – 9 µM urate hydroperoxide. Stock oxidant concentration was checked with the TMB (3.2.2) and FOX assay (2.2.3). The cuvettes were incubated for 10 min at room temperature and assayed with DTNB (3.2.3).

3.3 Results

3.3.1 DTNB Assay

I wanted to use the DTNB assay to quantify reduced thiol concentration and depletion with exposure to oxidants. A discontinuous system was used to treat cysteine and glutathione with oxidants. A standard curve was made for cysteine, glutathione, cystine and glutathione disulfide absorbance during the DTNB assay (Appendix 1, figure 34 A). Cysteine and glutathione linearly absorbed light at 412 nm, whereas the absorbance of the oxidized forms was negligible. Thus, the DTNB assay was exclusive to reduced form of these thiols. The reduced thiols were exposed to the individual substances of the xanthine oxidase/lactoperoxidase system and the resulting thiol concentration was measured (Appendix 1, figure 34 B and 35). Urate and lactoperoxidase deplete cysteine, thus interfered with the assay.

3.3.1.1 Reduced Thiol Depletion by Urate Hydroperoxide

In this experiment I sought to measure the effect of urate hydroperoxide on cysteine and glutathione. The DTNB assay was performed on these thiols following treatment with samples for the xanthine oxidase/lactoperoxidase system. The urate hydroperoxide concentration for the full system in both experiments was 10 µM.

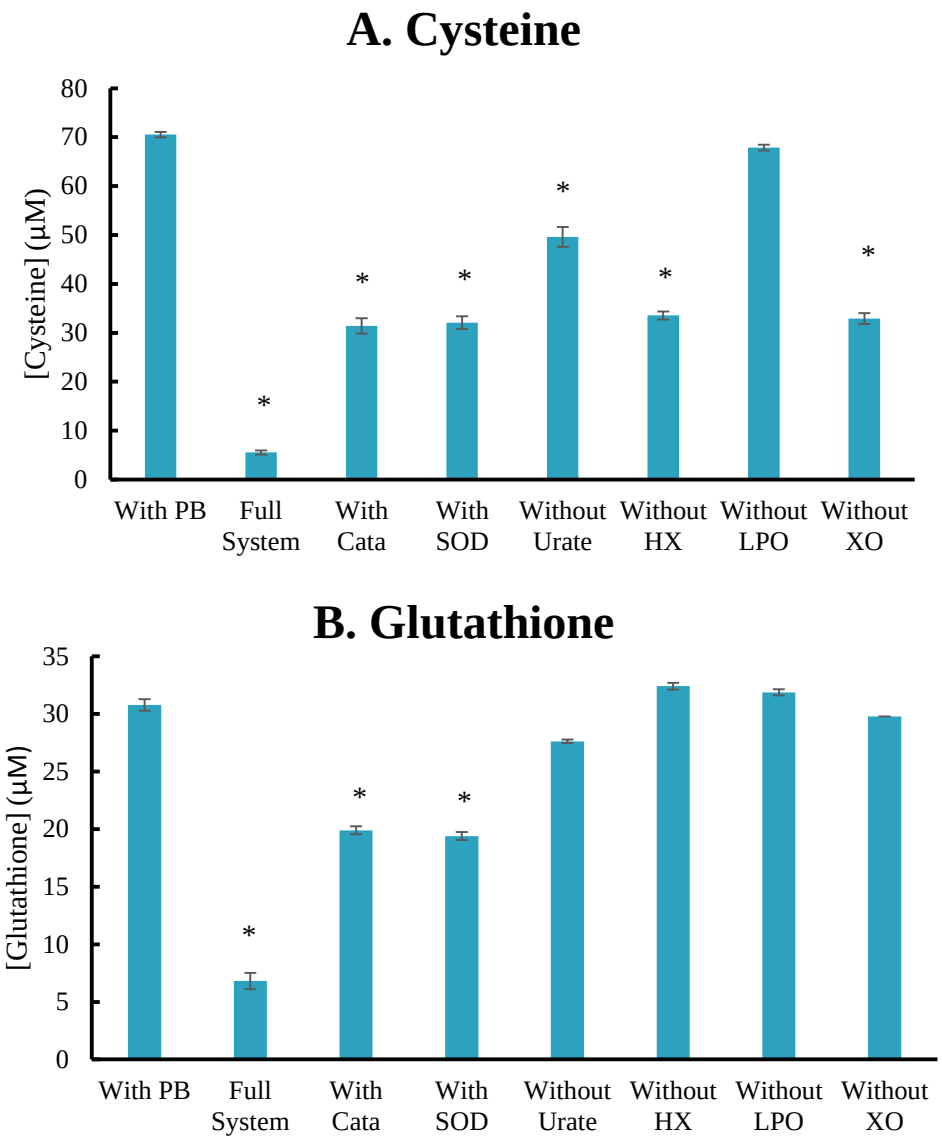

Figure 16: Depletion of free thiols by urate hydroperoxide. A. Depletion of cysteine by urate hydroperoxide. **B.** Depletion of glutathione by urate hydroperoxide. The xanthine oxidase/lactoperoxidase system was incubated with 70 µM cysteine 30 µM glutathione for 10 min and DTNB assay was performed. The hydroperoxide concentration of each sample (for both cysteine and glutathione) were 0, 12, 16.3, 3.2, 5.8, 2.8, 2.1 and 1.7 µM. Thus, when the baseline absorbance was removed, the urate hydroperoxide concentration of the full system was 10 µM. These graphs were representative of two experiments. The error bars represented the standard deviation of triplicate readings for one experiment. One-way ANOVA followed by Holm-Sidak multiple comparison on triplicate readings was used to identify samples that were significantly different from the phosphate buffer control (* $p < 0.05$).

When 70 µM cysteine was discontinuously exposed to urate hydroperoxide (full system) the reduced thiol concentration dropped to approximately 5 µM (figure 16 A). The addition of catalase and superoxide dismutase limited the reduced thiol depletion to approximately 30 µM. When hypoxanthine and xanthine oxidase were excluded from the system the concentration of cysteine dropped to 30 µM. When urate and

lactoperoxidase were excluded the reduced thiol concentration was close to the thiol concentration in phosphate buffer, 50 and 70 µM respectively. Thus, urate and lactoperoxidase depleted cysteine, as seen with the control experiment (Appendix 1, figure 35 A). It was clear that urate hydroperoxide (full system) depleted cysteine compare to the control (without hypoxanthine), however the sole effect of urate hydroperoxide was obscure. Dose-dependent depletion of cysteine by urate hydroperoxide was not performed because the interference by urate and lactoperoxidase were too strong and inconsistent.

When approximately 30 µM glutathione was exposed to urate hydroperoxide the reduced thiol concentration dropped to approximately 7 µM (full system, figure 16 B). The addition of catalase and superoxide dismutase limited the depletion to approximately 20 µM. The control solutions without urate and xanthine oxidase had similar glutathione concentrations as the phosphate buffer control. There was a small increase in reduced thiol concentration when hypoxanthine and lactoperoxidase were left out of the system. This was most likely interference by catalase. Formation of urate hydroperoxide depleted glutathione (full system) compared to the control (without hypoxanthine).

3.3.1.2 Dose-Dependent Depletion of Reduced Thiols by Taurine Chloramine

I sought to determine the stoichiometry of cysteine and glutathione depletion by taurine chloramine. These thiols were dose-dependently exposed to taurine chloramine and the resulting reduced thiol concentration was measured with DTNB. Approximately 25 or 15 µM cysteine or glutathione was exposed to 0 – 13 µM taurine chloramine.

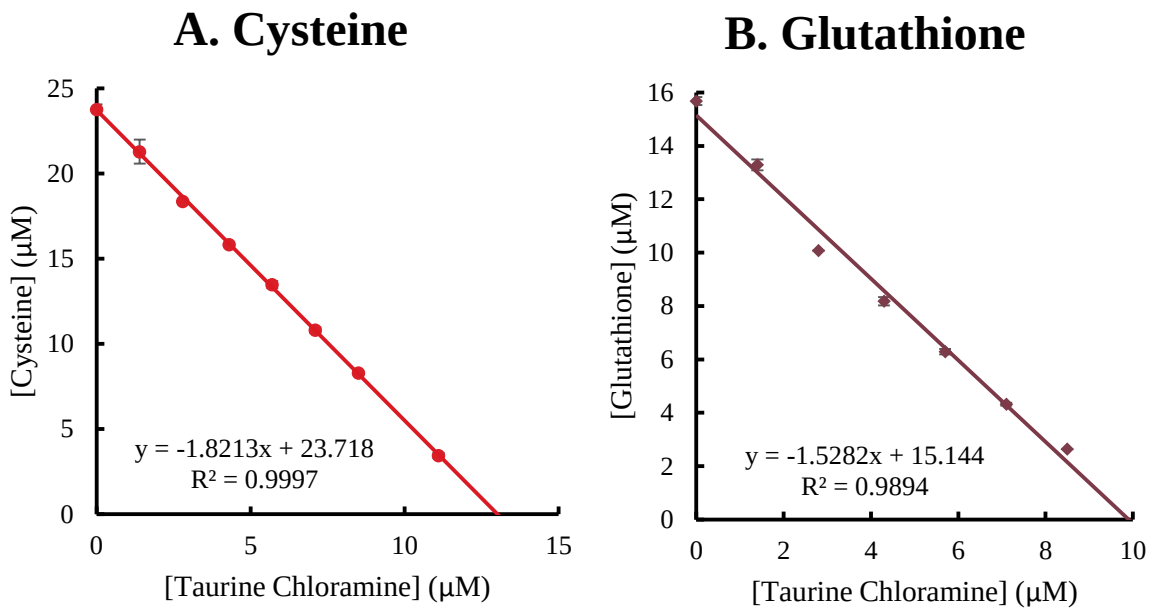

Figure 17: Exposure of free thiols to dose-dependent taurine chloramine. **A.** Dose-dependent depletion of cysteine by taurine chloramine. **B.** Dose-dependent depletion of glutathione by taurine chloramine. The taurine chloramine treatment was varied by exposing the thiols to different volumes of a 20 µM stock. The absorbance of taurine chloramine at 412 nm when treated with DTNB was negligible. These graphs were representative of three experiments. The error bars represented the standard deviation of triplicate readings from one experiment.

Taurine chloramine reaction with cysteine or glutathione resulted in a linear loss of absorbance at 412 nm as the thiols were oxidized (figure 17). The stoichiometry for the depletion of cysteine by taurine chloramine was 2:1, whereas glutathione depletion by taurine chloramine was 3:2 ratio. These ratios were close to 2:1 and imply that taurine chloramine dimerised reduced thiols. Thus, one taurine chloramine depleted two reduced thiols. These results were similar to Peskin and Winterbourn (142), who determined the stoichiometry of thiol oxidation to be 2.1:1 for cysteine and 1.8:1 for glutathione with taurine chloramine.

3.3.1.3 Dose-Dependent Depletion of Glutathione by Urate Hydroperoxide

Glutathione was exposed to urate hydroperoxide in a dose-dependent manner to determine the stoichiometry of its oxidation. Approximately 25 µM glutathione was treated with 0 – 10 µM urate hydroperoxide. The resulting thiol concentration was measured with the DTNB assay.

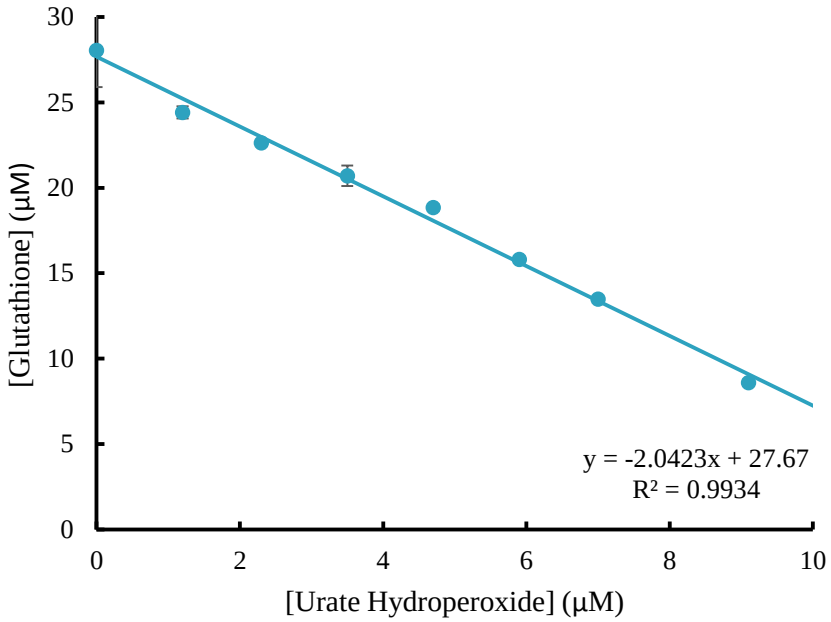

Figure 18: Dose-dependent depletion of glutathione by urate hydroperoxide. Glutathione was incubated with increasing concentrations urate hydroperoxide. This graph was representative of two experiments. The error bars represented the standard deviation for triplicate readings for one experiment.

Urate hydroperoxide linearly depleted glutathione (figure 18). The stoichiometry of glutathione oxidation by urate hydroperoxide was 2:1. This ratio was identical to results by Patrício et al. (20) and taurine chloramine depletion of reduced thiols (figure 17). This ratio implies a urate hydroperoxide molecule oxidises glutathione to glutathione disulfide, thus depleting two reduced thiols.

3.4 Discussion

The depletion of reduced thiols by taurine chloramine and urate hydroperoxide was measured through loss of DTNB absorbance at 412 nm. Lactoperoxidase interfered with the depletion of cysteine by urate hydroperoxide, but it was apparent from Figure 16 A. that urate hydroperoxide oxidises this amino acid. Lactoperoxidase and urate seem to deplete cysteine (figure 16 A and 35 A). Cysteine could bind lactoperoxidase in the absence of hydrogen peroxide, then enter the peroxidase cycle to be oxidized to cystine (146-149). Cysteine has antioxidant properties and may scavenge oxidized urate (74). This result was consistent with previous work by Kuzkaya et al. (74), wherein urate's antioxidant capacity was extended by the presence of cysteine to reduce the urate radical.

Glutathione was depleted by urate hydroperoxide at ratio 2:1. This ratio suggests glutathione passed a hydride to urate hydroperoxide and dimerised to glutathione disulfide. Thus, urate hydroperoxide did not form an adduct to the thiol. Patrício et al. (20) published mass spectrometry data with the same ratio for glutathione depletion by this oxidant. Together, this was strong evidence that urate hydroperoxide oxidises glutathione to glutathione disulfide. Lactoperoxidase marginally depleted glutathione, thus it was unlikely to enter this enzyme's peroxidase cycle (figure 16 B and 35 B). Steric hindrance by the glycine and glutamate side-chains may have prevented oxidation by lactoperoxidase (150).

Cysteine is an essential building block for biomolecules, thus urate hydroperoxide depletion of this molecule will affect anabolism of the cell. Dose-dependent depletion of cysteine by urate hydroperoxide could be performed with the riboflavin photooxidation system to bypasses interference by lactoperoxidase. My findings could be expanded to other important thiol-containing compounds such as cysteine analogue, homocysteine; or glutathione precursor, cysteinylglycine (151). Also, the glutathione to glutathione disulfide ratio could be measured for cells exposed to urate hydroperoxide. Mass spectrometry should be performed on cysteine and glutathione treated with urate hydroperoxide to confirm that this oxidant did not form an adduct to cysteine or glutathione.

Urate hydroperoxide will deplete cysteine at inflammatory sites, hence starving the surrounding cells of this essential amino acid. Serum cysteine is mainly protein-bound or oxidized; the concentration of free cysteine is only 10 μM (151). Therefore, urate hydroperoxide may have a more significant effect on protein-bound cysteine used by enzymes for catalysis. Urate hydroperoxide formation will aggravate oxidative stress by depleting antioxidants like glutathione, leading to exposure of the cell to oxidants and toxins. However, glutathione is a minor antioxidant in blood serum and is present at 4 μM (151). For urate hydroperoxide to affect the glutathione pool it must be uptaken into cells where the concentration is up to 10 mM (152). Urate hydroperoxide is unlikely to achieve concentrations of 5 mM to deplete this pool, hence it must work in conjunction with other oxidants. We would expect oxidants to be abundant during oxidative stress induced by hyperuricemia.

Chapter 4. Urate Hydroperoxide and Glyceraldehyde-3-Phosphate Dehydrogenase

4.1 Introduction

Inactivation of thiol-dependent enzymes by urate hydroperoxide could be the link between hyperuricemia and inflammatory disease. Enzymes that rely on a cysteine residue for catalysis, or thiol-dependent enzymes, are ubiquitous in biology (24). Catalytic cysteines are powerful soft nucleophiles with highly polarizable empty d-orbitals. They are often paired with a histidine residue, which lowers the pKa of cysteine from 8.3 to 2.5 – 8 (153, 154). These attributes make catalytic cysteines vulnerable to electrophilic oxidants like urate hydroperoxide (154, 155). Oxidation of catalytic cysteines inactivates the enzyme (23, 153). Metabolic pathways affected by thiol-dependent enzyme inactivation include glycolysis, electron transport, oxidative signalling and glutathione metabolism. These pathways are essential for cell function, therefore cell survival may be affected by electrophilic oxidants (24). The aim of this chapter is to determine whether urate hydroperoxide inactivates a thiol-dependent enzyme and the resulting modification. I used GAPDH as a model for thiol-dependent enzymes.

GAPDH catalyses the sixth step of glycolysis and is essential for the function of all cells (29). This enzyme also functions in cell proliferation, oxidative signalling, apoptosis, membrane transport, cytoskeleton dynamics, DNA replication and repair (29, 156, 157). GAPDH catalyses the addition of an inorganic phosphate to GAP using cofactor oxidized nicotinamide adenine dinucleotide (NAD^+), the products are 1,3-bisphosphoglycerate (BPG) and reduced nicotinamide adenine dinucleotide (NADH). The mechanism for catalysis is hydride transfer from GAP to NAD^+, in which the catalytic cysteine (Cys149) forms a covalent bond to GAP (158-162) (figure 19). GAPDH inactivation uncouples oxidation and phosphorylation during glycolysis, preventing the production of ATP and leading to cell death (27, 163). Loss of function for this enzyme has repercussions for breakdown of glucose for energy (29).

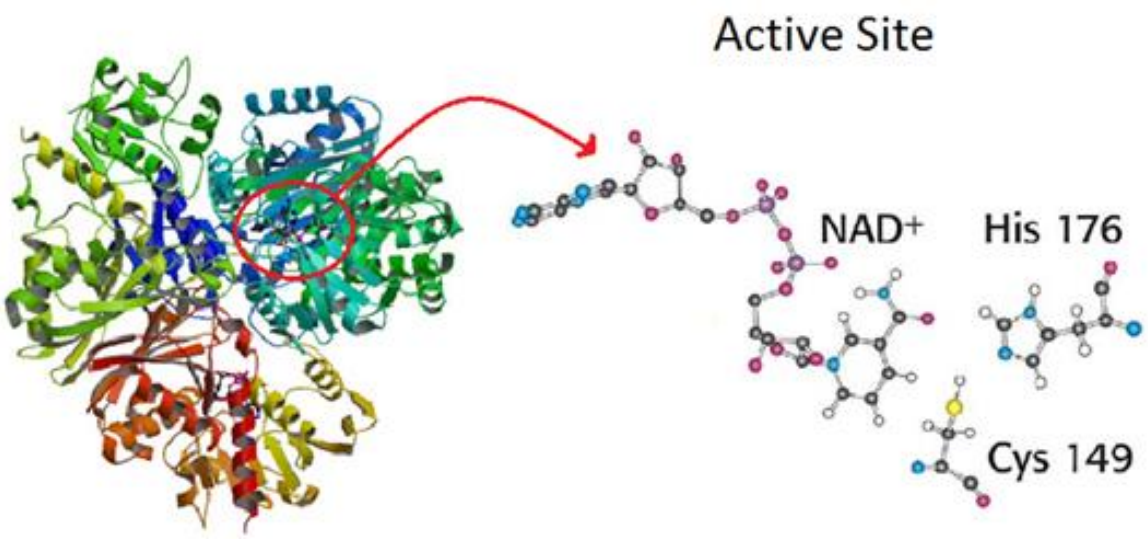

Figure 19: Crystal structure and active site configuration of rabbit muscle GAPDH. This enzyme is a homotetramer with the active site is a NAD-binding Rossman fold domain. The essential cysteine is positioned to covalently bind GAP. His176 transfers a hydride from the intermediate to NAD^+, producing NADH. Figure adapted from (28).

The essential GAPDH thiol can undergo a number of modifications, following oxidant exposure, resulting in inactivation (figure 20). Cys149 is consecutively oxidized to sulfenic, sulfinic and sulfonic acid. Sulfenic acid is highly reactive and forms a disulfide bond between Cys149 and Cys153 in rabbit muscle GAPDH, or mixed a disulfide bond with other thiol molecules (27, 143). Though, it is debatable whether Cys149 and Cys153 are close enough to form a disulfide bond (27, 162). This modification is reversible with reduction by glutathione. Sulfinic acid is stable and is solely removed by sulfiredoxin, whether this occurs *in vivo* is unclear (164). Sulfonic acid is the final state of overoxidation and is essentially irreversible (23). Oxidants and alkylating agents form adducts to Cys149, resulting in permanent loss of activity (26, 165).

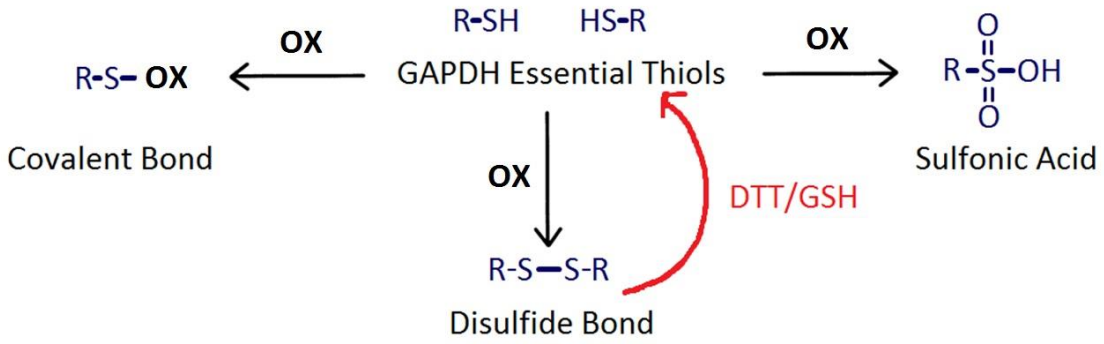

Figure 20: Modifications of the GAPDH essential thiol formed during inactivation by oxidants. Cys149 can form a disulfide bond with an adjacent cysteine reside (Cys153). This modification is made by taurine chloramine and is reversible by dithiothreitol (DTT)/glutathione. Cys149 can be overoxidized to sulfenic, sulfinic or sulfonic acid. Formation of sulfonic acid is irreversible *in vivo*. Oxidants or alkylating agents can form irreversible adducts to Cys149. Figure adapted from (27).

Urate hydroperoxide inactivation of thiol-dependent enzymes may link hyperuricemia and tissue damage during inflammatory disease. I hypothesize that urate hydroperoxide inactivates the thiol-dependent enzyme GAPDH and oxidises its cysteine residues. My basis for this hypothesis is that electrophilic oxidants induce modifications to thiol-dependent enzymes (24). As a hydroperoxide, urate hydroperoxide is a highly reactive oxidant (20). GAPDH was chosen as a model for thiol-dependent enzymes because it is an abundant and essential enzyme in all cells. I aim to determine the concentration of urate hydroperoxide that was required to inactivate GAPDH, whether inactivation was reversible and the structural modification that occurred.

4.2 Materials and Methods

4.2.1 Materials

Substances and solutions used throughout experimental work were put in table 4.

Table 4: Description of substances and solutions used to perform the GAPDH assay, gel electrophoresis and mass spectrometry. The preparation and company sourced were described. Buffers were autoclaved before use.

Substance	Preparation	Company
4% Acrylamide stacking gel	In MilliQ: 4% Acrylamide/bis, 0.6 M Tris HCl (pH 8.8), 0.1% SDS, 0.05% APS and 0.16% TEMED.	
15% Acrylamide resolving gel	In 0.6 M Tris HCl (pH 8.8): 25% Acrylamide/bis, 0.15% SDS, 0.08% APS, 0.2% TEMED.	
40% Acrylamide/bis solution	Acrylamide to Bis = 37.5:15	BioRad, 1610148
Ammonium persulfate (APS)	Stock of 10% (w/v) dissolved in MilliQ.	Sigma, A3678
Ammonium Bicarbonate		
Bio-gel polyacrylamide beads	Bio-gel P-6DG desalting gel, 990-180 µM.	BioRad, 150-0738
Bromophenol blue		Sigma, B1131
DL-dithiothreitol (DTT)	0.1 M was dissolved in 50 mM phosphate buffer. For SDS-PAGE used 1 M DTT.	Sigma, D9779
Electrode buffer	In MilliQ: 25 mM Tris, 192 mM glycine, 0.1% SDS, pH adjusted to 8.3.	
Formic acid		Merck, 1.00263.100
GAP	Diluted from 45 mg/mL to 10 mM in phosphate buffer.	Sigma, G-5251
Glycerol		Sigma, G5516
Glycine (Gly)		Sigma, G8898
β-mercaptoethanol		Sigma, 63699
NAD^+	Stock of 10 mM dissolved in phosphate buffer.	Sigma, N-7004
NADH	Stock of 1 mM dissolved in phosphate buffer.	Sigma, N8129
Protein Standard Dual Colour	Protein ladder for SDS-PAGE.	Precision Plus, #16103744110029
Rabbit Muscle GAPDH	Dissolved in 50 mM TEA buffer, ε(280) = 149 $mM^{-1}cm^{-1}$ (166).	ICN Biomedical Inc., [9001-50-7]
Sodium dodecyl sulfate (SDS)		Fisher Science, SP53053
Solvent A (mobile phase)	In MilliQ: 0.1% formic acid	
Solvent B (mobile phase)	In acetonitrile: 0.1% formic acid	
Tetramethylethylenediamine (TEMED)		Sigma, T9281
Triethanolamine (TEA)		BDH, 103704U
TEA buffer	In MilliQ: 50 mM TEA and 50 mM NaH_2PO_4 anhydrous, pH adjusted to 8.5 with HCl.	
Tris(hydroxymethyl)aminomethane-HCl (Tris-HCl)		Roche, 10708976001
Sample Buffer for sodium dodecyl sulfate-polyacrylamide gel electrophoresis (SDS-PAGE)	In MilliQ: 60 mM Tris-HCl (pH 6.8), 20% (v/v) glycerol, 2% (v/v) SDS, 5% (v/v) β-mercaptoethanol and 0.25 M bromophenol blue.	

4.2.2 GAPDH Assay

The GAPDH assay was used to assess the enzymes activity after various treatments. This assay exposed GAPDH to its substrates and measured the formation of NADH at 340 nm. This method was optimised from Seidler (167). The assay was performed with a Hitachi spectrophotometer and 1 mL quartz cuvette. The spectrophotometer was set to measure -0.1 – 1 absorbance at 340 nm for 300 sec, spectral band width = 2 at 25ºC. The assay required approximately 60 nM GAPDH, 0.5 mM GAP, 1 mM NAD^+ and 50 µM DTPA, dissolved in 1 mL TEA buffer. The spectrophotometer was blanked with all substances except GAPDH, which initiated the assay. The initial rate of GAPDH activity was calculated as $A.min^{-1}$ over 10 – 50 sec. GAPDH activity was expressed as a percent by designating GAPDH diluted in phosphate buffer as 100% activity. Graphs were plotted for GAPDH activity (%) vs. substance or concentration of oxidant.

4.2.2.1 Optimising the GAPDH Assay

The concentration of NAD^+ and DTT used during the GAPDH assay was optimised to achieve high activity ($A.min^{-1}$). GAPDH activity was assayed over a number of concentrations of NAD^+ to determine the saturation concentration for this substrate. The concentration of NAD^+ was varied by diluting a10 mM stock of in phosphate buffer to make a dilution series. Each dilution (100 µL) was transferred into the assay cuvette (with 2 mM DTT) to achieve final concentrations 0 – 1.4 µM. Next the concentration of DTT required to activate the enzyme was determined. The concentration of DTT was high enough to reduce the enzyme yet easily removed with spin columns. Stock DTT (100 mM) was added at different volumes to the assay cuvette to achieve final concentrations 0 – 7.5 mM. The other substances of the assay were diluted in TEA buffer and the assay was performed (4.2.2).

The linearity of GAPDH activity with concentration was determined by creating a standard curve. GAPDH (25 µM) was diluted in TEA buffer. The concentration of GAPDH in the cuvette was 0 – 400 nM.

4.2.2.2 Preparation of Reduced GAPDH with Spin Columns

GAPDH was isolated from DTT with spin columns to allow treatment of the enzyme with oxidants in later experiments. GAPDH was reduced with 2 mM DTT for

30 min. Mini-Bio-Spin® chromatography columns were prepared by adding 700 µL wet Bio-Gel polyacrylamide and allowing excess liquid to flow through. Columns were washed four times with MilliQ and once with TEA buffer. The columns were packed by centrifugation at 1000 g for 2 min. GAPDH and DTT samples were injected on top of each column at a maximum volume of 75 µL. The columns were centrifuged at 1000 g for 4 min to elute GAPDH.

The effectiveness of spin column isolation was assessed by measuring concentration and activity for each step of GAPDH reduction and isolation (Initial, addition of DTT and isolation with spin columns). The assay cuvette did not have additional DTT (4.2.2).

4.2.3 NAD^+ and NADH Photometry

The purpose of this experiment was to determine whether taurine chloramine or urate hydroperoxide oxidised NAD^+ or NADH, thus creating interference with the GAPDH assay. NAD^+ absorbed light at 260 nm while NADH absorbed at 260 and 340 nm (168). Photometric measurement at 340 nm was used to show the formation or depletion of NADH. The Agilent spectrophotometer was blanked with phosphate buffer in a 1 mL quartz cuvette. The buffer was replaced with the NAD solution dissolved in phosphate buffer and triplicate readings were made. The extinction coefficients were: $\varepsilon_{(260)}$ = 18,000 $M^{-1}cm^{-1}$ and $\varepsilon_{(340)}$ = 6,220 $M^{-1}cm^{-1}$ (168). NAD concentration was plotted vs. concentration of oxidant.

Standard curves were made for NAD^+ and NADH absorbance at 260 and 340 nm. NAD^+ or NADH (10 mM) was diluted with phosphate buffer to make a dilution series. The NAD dilutions (100 µL) were added to 900 µL phosphate buffer and the absorbance at 260 and 340 nm was measured for both oxidation states. The final concentrations for NAD^+ and NADH were 0 – 20 and 0 – 150 µM respectively.

4.2.3.1 Dose-Dependent Treatment of NAD^+ and NADH with Oxidants

The oxidation state of NAD was photometrically measured following dose-dependent treatment with oxidants. NAD^+ and NADH were exposed to varying volumes of taurine chloramine or urate hydroperoxide and incubated for 10 min at room temperature. Samples were transferred into a 100 µL quartz cuvette. The absorbance

was read at 260 and 340 nm, having blanked the Agilent spectrophotometer with the same concentration of oxidant (4.2.3).

In Eppendorf tubes, NAD^+ (25 µL of 80 µM) was exposed to varying volumes of 30 µM taurine chloramine and the volume was equalled at 375 µL with phosphate buffer. The final concentrations of taurine chloramine were 0 – 28 µM. NADH (40 µM) was treated with 0 – 159 µM taurine chloramine. The same method was used to dose-dependently treat NAD with urate hydroperoxide. NAD^+ (40 µL of 60 µM) and NADH (40 µM) were treated with varying volumes of 8 µM urate hydroperoxide (2.3.3.3). Samples were made up to 600 µL with phosphate buffer. The final urate hydroperoxide concentrations were 0 – 3.8 µM or 0 – 7 µM. Due to interference by the xanthine oxidase/lactoperoxidase system, only samples with the five lowest concentrations of urate hydroperoxide could be read.

4.2.4 Continuous Inactivation of GAPDH by Urate Hydroperoxide

The GAPDH assay was combined with the xanthine oxidase system in a quartz cuvette and the GAPDH activity was assayed. This was a continuous system where urate hydroperoxide was formed as GAPDH activity was assayed at 340 nm (4.2.2). Samples were made in triplicate to represent the full xanthine oxidase/lactoperoxidase system, removal of a substance or addition of quenchers (Appendix 2, table 10). The final concentration of the xanthine oxidase/lactoperoxidase system were 100 µM hypoxanthine, 250 µM urate, 200 nM lactoperoxidase and 1.8 µM xanthine oxidase. All samples had 60 nM GAPDH (DTT-reduced), 0.5 mM GAP, 1 mM NAD^+ and 50 µM DTPA in 1 mL TEA buffer. The spectrophotometer was blanked before the addition of xanthine oxidase and GAPDH as initiators for the two systems. As a control, the substances used to assay GAPDH activity were diluted in TEA buffer to represent 100% GAPDH activity.

The raw data (absorbance vs. time) for one replicate per sample was collated as a graph. The GAPDH activity for each triplicate was calculated for time periods: 30 – 60, 60 – 120, 120 – 180, 180 – 240 and 240 – 360 sec. These rates were plotted at time points 45, 90, 150, 210 and 270 sec vs. percent GAPDH activity.

4.2.5 Discontinuous Inactivation of GAPDH by Oxidants

A discontinuous system was used to measure the inactivation of GAPDH by taurine chloramine or urate hydroperoxide. GAPDH and the oxidants were prepared separately and mixed together in Eppendorf tubes as samples. GAPDH was reduced and isolated with a spin column at a high concentration (10 µM) and diluted 10 times in the samples with the oxidant. This experimental design allowed a maximum concentration of oxidant in the samples whilst the GAPDH concentration was constant with measurable activity.

4.2.5.1 GAPDH Inactivation by Urate Hydroperoxide

GAPDH was treated with the substances of the xanthine oxidase/lactoperoxidase system and assayed for change in enzyme activity. The final concentrations were the same as later experiments for inactivation of GAPDH by urate hydroperoxide (next paragraph). Each substance of the xanthine oxidase/lactoperoxidase system was diluted in 180 µL phosphate buffer. The concentrations were: 100 µM hypoxanthine, 400 µM urate, 200 nM lactoperoxidase, 1.8 µM xanthine oxidase or 50 mM phosphate buffer. Next, 20 µL of 10 µM GAPDH was added to each solution. After 10 min incubation the GAPDH activity for each sample was measured (4.2.2).

Xanthine oxidase/lactoperoxidase system samples (Appendix 2, table 11) were made in Eppendorf tubes. After 20 min incubation, having stopped the reaction with the quenchers, the hydroperoxide concentration was measured with the FOX assay. GAPDH (1 µM) was treated with 180 µL of each sample. After 10 min incubation GAPDH activity was assayed. A control was made with 1 µM GAPDH diluted in catalase-treated phosphate buffer to represent the active enzyme. The final concentration of substances were approximately 80 µM hypoxanthine, 330 µM urate, 160 nM lactoperoxidase, 1.5 µM xanthine oxidase, 80 µg/mL catalase (160 µg/mL for G.) and 8 µg/mL superoxide dismutase (16 µg/mL for F.).

4.2.5.2 Dose-Dependent Inactivation of GAPDH by Oxidants

The GAPDH assay was used to assess the effect of oxidants on enzyme activity. GAPDH (20 µl of 10 µM) was treated with a varying volume of 20 µM taurine chloramine or 7 µM urate hydroperoxide. Catalase-treated phosphate buffer was added to equal the volume of samples at 200 µL. The final concentration of oxidants were 0 –

16 µM taurine chloramine or 0 – 6 µM urate hydroperoxide (2.3.3.3). Samples were incubated at room temperature for 10 min and assayed for GAPDH activity (4.2.2). The stock concentrations of taurine chloramine and urate hydroperoxide were confirmed with the TMB (3.2.2) and FOX (2.2.4) assay respectively.

4.2.6 Inactivation Kinetics for GAPDH

The GAPDH assay was performed at various time points during discontinuous inactivation by oxidants. GAPDH was exposed to the oxidant in an Eppendorf tube and at set time points this solution was injected into the spectrophotometer and assayed for GAPDH activity. Three cuvettes were prepared in the Hitachi spectrophotometer with all the substances for the GAPDH assay, bar GAPDH. The spectrophotometer measured 340 nm throughout the experiment. In an Eppendorf tube, 20 µl of 10 µM GAPDH was combined with 180 µL of the oxidant and the stopwatch was immediately started. At three given time points, 60 µL of the sample was injected into a quartz cuvette. Four samples were made with staggered time points. The time points for a given sample were at least 45 sec apart to allow a linear slope to be made. Time points for samples:

1. 10, 60, 100 sec
2. 20, 75, 120 sec
3. 30, 90, 170 sec
4. 45, 140, 200 sec

The kinetics experiment was repeated three times for each oxidant. GAPDH activity (%) was plotted vs. time.

GAPDH (20 µL of 10 µM) was mixed with 180 µL of 20 µM taurine chloramine or 3 µM urate hydroperoxide. Taurine chloramine degrades slowly at room temperature, thus its concentration was similar for all the time points. Urate hydroperoxide degrades quickly, hence each sample was made from a new urate hydroperoxide solution. This increased the variability in the experiment because the urate hydroperoxide concentration was not identical per sample.

4.2.7 Reactivation of GAPDH Following Dose-Dependent Inactivation by Oxidants

This experiment assayed the reversibility of GAPDH inactivation by oxidants by reactivating the enzyme with DTT. Two sets of samples were made to represent before and

after inactivated GAPDH was exposed to DTT. Both samples sets were dose-dependently exposed to oxidants (4.2.5.2). One sample was exposed to catalase-treated phosphate buffer and served as a control to measure GAPDH inactivation. The second sample set was reduced with 2 mM DTT. All samples had a uniform concentration of substances.

GAPDH (1 µM) was dose-dependently exposed to 20 µM taurine chloramine (Appendix 2, table 12) or 7 µM urate hydroperoxide (Appendix 2, table 13). After 10 min incubation, the samples sets were either treated with DTT (2 mM) or diluted with catalase-treated phosphate buffer. Samples were incubated for 30 min before measuring the GAPDH activity. The final concentrations of oxidants were 0 – 18 µM taurine chloramine or 1 – 6 µM urate hydroperoxide. GAPDH was diluted in catalase-treated phosphate buffer and reduced with DTT to represent 100% GAPDH activity. GAPDH activity (%) was plotted against oxidant concentration for inactivate and reactivated samples.

4.2.8 DTNB Measurement of Cysteine Residues on GAPDH

The DTNB assay was used to measure depletion of cysteine residues on GAPDH by oxidants. This assay was modified to measure reduced thiol concentration in quartz cuvettes (162). GAPDH was reduced with DTT for 30 min and passed through spin columns twice to isolate GAPDH (4.2.2.2). The 380 µL samples were treated with 20 µL of 10 mM DTNB reagent and incubated for approximately 10 min in the dark. The Agilent spectrophotometer was blanked with TEA buffer treated with DTNB reagent. The assay solution was transferred into a 100 µL quartz cuvette and the absorbance was read at 412 nm on an Agilent spectrophotometer as previously described (3.2.3). The reduced thiol concentration was calculated with the DTNB extinction coefficient and plotted against substance or oxidant concentration.

A standard curve was made by varying the concentration of GAPDH exposed to DTNB. A stock of 1 µM GAPDH was diluted to 0 – 1200 nM with TEA buffer to make a dilution series. GAPDH (3 µM) was also treated with the substances of the xanthine oxidase/lactoperoxidase system to determine their interference with the assay. The final concentrations were the same as section 4.2.8.1: 50 mM phosphate buffer, 90 µM hypoxanthine, 360 µM urate, 190 nM lactoperoxidase, 1.7 µM xanthine oxidase, 95 µg/mL catalase and 9.5 µg/mL superoxide dismutase. After 10 min incubation the DTNB assay was performed.

4.2.8.1 Dose-Dependent Depletion of Cysteine Residues on GAPDH by Oxidants

The DTNB assay was used to measure the concentration of cysteine residues on GAPDH following dose-dependent exposure to oxidants (4.2.8). GAPDH (3 µM) was treated with varying volumes of 20 µM taurine chloramine or 9 µM urate hydroperoxide (2.3.3.3) discontinuously. The volume was made up to 190 µL with phosphate buffer. After 10 min incubation the DTNB assay was performed (4.2.8). The stock oxidant concentrations were determined with the TMB (3.2.2) and FOX assay (2.2.4).

4.2.9 Polyacrylamide Gel Electrophoresis

Laemmli-SDS-PAGE was performed to separate and visualise GAPDH and the xanthine oxidase/lactoperoxidase system (169). SDS-PAGE involved the movement of proteins through a polyacrylamide gel matrix with the applied electrical current. Proteins were separated by mass and charge, with small proteins travelling faster through the matrix. SDS, an anionic detergent, was used to promote the movement of the protein with the charge. Proteins were treated with coomassie brilliant blue, which stains proteins blue (170).

Two stacking gels were made from a 15% acrylamide resolving gel and 4% stacking gel. The composition of the gels was given in table 4. The resolving gel was poured first and was dried at room temperature for 20 min. The stacking gel was poured on top and wells were created with a comb. The following samples were made to 100 µM using a discontinuous system as previously described. The final concentration of substances were 1.5 µM GAPDH and 0 – 10.5 µM urate hydroperoxide (2.3.3.3).

1. Protein marker (Precision Plus protein standards dual colour)
2. GAPDH
3. Urate hydroperoxide
4. 1:1 GAPDH and urate hydroperoxide
5. 2:7 GAPDH and urate hydroperoxide
6. 1:7 GAPDH and urate hydroperoxide

For the non-reducing gel, 20 µL of each sample was transferred into an Eppendorf tube with 2.5 µL phosphate buffer and 5 µL non-reducing sample buffer. For the reducing gel, the phosphate buffer was replaced with 2.5 µL of 1 M DTT. Samples (28 µL) were injected into the following wells of the gel: well 4 – sample 1, well 5 – sample 2, well 6 –

sample 3, well 7 – sample 4 and well 8 – sample 5. The protein marker Precision Plus protein Standards Dual Colour was injected (3 µM) into well 3. The gel tanks were filled with Tris-Gly, pH 8.3 electrode buffer and ran for 60 min at 200 V. A BioRad gel dock (universal hood 11-S.N.765/00260) was used to visualise the protein. Documentation was performed with Quality One Chemidoc XRS (version 4.6.1.build 05). The gels where exposed to light for 500 sec and an image was taken.

4.2.10 GAPDH Mass Spectrometry

Whole protein mass spectrometry was performed on samples of GAPDH treated with urate hydroperoxide (2.3.3.3) and/or DTT in a discontinuous system. This method allowed identification of molecular weight changes to the GAPDH monomer with treatments. Proteins entered the mass spectrometer from the high performance liquid chromatography (HPLC) column. Electrospray ionisation applied a high voltage and temperature to the protein to form an ionised aerosol. This method minimised fragmentation of the proteins. The ionised proteins were separated based on their mass-to-charge (m/z) ratio by the quadrupole ion trap and were sent to the detector (171). Molecular weight was calculated from m/z and charge of the ionised protein:

$$\frac{m}{z} = \frac{(\mathrm{m} + \mathrm{nH}^{+})}{\mathrm{n}}$$

Where: m/z = mass-to-charge ratio, m = mass (Da), H^+ = mass of hydrogen (1.008 Da) and n = number of charges. GAPDH (4.2 µM) was incubated with urate hydroperoxide (3.5 µM) (2.3.3.3) for 10 min. Samples were then treated with 2 mM DTT for 30 min or were diluted with phosphate buffer. The final volume was 100 µL:

A. GAPDH
B. GAPDH and DTT
C. GAPDH and urate hydroperoxide
D. GAPDH, urate hydroperoxide and DTT

The Velos Pro ion-trap mass spectrometer (Thermo Scientific) was set to positive ion mode. The resulting mass spectrums were deconvoluted with ProMass for Xcalibur. The full description for the conditions of HPLC and mass spectrometry was put in Appendix 2 (5.3.1).

4.3 Results

4.3.1 Optimising the GAPDH Assay

In these experiments I wanted to optimise the GAPDH assay to allow assessment of GAPDH activity after oxidant treatments. The concentration of NAD^+ and DTT were varied from 0 – 1.4 µM and 0 – 7.5 mM respectively in the assay cuvette. The resulting GAPDH activity was measured at 340 nm.

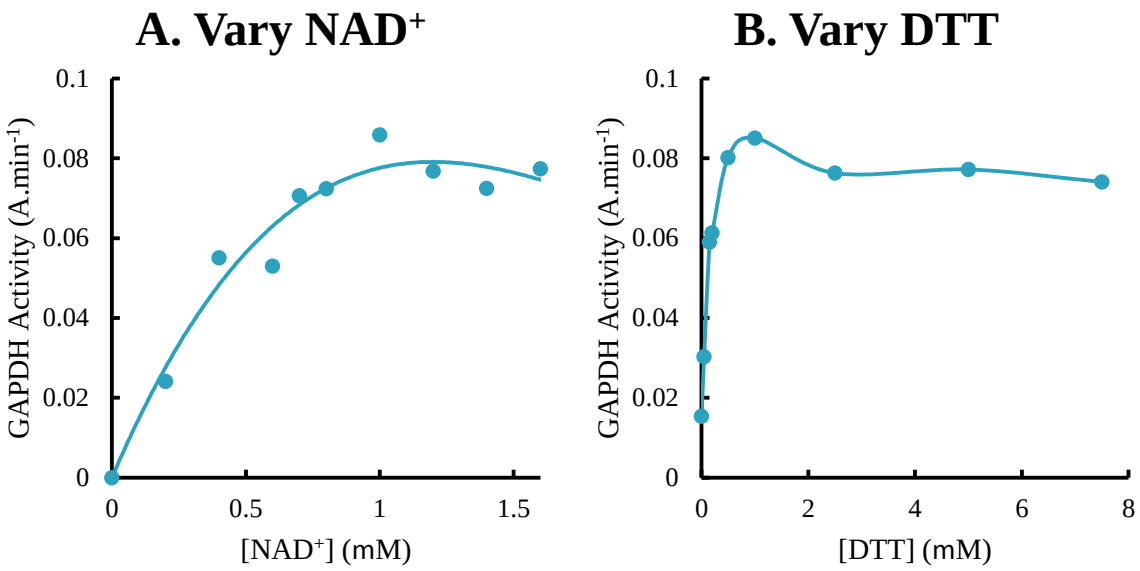

Figure 21: Optimising the GAPDH assay. A. Optimising the NAD^+ concentration used for the GAPDH assay. The concentration of NAD^+ was varied in the cuvette during the GAPDH assay. The concentrations for all other substances were constant for the assay. **B.** Optimising the DTT concentration used for the GAPDH assay. The concentration of DTT was varied in the cuvette during the GAPDH assay. The concentrations for all other substances were constant. These graphs represented two experiments.

During NAD^+ optimisation, GAPDH activity reached a maximum of 0.08 $A.min^{-1}$ at 1 mM NAD^+, after which the activity plateaued (figure 21 A). The addition of DTT to the assay cuvette dramatically increased the GAPDH activity (figure 21 B). The enzyme activity reached a maximum at 1 mM DTT, at a rate six times greater than in the absence of DTT. There was some loss of GAPDH activity with DTT concentrations > 1 mM, but the activity was still high. Based on these results, GAPDH was reduced with 2 mM DTT and isolated with spin columns. GAPDH was assayed with 1 mM NAD^+. The optimised GAPDH assay used concentrations: 60 nM GAPDH (reduced with 2 mM DTT), 0.5 mM GAP, 1 mM NAD^+ and 50 µM DTPA in TEA buffer.

A series of experiments were preformed to assess the interference of the xanthine oxidase/lactoperoxidase system on GAPDH activity. GAPDH activity was linear with

concentration in the presence of DTT (Appendix 1, figure 36). This enzyme was isolated from DTT with spin columns with a workable concentration and activity (Appendix 1, figure 37). NAD absorbance at 260 and 340 nm was used to assess the oxidation state (Appendix 1, figure 38). Exposure of this cofactor to taurine chloramine and urate hydroperoxide did not affect the oxidation state at concentrations used for GAPDH inactivation assay (Appendix 1, figure 39 and 40).

4.3.2 GAPDH Inactivation by Continuous Urate Hydroperoxide Formation

In this experiment I sought to measure the effect of urate hydroperoxide on GAPDH as it was formed by the xanthine oxidase/lactoperoxidase system. In a quartz cuvette the GAPDH assay and the xanthine oxidase/lactoperoxidase systems were mixed in TEA buffer. The absorbance at 340 nm was monitored. None of the substances used to make urate hydroperoxide affected GAPDH activity (Appendix 1, figure 41).

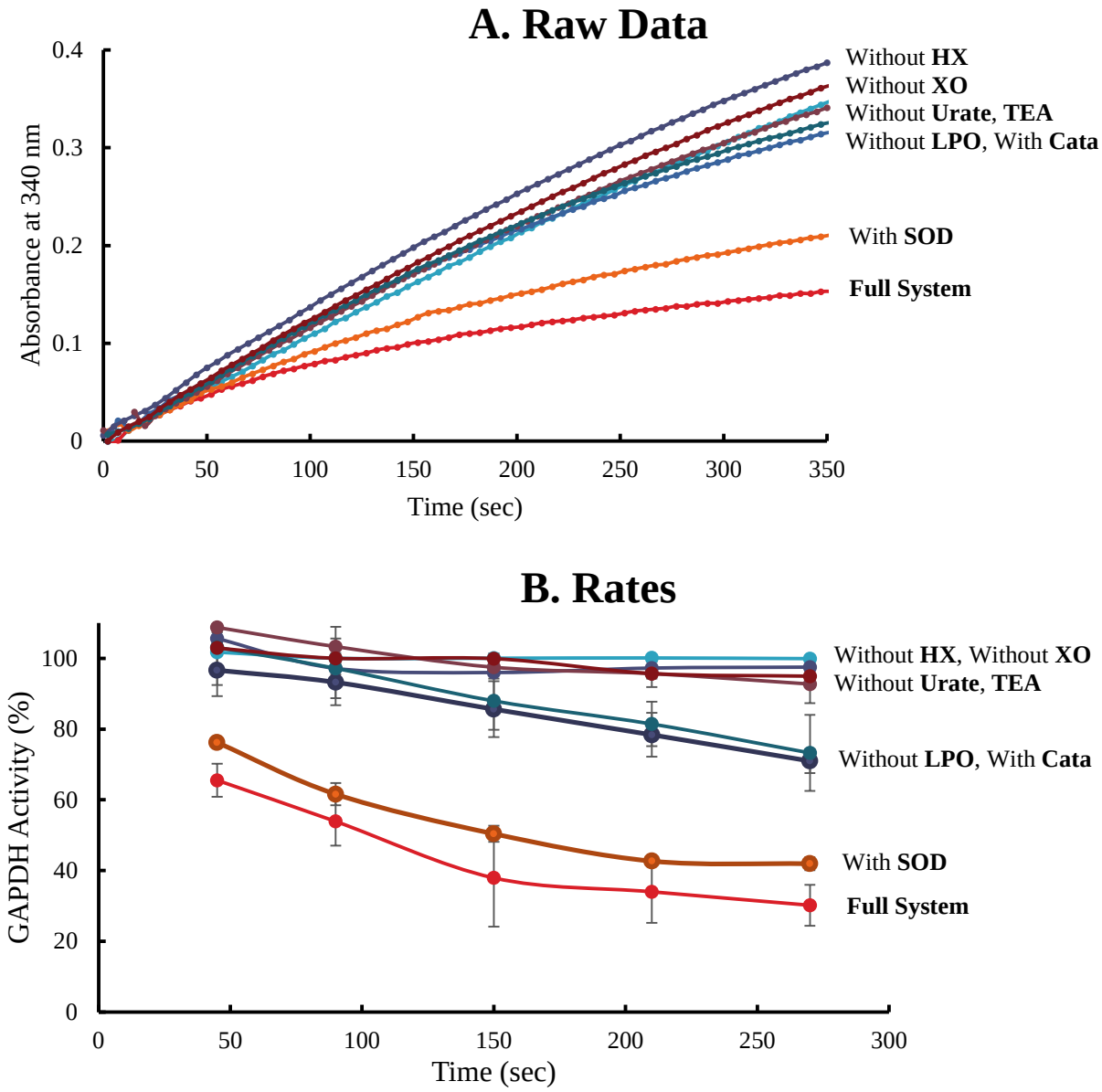

Figure 22: GAPDH inactivation during continuous formation of urate hydroperoxide. The substances of the GAPDH assay and xanthine oxidase/lactoperoxidase system were mixed in a quartz cuvette. Xanthine oxidase and GAPDH were the initiators. Each sample represented the removal of a substance from the xanthine oxidase/lactoperoxidase system or addition of catalase and superoxide dismutase. The control 'TEA buffer' only had the substances for the GAPDH assay to represent 100% GAPDH activity. **Top**: Raw data of each sample's absorbance at 340 nm. **Bottom**: GAPDH activity vs. time for each sample expressed as a percent. These graphs represented one experiment and the error bars were standard deviation for triplicate readings.

Figure 22 illustrates how the xanthine oxidase/lactoperoxidase system *in situ* effects GAPDH activity. Compared with the TEA buffer control, the full system had a significantly lower maximum absorbance (figure 22 A). The addition of superoxide dismutase was not effective in increasing the maximum absorbance, whereas the addition of catalase protected formation of NADH. All other controls (without hypoxanthine, urate,

lactoperoxidase and xanthine oxidase) had similar absorbance to TEA buffer. When the GAPDH activity was converted into a percent, the effect of urate hydroperoxide formation became distinct (figure 22 B). Initially, the full system caused a 40% loss of activity, this increased to approximately 70% in 4 min. During this time period approximately 5 µM urate hydroperoxide was made (figure 14). The addition of superoxide dismutase did not prevent the inactivation of GAPDH. All other samples had similar GAPDH activities.

The loss of GAPDH activity with the full xanthine oxidase/lactoperoxidase system implies a urate oxidant was responsible. Urate hydroperoxide was not solely responsible for inactivation of GAPDH since other oxidants were formed. Next, a discontinuous system was used to determine inactivation of GAPDH by urate hydroperoxide. The advantage of this system was that urate hydroperoxide dominated the oxidants formed.

4.3.3 Discontinuous Inactivation of GAPDH

4.3.3.1 Inactivation of GAPDH by Urate Hydroperoxide

For this experiment, I sought to determine whether the xanthine oxidase/lactoperoxidase system effected GAPDH activity. GAPDH was discontinuously exposed to samples for this system and the enzyme activity was assayed. The urate hydroperoxide concentration for the full system was 5 µM.

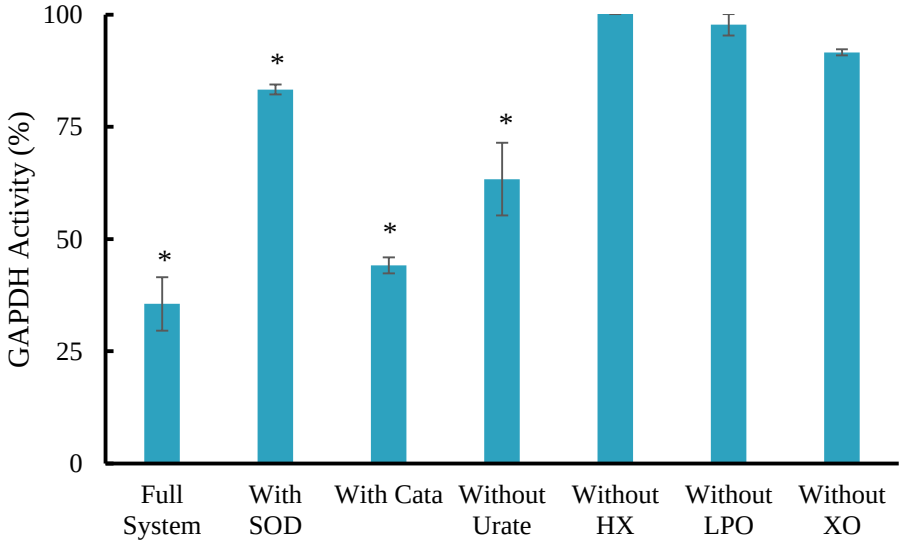

Figure *23*: Inactivation of GAPDH by urate hydroperoxide. GAPDH was treated with samples for the xanthine oxidase/lactoperoxidase system. These samples included the full system, removal of a substance or addition of catalase or superoxide dismutase. The hydroperoxide concentrations for samples A – G were 5, 2.7, 3.6, 0.9, 0.3, 0.1 and 0.2 µM. This graph was representative of two experiments. The error bars represented the standard deviation of triplicate readings for one experiment. One-way ANOVA followed by Holm-Sidak multiple comparison on triplicate readings was used to identify samples that were significantly different from the phosphate buffer control (* $p < 0.05$).

GAPDH was treated with the xanthine oxidase system to determine the effect of urate hydroperoxide on enzyme activity (figure 23). The full system with 5 µM urate hydroperoxide caused a 60% loss of GAPDH activity. The addition of catalase to the xanthine oxidase/lactoperoxidase system did not prevent GAPDH inactivation, whereas superoxide dismutase minimised the loss of activity to 20%. Hence, superoxide was essential for oxidant formation and GAPDH inactivation. When urate was removed from the system, 2.7 µM urate hydroperoxide was formed and approximately 40% of GAPDH activity was lost. Hypoxanthine, lactoperoxidase and xanthine oxidase were essential for urate hydroperoxide formation. When they were removed from the system there was minimal loss of GAPDH activity. These controls provide strong evidence that the loss of GAPDH activity was due to urate hydroperoxide as opposed to superoxide, hydrogen peroxide or other products formed.

4.3.3.2 Dose-Dependent Inactivation of GAPDH by Taurine Chloramine and Urate Hydroperoxide

The purpose of this experiment was to determine the stoichiometry of GAPDH inactivation by taurine chloramine and urate hydroperoxide. GAPDH (1 µM) was exposed to 0 – 12 µM taurine chloramine or 0 – 6 µM urate hydroperoxide in a dose-dependent manner.

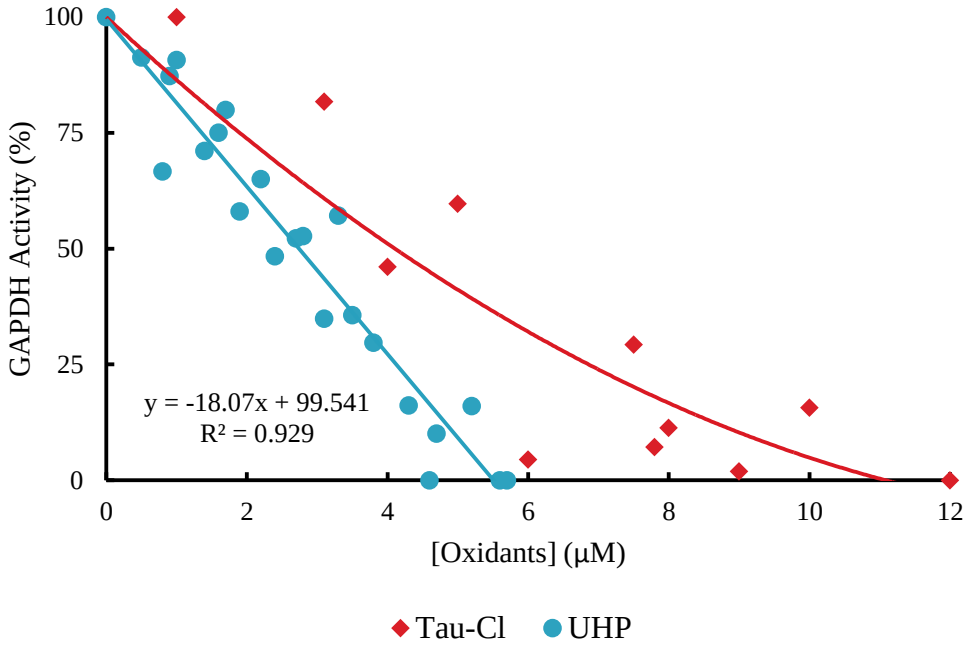

Figure 24: Dose-dependent inactivation of GAPDH by taurine chloramine or urate hydroperoxide. Reduced GAPDH was incubated with for 10 min with varying concentrations of oxidant. The resulting activity of GAPDH was quantified by measuring the formation of NADH at 340 nm on a spectrophotometer. GAPDH activity was lost with increasing concentration of oxidant. The concentration of GAPDH was approximately 1 µM. This graph combines at least three experiments.

Treatment of GAPDH with 10 µM taurine chloramine caused complete loss of activity (figure 24). The stoichiometry of inactivation for taurine chloramine to GAPDH was approximately 10:1. Urate hydroperoxide also showed dose-dependent inactivation of GAPDH. Approximately 5 µM urate hydroperoxide completely inactivated 1 µM GAPDH, hence the ratio of inactivation was approximately 5:1. The rate of inactivation was -18% activity per µM urate hydroperoxide. Urate hydroperoxide was a more successful inactivator of GAPDH than neutrophil derived oxidant taurine chloramine.

4.3.4 Inactivation Kinetics for GAPDH

I studied the kinetics of GAPDH inactivation by taurine chloramine and urate hydroperoxide to determine the reactivity of these oxidants. GAPDH was exposed to an oxidant in a discontinuous system and the resulting solution was immediately injected into the solution into assay cuvettes at different time points. Thus, the loss of GAPDH activity was measured with time.

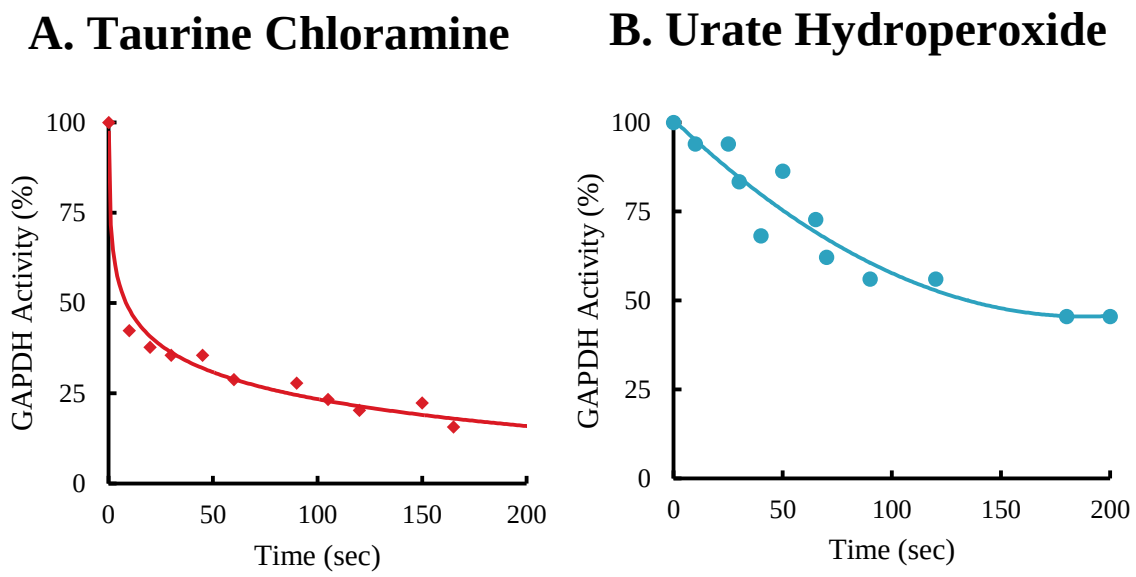

Figure 25: **Kinetics of GAPDH inactivation by oxidants.** GAPDH was exposed to oxidants and the resulting activity was assayed at three time points. This method was repeated three times and the time points measured were staggered. Time = 0 was the GAPDH activity in catalase-treated phosphate buffer. **A.** Kinetics of GAPDH exposure to taurine chloramine. **B.** Kinetics of GAPDH inactivation by urate hydroperoxide. These graphs were representative of three experiments.

Half of GAPDH activity was instantly lost upon exposure to taurine chloramine (figure 25 A). GAPDH activity continued to decline over the span of minutes. These results suggested GAPDH inactivation by taurine chloramine had two reactions: a fast and slow reaction. The fast reaction was not be characterised and represented the greater loss of GAPDH activity. The decline from 10 sec to 3 min represented a decline of approximately 9% per min. The concentrations of GAPDH and taurine chloramine were approximately 1 and 18 μM respectively.

GAPDH exposure to urate hydroperoxide was met with a fast loss of GAPDH activity over 2 min (figure 25 B). The decline in activity was smooth, hence the cause of inactivation might be a one-step reaction. GAPDH activity declined at a rate of approximately 23% per min. For this experiment, a low concentration of urate hydroperoxide (approximately 3 μM) was used which only inactivated half of the enzyme. Inactivation of GAPDH with higher concentrations of urate hydroperoxide was too quick to make a curve with multiple points.

4.3.5 Reactivation of GAPDH with DTT

This series of experiments explored whether inactivation of GAPDH by taurine chloramine or urate hydroperoxide was irreversible by reactivating the enzyme with DTT. I sought to confirm experiments by Peskin and Winterbourn (143) that taurine chloramine inactivation of GAPDH was reversible. GAPDH was exposed to taurine chloramine in a dose-dependent manner then samples were reduced with 2 mM DTT.

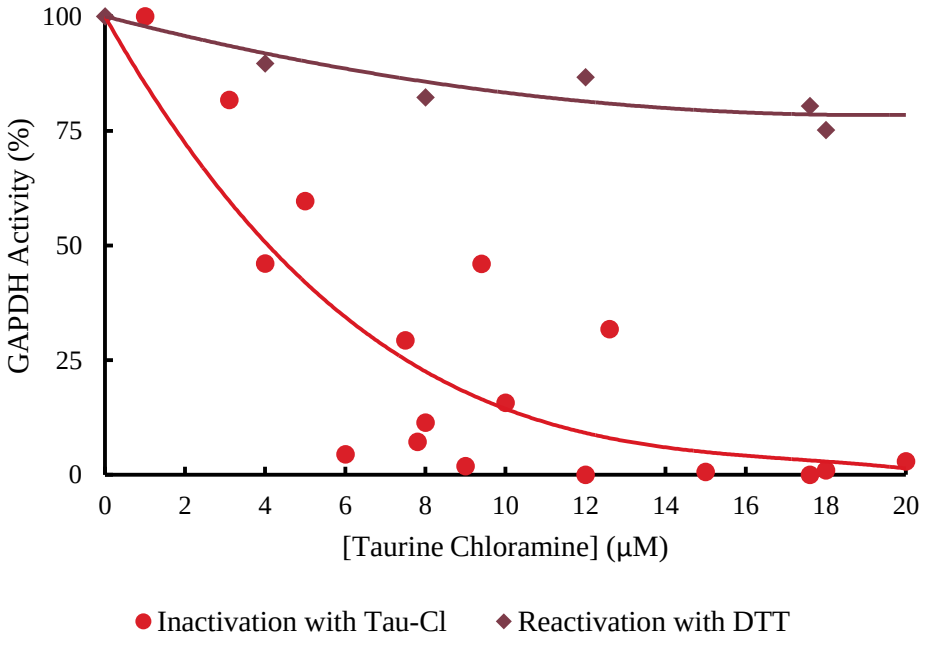

Figure 26: Reactivation of GAPDH following inactivation with taurine chloramine. GAPDH was dose-dependently exposed to taurine chloramine for 10 min. DTT (2 mM) was added to reactivate half of the samples and incubated for a further 30 min before measuring GAPDH activity. This graph combines at least three experiments.

Figure 26 illustrates how GAPDH was reactivated following exposure to taurine chloramine. GAPDH treatment with taurine chloramine resulted in a dose-dependent loss of GAPDH activity as previously described (4.3.3.2). Reduction by DTT recovered at least 80% of GAPDH activity regardless of taurine chloramine concentration. These results were similar to Peskin and Winterbourn (143) and confirms that taurine chloramine inactivation of GAPDH was reversible by reduction. Taurine chloramine likely inactivates GAPDH by forming disulfide bond with the essential thiol, and may pass through a sulfinic acid intermediate (143).

Next, the reactivation experiment was performed with GAPDH exposed to urate hydroperoxide.

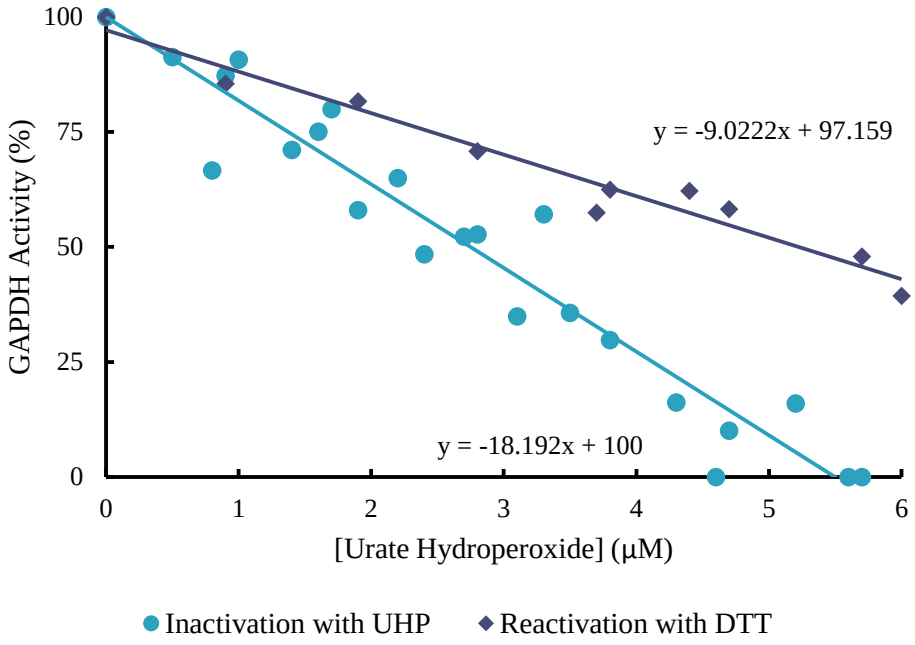

Figure 27: Reactivation of GAPDH following inactivation with urate hydroperoxide. GAPDH was dose-dependently treated with urate hydroperoxide for 10 min. Half of the samples were reduced with 2 mM DTT and incubated the samples for a further 30 min before measuring GAPDH activity. This graph combines at least three experiments.

Urate Hydroperoxide completely inactivated GAPDH, as shown in section 4.3.3.2. Reduction of the inactivated samples by DTT recovered approximately half of the activity lost (figure 27). This indicates GAPDH inactivation by urate hydroperoxide could be caused by reversible and irreversible modification.

4.3.6 Depletion of Cysteine Residues on GAPDH by Oxidants

This experiment served as a link between GAPDH inactivation and modification by oxidants. I wanted to determine whether cysteine residues on GAPDH were oxidized by taurine chloramine and urate hydroperoxide. The DTNB assay was performed on GAPDH discontinuously treated with oxidants in quartz cuvettes. Cysteine and GAPDH linearly absorbed light at 412 nm (Appendix 1, figure 42). The substances of the xanthine oxidase/lactoperoxidase system did not interfere with the assay (Appendix 1, figure 43).

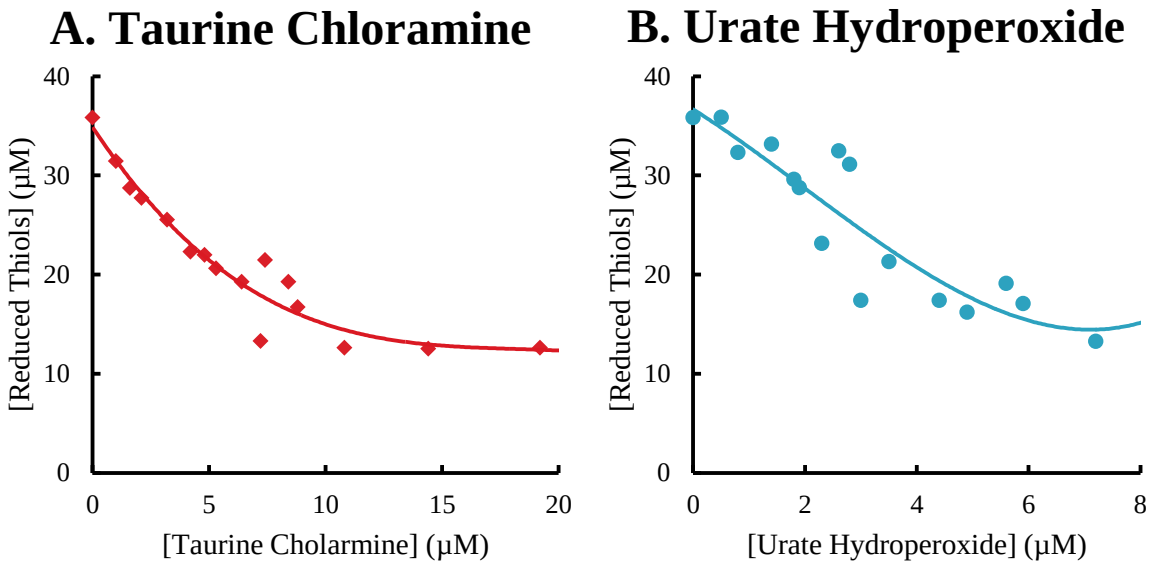

Figure 28: Dose-dependent depletion of cysteine residues on GAPDH by oxidants. **A.** Dose-Dependent depletion of GAPDH thiols by taurine chloramine. **B.** Dose-dependent depletion of cysteine residues on GAPDH by urate hydroperoxide. The final concentration of the GAPDH monomer was approximately 3 µM. These graphs combine three experiments which were normalised to a reduced thiol concentration of 36 µM.

The DTNB assay of 3 µM GAPDH revealed 36 cysteine residues. Treatment of GAPDH with taurine chloramine oxidized 23 µM of the cysteine residues measured with DTNB (figure 28 A). The reduced thiol concentration plateaued at approximately 10 µM taurine chloramine. Similar results were seen for treatment of GAPDH with urate hydroperoxide (figure 28 B). Approximately 7 µM urate hydroperoxide was required to deplete 23 µM of cysteine residues on GAPDH.

A GAPDH concentration of 3 µM should have produced 48 µM reduced thiols. However, as shown with the standard curve (Appendix 1, figure 42 B), one quarter of the cysteine residues on GAPDH were not measurable with DTNB. Thus, taurine chloramine and urate hydroperoxide depleted half of the cysteine residues on GAPDH. Previous studies determined that half of the cysteine residues on GAPDH were vulnerable to oxidants (27, 172).

4.3.7 Polyacrylamide Gel Electrophoresis of GAPDH

I performed SDS-PAGE on GAPDH samples treated with urate hydroperoxide to determine if there were major structural changes to the proteins. GAPDH and the proteins

of the xanthine oxidase/lactoperoxidase system were separated under reducing and non-reducing conditions.

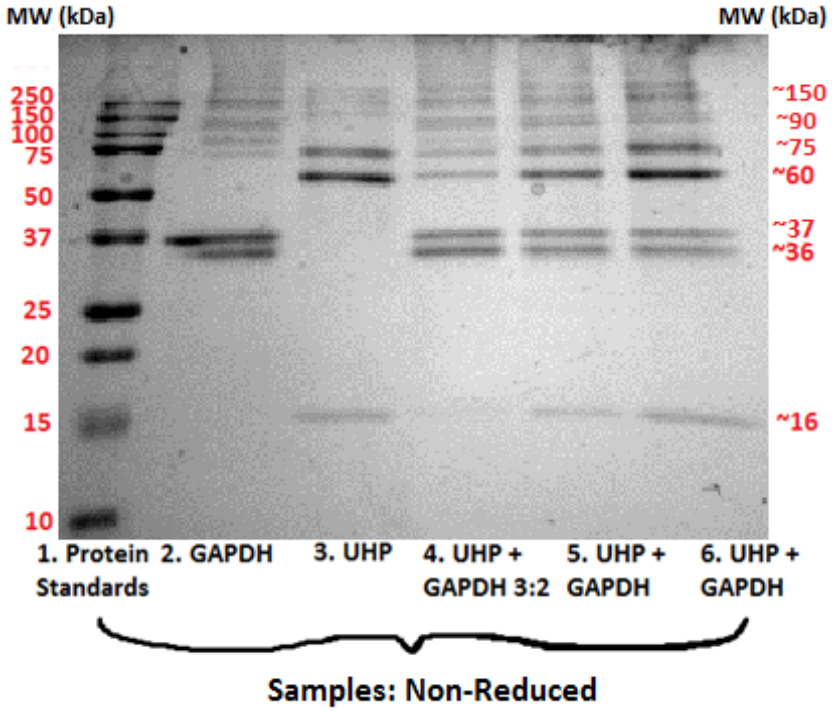

Figure 29: Non-reducing gel for the inactivation of GAPDH by urate hydroperoxide. GAPDH was exposed to urate hydroperoxide in a dose-dependent manner. The controls consisted of a protein marker, GAPDH and urate hydroperoxide. Lane 1: protein marker. Lane 2: 1.5 µM GAPDH. Lane 3: 10.5 µM urate hydroperoxide. Lane 4: 2.2 µM urate hydroperoxide + 1.5 µM GAPDH (approximately 3:2). Lane 5: 5.5 µM urate hydroperoxide + 1.5 µM GAPDH (7:2). Lane 6: 10.5 µM urate hydroperoxide + 1.5 µM GAPDH (7:1).

Separation of samples under non-reducing conditions allowed visualisation of the quaternary structure of GAPDH (figure 29). The GAPDH control produced two major bands at approximately 36 and 37 kDa (lane 2). These species were likely the GAPDH monomers. The species formed above 75 kDa were impurity or other quaternary structures. The faint band at 150 kDa was likely the native homodimer of GAPDH (144 kDa (173)). The xanthine oxidase/lactoperoxidase system (lane 3) produced bands at 16, 60, 80 and 150 kDa. These bands represent superoxide dismutase monomer (16 kDa (174)), catalase monomer (57.5 kDa (175)), lactoperoxidase dimer (77.5 kDa (176)) and xanthine oxidase monomer (150 kDa (177)) respectively. Dose-dependent exposure of GAPDH to urate hydroperoxide (lanes 4 – 6) produced bands which were a combination of the two controls (lane 2 and 3). Thus there were no large molecular weight change for GAPDH exposed to urate hydroperoxide.

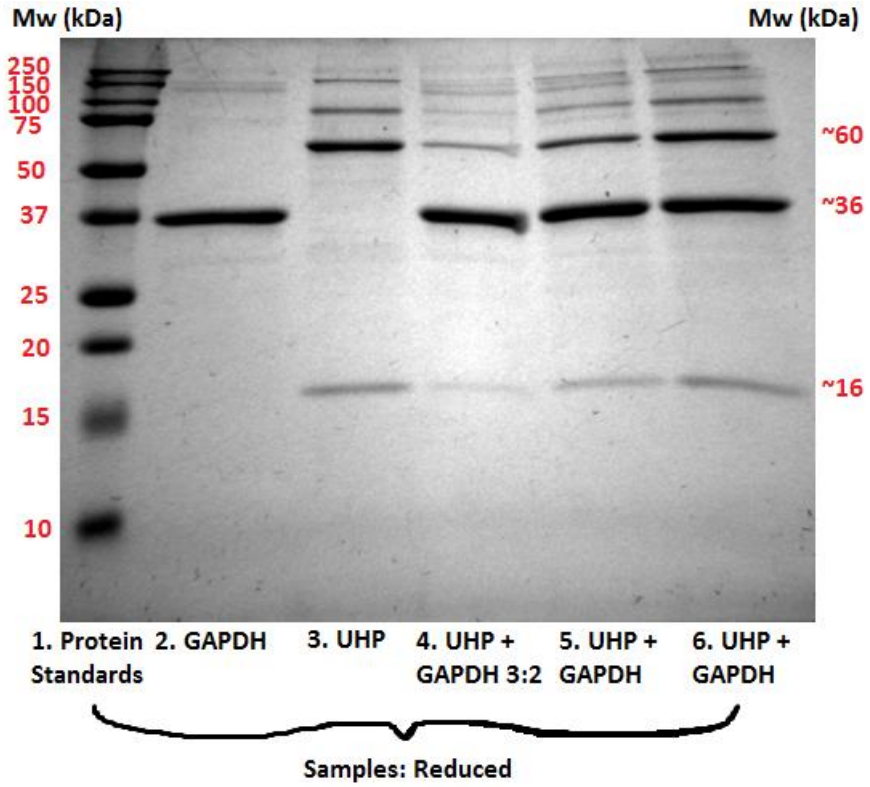

Figure 30: Reducing gel for the inactivation of GAPDH by urate hydroperoxide. GAPDH was exposed to urate hydroperoxide in a dose-dependent manner. The controls consisted of a protein marker, GAPDH and urate hydroperoxide. **Lane 1**: protein marker. **Lane 2**: 1.5 µM GAPDH. **Lane 3**: 10.5 µM urate hydroperoxide. **Lane 4**: 2.2 µM urate hydroperoxide + 1.5 µM GAPDH (approximately 3:2), **Lane 5**: 5.5 µM urate hydroperoxide + 1.5 µM GAPDH (7:2). **Lane 6**: 10.5 µM urate hydroperoxide + 1.5 µM GAPDH (7:1).

Separation of samples under reducing conditions allowed visualisation of the tetrameric structure of GAPDH (figure 30). GAPDH ran as a single band at approximately 36 kDa in reducing conditions (lane 2). This band represented the GAPDH monomer. The major bands for the xanthine oxidase/lactoperoxidase system were the same as non-reducing conditions (figure 29) (lane 3). Dose-dependent exposure of GAPDH to urate hydroperoxide produced a combination of bands seen in the controls (lane 4 – 6). A faint band formed at approximately 70 kDa which was not present in the GAPDH or urate hydroperoxide samples. However, it was too faint to be a significant modification. The results for reducing and non-reducing conditions were consistent. There was no major change in GAPDH's molecular weight following exposure to urate hydroperoxide.

4.3.8 Mass Spectrometry of GAPDH

Using mass spectrometry, I hoped to identity modifications to residues to explain the loss of GAPDH activity following exposure to urate hydroperoxide. All work with the mass spectrometer and analysis was carried out by Dr. Louise Paton. I prepared the samples for mass spectrometry and performed the tryptic digest. GAPDH was treated with urate hydroperoxide and/or DTT. The samples ran through the mass spectrometer as complete proteins.

Table 5: Species found during whole protein mass spectrometry of GAPDH treated with a low concentration of urate hydroperoxide. For this experiment a ratio of 1:1 GAPDH to urate hydroperoxide was used. Only species that represented > 5% of the total were listed. The GAPDH monomer and the species that may have an adduct were highlighted yellow.

A. GAPDH			B. GAPDH + DTT			C. GAPDH + UHP			D. GAPDH + UHP + DTT		
Mw (Da)	Δ mass (Da)	Total (%)	Mw (Da)	Δ mass (Da)	Total (%)	Mw (Da)	Δ mass (Da)	Total (%)	Mw (Da)	Δ mass (Da)	Total (%)
35,734	0	28.1	35,732	0.0	48	35,732	0	38	35,734	0	41.2
35,691	-43	26.1	35,807	75	32	35,805	72	34	35,810	77.4	27.7
35,775	41	24.2	35,877	145	7	35,865	132	13	35,865	132	10.7
35,846	112	11.4									

The mass spectrums had a small population of species at 36 kDa, indicating HPLC successfully separated GAPDH (Appendix 1, figure 44). The species found per sample and delta masses were presented in table 5. The m/z values for the GAPDH monomer was seen in sample A. The species found were approximately 36 kDa and differed by 155 Da. When DTT was added (sample B) the 35,732 Da species became distinct and likely represented the reduced GAPDH monomer. GAPDH was treated with urate hydroperoxide (sample C) and three major species were found. The main species represented the reduced GAPDH monomer (35,732 Da). The 35,805 Da species had a similar molecular weight and percent to a species formed when GAPDH was reduced with DTT (35,807 Da) (samples B). Thus, this species was not unique to urate hydroperoxide treatment. Of interest was the species with a molecular weight of 35,865 Da (sample C). This species was formed during urate hydroperoxide treatment and remained after DTT reduction (sample D). A delta mass of 132 was too low to be the 35,877 Da species of sample B.

The 35,865 Da species of sample C may have been the cause of irreversible inactivation of GAPDH following treatment with urate hydroperoxide. A delta mass of 132 indicated the formation of a urate adduct. However, the molecular weight of urate was 168. The purine ring of urate may have degraded during mass spectrometry to lose atoms. A tryptic digest of GAPDH with trypsin was performed and the resulting peptides were measured with tandem mass spectrometry. The sequence coverage of GAPDH by the peptides was too low to determine the oxidative modification to GAPDH.

4.4 Discussion

Urate hydroperoxide is a powerful oxidant of thiol-dependant GAPDH. When I exposed GAPDH to urate hydroperoxide the activity was lost in a dose-dependent manner. The inactivation ratio for urate hydroperoxide to GAPDH was 5:1. In comparison, taurine chloramine required twice the concentration to inactivate the same concentration of GAPDH. Urate hydroperoxide was therefore a stronger oxidant of GAPDH than taurine chloramine and hydrogen peroxide (143). DTT only recovered half of GAPDH activity following inactivation by urate hydroperoxide. The same concentration of DTT completely removed the effects of taurine chloramine on GAPDH. These results indicate urate hydroperoxide partially permanently inactivates GAPDH. Permanent inactivation of enzymes affect a cell's ability to survive and proliferate since the enzyme would have to be broken down and replaced (24).

Neither taurine chloramine nor urate hydroperoxide completely oxidized the cysteine residues on GAPDH during the DTNB assay. This finding was consistent with previous work by Ishii et al. (27). Of the four cysteine residues on the GAPDH monomer, Cys149 and Cys153 quickly cleave DTNB, whereas Cys244 and Cys281 reacts slowly with DTNB. Oxidants only deplete Cys149 and Cys153, hence the DTNB assay measures approximately half the reduced thiols following oxidant treatment (27). Urate hydroperoxide depletion of cysteine residues on GAPDH was too variable to determine the stoichiometry of depletion. This may become apparent with repeat experiments. Future experiments could include measurement of the kinetics of oxidation of cysteine residue on GAPDH with the DTNB assay.

Urate hydroperoxide increased the mass of the GAPDH monomer by 132 Da during whole protein mass spectrometry. This could be an adduct of urate to GAPDH. However,

the molecular weight of urate is 168 Da and it is difficult to speculate what loss of mass allows an addition of 132 Da. The purine ring may have collapsed resulting in the loss of some atoms. Urate adducts of 140 and 166 Da have been seen in our lab (Rufus Turner, unpublished data). A tryptic digest was performed on GAPDH treated with urate hydroperoxide however the sequence coverage for the resulting peptides was only 35%. This coverage was too poor to determine which residue the urate formed on. The tryptic digest must be optimised to deliver more GAPDH peptides. This could be achieved by performing a double protease digest with trypsin and chymotrypsin to maximise the number of cleavage sites. I plan to perform a trypsin/chymotrypsin digest, followed by mass spectrometry in the future.

Chapter 5. Conclusions

5.1 Summary of Findings

My research describes a new mechanism for urate acting as pro-oxidant through formation of the novel oxidant urate hydroperoxide. I studied the formation and reactivity of urate hydroperoxide with thiols. An enzyme system with xanthine oxidase and lactoperoxidase was used to form urate hydroperoxide. The concentration of this oxidant was measured with the FOX assay. Urate hydroperoxide formation was optimised using a maximum concentration of hypoxanthine, urate and xanthine oxidase. The optimised system formed approximately 15 µM urate hydroperoxide in 20 min at initial rate 3.2 $\mu M min^{-1}$. This was a useful concentration for future experiments. Urate hydroperoxide depleted cysteine and glutathione. The depletion of glutathione by urate hydroperoxide was at a 2:1 ratio, which implies glutathione was oxidised to glutathione disulfide and did not form an adduct.

Urate hydroperoxide caused a dose-dependent loss of activity in thiol-dependent enzyme GAPDH. The ratio of inactivation was approximately 5:1. The inactivated enzyme was reduced with DTT and half of the activity was recovered. Hence, urate hydroperoxide partially, permanently inactivates GAPDH. Using mass spectrometry I identified a 132 Da increase in mass of GAPDH after treatment with urate hydroperoxide. This modification could be a urate adduct, however I could not confirm this theory with a tryptic digest followed by tandem mass spectrometry. Urate hydroperoxide oxidised half of the cysteine residues on GAPDH and may have formed the urate adduct to the catalytic cysteine. However, I could not confirm oxidation of cysteine was responsible for permanent loss of activity. Overall, these results suggest that urate hydroperoxide could be a strong oxidant of thiol-dependent enzymes. The mechanism of inactivation requires more work to elucidate.

Urate hydroperoxide may be produced by neutrophil oxidative bursts during hyperuricemia (figure 31). Thus, this research links hyperuricemia and tissue damage leading to inflammatory disease. Urate hydroperoxide could deplete cysteine and glutathione, hence starving the cell of essential biomolecules and aggravating oxidative stress. Thiol-dependent enzymes; such as glycolytic enzymes, protein tyrosine phosphatase and cysteine protease; could be irreversible inactivated by urate hydroperoxide. Since thiol-dependent enzymes are ubiquitous in biology, permanent loss of these enzymes may

lead to loss of cell function and death. Factors secreted during apoptosis or necrosis recruits inflammatory cells. This is positive feedback for inflammation, oxidative stress and urate hydroperoxide formation.

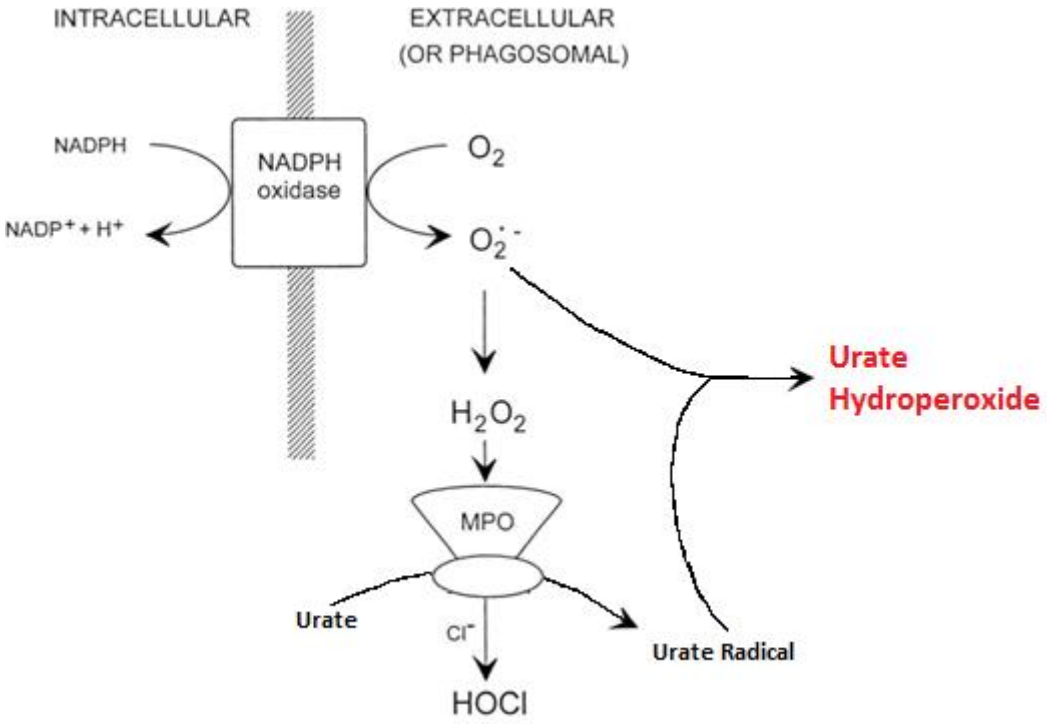

Figure 31: Neutrophil activity at inflammatory sites, during hyperuricemia, could produce urate hydroperoxide. Membrane-bound NADPH oxidase generates superoxide using NADPH as a cofactor. Superoxide can dismutate to hydrogen peroxide, which is a substrate for neutrophil myeloperoxidase. Myeloperoxidase produces hypochlorous acid from chloride and hydrogen peroxide. It also converts urate to a radical. Superoxide and the urate radical are in proximity to combine and form urate hydroperoxide. Figure adapted from (108).

Urate hydroperoxide formation explains the pro-oxidant effects of urate during hyperuricemia. Previous studies found that urate promoted lipid peroxidation and enzyme inactivation. Urate hydroperoxide may have formed during these experiments and led to the oxidation of the biomolecules studied. For example, urate hydroperoxide may have formed during Aruoma and Halliwell's (91) radiolysis of A1AT. A1AT relies on a cysteine residue for activity, thus urate hydroperoxide may have formed an adduct to this enzyme analogous to my findings with GAPDH (178). In support of this, the authors proposed a urate peroxyl radical inactivated the enzyme. Peroxyl radicals degrade to hydroperoxides, thus our theories are analogous (67).

5.2 Strengths and Limitations

To the best of my knowledge, no other study has measured urate hydroperoxide's effect on enzymes. I presented strong *in vitro* evidence that urate hydroperoxide inactivates GAPDH. Urate hydroperoxide inactivation of thiol-dependent enzyme GAPDH is new and important for understanding the pro-oxidant effects of urate during hyperuricemia. My research provides a new mechanism for the numerous pro-oxidant effects of urate, which were previously unexplained. This research paves the way for in-depth research on urate hydroperoxide.

A major limitation of this study is that there is no evidence urate hydroperoxide is formed *in vivo*. However, neutrophils, which are abundant at inflammatory sites, have all the machinery to produce this oxidant. Measuring urate hydroperoxide's presence *in vivo* is difficult due to its reactive and transient nature. The formation of a urate adduct to thiol-dependent enzymes could be used as a biomarker for urate hydroperoxide's formation *in vivo*. I cannot discern urate hydroperoxide's effect on all thiol-dependent enzymes based on its inactivation of GAPDH. A diverse pool of thiol-dependent enzymes should be studied to conclude that urate hydroperoxide inactivates thiol-dependent enzymes in general.

In this thesis I postulated that urate hydroperoxide could be formed at an inflammatory site extracellularly. However for urate to have a significant effect on thiols it must be uptaken into cells through a urate transporter. Urate is uptaken into vascular smooth muscle cells though anion transporter URAT1 (179), urate hydroperoxide could also be uptaken through this transporter. However, whether urate transporters allow uptake of oxidised urate has not been explored.

My work was completely *in vitro* and therefore has limited applicability to *in vivo*. *In vitro* experiments place the substrates in a proximity that might not be achieved *in vivo*. For example, urate hydroperoxide formation at an endothelium inflammatory site might be hindered by blood flow washing away the proteins. Also, neutrophils may only form urate hydroperoxide when the inflammatory site is overwhelmed by oxidative stress because antioxidants like ascorbate and glutathione reduce oxidants. During oxidative stress there would be a multitude of other oxidants which could be as powerful as urate hydroperoxide. At best, I argue that urate hydroperoxide could contribute to tissue damage by oxidative stress in conjunction with other oxidants.

5.3 Recommendation for Future Work

There is strong evidence that urate hydroperoxide inactivates GAPDH but I could not identify the modification. GAPDH treated with urate hydroperoxide may form an adduct, however the results from the tryptic digest were too poor to support this. I hope to optimise the tryptic digest and characterise the oxidative modification to GAPDH in the future.

This thesis described urate hydroperoxide's inactivation of one thiol-dependent enzyme. My work must be extended to other thiol-dependent enzymes such as protein tyrosine phosphatase, protein tyrosine kinase and other glycolytic enzymes. Urate hydroperoxide inactivation of these enzymes will build a picture of this oxidant's reactivity with thiol-dependent enzymes. Also, urate hydroperoxide could oxidise other biomolecules. In particular, urate hydroperoxide's depletion of ascorbate should be characterised. Urate hydroperoxide's ability to oxidise past the lipid-water barrier could also be characterised by measuring the oxidation of lipids and lipid-soluble antioxidants such as coenzyme, α-tocopherol and carotenes.

To give this research cellular context I suggest exposing cells and bacteria to urate hydroperoxide and measuring the change of cell viability. However, this requires urate hydroperoxide uptaken into cells and use of an appropriate cell model. Since the pathological context of this research is hyperuricemia I suggest cells to model the human endothelium. Cells could be exposed to hyperuricemia and the xanthine oxidase/lactoperoxidase system to make urate hydroperoxide *in situ*. Whether urate hydroperoxide could be uptaken by urate transporters should be explored. Additionally, we could determine the viability of urate hydroperoxide formation *in vivo* by exposing neutrophils to hyperuricemic conditions during their oxidative bursts and measuring hydroperoxide formation. There is also the possibility of creating antibodies for the urate adduct to GAPDH. This would allow detection of urate hydroperoxide's oxidation of GAPDH in cells.

The formation of urate adducts to enzymes has potential as a biomarker of urate hydroperoxide formation *in vivo*. Future experiments could include spiking clinical plasma samples with urate hydroperoxide and performing mass spectrometry to detect the formation of adducts on isolated thiol-dependent enzymes, depletion of antioxidants and other oxidized species. Also, urate adducts could be developed as a biomarker for hyperuricemia patients risk of heart disease. This would involve measuring urate adducts in

clinical samples from patients suffering hyperuricemia and a control population and correlating to risk of heart disease.

I will be continuing this project as summer studentship wherein I will study urate hydroperoxide inactivation of protein tyrosine phosphatase and the protective effects of ascorbate. I will optimise the riboflavin photooxidation system for urate hydroperoxide formation. The possibilities for future work with urate hydroperoxide are numerous and exciting. Research into this novel oxidant could provide a mechanism for hyperuricemia's pro-oxidant effects, therefore advancing our understanding of its association with inflammatory disease.

References

1. Becker BF. Towards the physiological function of uric acid. Free Radic Biol Med. 1993;14(6):615-31.
2. So A, Thorens B. Uric acid transport and disease. J Clin Invest. 2010;120(6):1791-9.
3. Ames BN, Cathcart R, Schwiers E, Hochstein P. Uric acid provides an antioxidant defense in humans against oxidant-and radical-caused aging and cancer: a hypothesis. Proc Natl Acad Sci. 1981;78(11):6858-62.
4. Oda M, Satta Y, Takenaka O, Takahata N. Loss of urate oxidase activity in hominoids and its evolutionary implications. Mol Biol Evol. 2002;19(5):640-53.
5. Stamp LK, Turner R, Khalilova IS, Zhang M, Drake J, Forbes LV, et al. Myeloperoxidase and oxidation of uric acid in gout: implications for the clinical consequences of hyperuricaemia. Rheumatology. 2014;53(11):1958-65.
6. Johnson RJ, Sautin YY, Oliver WJ, Roncal C, Mu W, Sanchez-Lozada LG, et al. Lessons from comparative physiology: could uric acid represent a physiologic alarm signal gone awry in western society? J Comp Physiol B. 2009;179(1):67-76.
7. Johnson RJ, Andrews P. The fat gene. Sci Am. 2015;313:64-9
8. Waring WS, Webb DJ, Maxwell SRJ. Systemic uric acid administration increases serum antioxidant capacity in healthy volunteers. J Cardiovasc Pharmacol. 2001;38(3):365-71.
9. Frei B, England L, Ames BN. Ascorbate is an outstanding antioxidant in human blood plasma. Proc Natl Acad Sci. 1989;86(16):6377-81.
10. Frei B, Stocker R, Ames BN. Antioxidant defenses and lipid peroxidation in human blood plasma. Proc Natl Acad Sci. 1988;85(24):9748-52.
11. Wen CP, David Cheng TY, Chan HT, Tsai MK, Chung WSI, Tsai SP, et al. Is high serum uric acid a risk marker or a target for treatment? Examination of its independent effect in a large cohort with low cardiovascular risk. Am J Kidney Dis. 2010;56(2):273-88.
12. Stamp LK, Khalilova IS, Tarr JM, Senthilmohan R, Turner R, Haigh RC, et al. Myeloperoxidase and oxidative stress in rheumatoid arthritis. Rheumatology. 2012;51(10):1796-803.
13. Kono H, Chen C-J, Ontiveros F, Rock KL. Uric acid promotes an acute inflammatory response to sterile cell death in mice. Clin Investig. 2010;120(6):1939.
14. Martinon F, Petrilli V, Mayor A, Tardivel A, Tschopp J. Gout-associated uric acid crystals activate the NALP3 inflammasome. Nature. 2006;440(7081):237-41.
15. Zharikov S, Krotova K, Hu H, Baylis C, Johnson RJ, Block ER, et al. Uric acid decreases NO production and increases arginase activity in cultured pulmonary artery endothelial cells. Am J Physiol Cell Physiol. 2008;295(5):C1183-C90.
16. Bagnati M, Perugini C, Cau C, Bordone R, Albano E, Bellomo G. When and why a water-soluble antioxidant becomes pro-oxidant during copper-induced low-density lipoprotein oxidation: A study using uric acid. Biochem J. 1999;340(1):143-52.
17. Meotti FC, Jameson GN, Turner R, Harwood DT, Stockwell S, Rees MD, et al. Urate as a physiological substrate for myeloperoxidase: implications for hyperuricemia and inflammation. J Biol Chem. 2011;286(15):12901-11.
18. Sautin YY, Nakagawa T, Zharikov S, Johnson RJ. Adverse effects of the classic antioxidant uric acid in adipocytes: NADPH oxidase-mediated oxidative/nitrosative stress. Am J Physiol Cell Physiol. 2007;293(2):C584-C96.
19. Seidel A, Parker H, Turner R, Dickerhof N, Khalilova IS, Wilbanks SM, et al. Uric Acid and Thiocyanate as Competing Substrates of Lactoperoxidase. J Biol Chem. 2014;289(32):21937-49.

20. Patrício ES, Prado FM, da Silva RP, Carvalho L, Prates MV, Dadamos TR, et al. Chemical characterization of urate hydroperoxide, a pro-oxidant intermediate generated by urate oxidation in inflammatory and photo-induced processes. Chem Res Toxicol. 2015.
21. Kidd PM. Glutathione: systemic protectant against oxidative and free radical damage. Altern Med Rev. 1997;2(3):155-76.
22. Lomaestro BM, Malone M. Glutathione in health and disease: pharmacotherapeutic issues. Ann Pharmacother. 1995;29(12):1263-73.
23. Giles GI. The redox regulation of thiol dependent signaling pathways in cancer. Curr Pharm Des. 2006;12(34):4427-43.
24. Giles NM, Giles GI, Jacob C. Multiple roles of cysteine in biocatalysis. Biochem Biophys Res Commun. 2003;300(1):1-4.
25. Leung-Toung R, Li W, Tam TF, Kaarimian K. Thiol-dependent enzymes and their inhibitors: a review. Curr Med Chem. 2002;9(9):979-1002.
26. Kato Y, Peskin AV, Dickerhof N, Harwood DT, Kettle AJ. Myeloperoxidase catalyzes the conjugation of serotonin to thiols via free radicals and tryptamine-4, 5-dione. Chem Res Toxicol. 2012;25(11):2322-32.
27. Ishii T, Sunami O, Nakajima H, Nishio H, Takeuchi T, Hata F. Critical role of sulfenic acid formation of thiols in the inactivation of glyceraldehyde-3-phosphate dehydrogenase by nitric oxide. Biochem Pharmacol. 1999;58(1):133-43.
28. Cowan-Jacob SW, Kaufmann M, Anselmo AN, Stark W, Grütter MG. Structure of rabbit-muscle glyceraldehyde-3-phosphate dehydrogenase. Acta Crystallogr D Biol Crystallogr. 2003;59(12):2218-27.
29. Sirover MA. New insights into an old protein: the functional diversity of mammalian glyceraldehyde-3-phosphate dehydrogenase. Biochim Biophys Acta. 1999;1432(2):159-84.
30. Kang D-H, Nakagawa T, Feng L, Watanabe S, Han L, Mazzali M, et al. A role for uric acid in the progression of renal disease. J Am Soc Nephrol. 2002;13(12):2888-97.
31. Mori MA, Bezy O, Kahn CR. Metabolic syndrome: is Nlrp3 inflammasome a trigger or a target of insulin resistance? Circ Res. 2011;108(10):1160-2.
32. Kolonel LN, Yoshizawa C, Nomura AM, Stemmermann GN. Relationship of serum uric acid to cancer occurrence in a prospective male cohort. Cancer Epidemiol Biomarkers Prev. 1994;3(3):225-8.
33. Fini MA, Elias A, Johnson RJ, Wright RM. Contribution of uric acid to cancer risk, recurrence, and mortality. Clin Transl Med. 2012;1(1):16.
34. Strasak AM, Rapp K, Hilbe W, Oberaigner W, Ruttmann E, Concin H, et al. Serum uric acid and risk of cancer mortality in a large prospective male cohort. Cancer Causes & Control. 2007;18(9):1021-9.
35. Qin L, Yang Z, Gu H, Lu S, Shi Q, Xing Y, et al. Association between serum uric acid levels and cardiovascular disease in middle-aged and elderly Chinese individuals. BMC Cardiovasc Disord. 2014;14.
36. Chuang S-Y, Chen J-H, Yeh W-T, Wu C-C, Pan W-H. Hyperuricemia and increased risk of ischemic heart disease in a large Chinese cohort. Int J Cardiol. 2012;154(3):316-21.
37. Kivity S, Kopel E, Maor E, Abu-Bachar F, Segev S, Sidi Y, et al. Association of serum uric acid and cardiovascular disease in healthy adults. Am J Cardiol. 2013;111(8):1146-51.
38. Chen JH, Chuang SY, Chen HJ, Yeh WT, Pan WH. Serum uric acid level as an independent risk factor for all‐cause, cardiovascular, and ischemic stroke mortality: A chinese cohort study. Arthritis Care Res. 2009;61(2):225-32.

39. Strasak AM, Rapp K, Hilbe W, Oberaigner W, Ruttmann E, Concin H, et al. The role of serum uric acid as an antioxidant protecting against cancer: prospective study in more than 28 000 older Austrian women. Ann Oncol. 2007;18(11):1893-7.
40. Zalawadiya SK, Veeranna V, Mallikethi-Reddy S, Bavishi C, Lunagaria A, Kottam A, et al. Uric acid and cardiovascular disease risk reclassification: Findings from NHANES III. Eur J Prev Cardiol. 2015;22(4):513-8.
41. Ito H, Abe M, Mifune M, Oshikiri K, Antoku S, Takeuchi Y, et al. Hyperuricemia is independently associated with coronary heart disease and renal dysfunction in patients with type 2 diabetes mellitus. PLoS One. 2011;6(11):e27817.
42. Wang J, Wang Y, Zhao D, Guo X, Zhong JQ. Association between serum uric acid and mortality in a Chinese population of hypertensive patients. Renal Fail. 2015;37(1):73-6.
43. Kawai T, Ohishi M, Takeya Y, Onishi M, Ito N, Yamamoto K, et al. Serum uric acid is an independent risk factor for cardiovascular disease and mortality in hypertensive patients. Hypertens Res. 2012;35(11):1087-92.
44. Silbernagel G, Hoffmann MM, Grammer TB, Boehm BO, März W. Uric acid is predictive of cardiovascular mortality and sudden cardiac death in subjects referred for coronary angiography. Nutr Metab Cardiovasc Dis. 2013;23(1):46-52.
45. Hamaguchi S, Furumoto T, Tsuchihashi-Makaya M, Goto K, Goto D, Yokota T, et al. Hyperuricemia predicts adverse outcomes in patients with heart failure. Int J Cardiol. 2011;151(2):143-7.
46. Levantesi G, Marfisi RM, Franzosi MG, Maggioni AP, Nicolosi GL, Schweiger C, et al. Uric acid: A cardiovascular risk factor in patients with recent myocardial infarction. International Journal of Cardiology. 2013;167(1):262-9.
47. Strazzullo P, Puig JG. Uric acid and oxidative stress: relative impact on cardiovascular risk. Nutr Metab Cardiovasc Dis. 2007;17(6):409-14.
48. Ioachimescu AG, Brennan DM, Hoar BM, Hazen SL, Hoogwerf BJ. Serum uric acid is an independent predictor of all-cause mortality in patients at high risk of cardiovascular disease: A Preventive Cardiology Information System (PreCIS) database cohort study. Arthritis Rheum. 2008;58(2):623-30.
49. Matzinger P. Tolerance, danger, and the extended family. Annu Rev Immunol. 1994;12(1):991-1045.
50. Janeway CA, editor Approaching the asymptote? Evolution and revolution in immunology. Cold Spring Harb Symp Quant Biol; 1989: Cold Spring Harbor Laboratory Press.
51. Cardella CJ, Davies P, Allison AC. Immune complexes induce selective release of lysosomal hydrolases from macrophages. Nature. 1974;247:46-8.
52. Denoble AE, Huffman KM, Stabler TV, Kelly SJ, Hershfield MS, McDaniel GE, et al. Uric acid is a danger signal of increasing risk for osteoarthritis through inflammasome activation. Proc Natl Acad Sci. 2011;108(5):2088-93.
53. Gasse P, Riteau N, Charron S, Girre S, Fick L, Pétrilli V, et al. Uric acid is a danger signal activating NALP3 inflammasome in lung injury inflammation and fibrosis. Am J Respir Crit Care Med. 2009;179(10):903-13.
54. Tschopp J, Schroder K. NLRP3 inflammasome activation: The convergence of multiple signalling pathways on ROS production? Nat Rev Immunol. 2010;10(3):210-5.
55. Gersch C, Palii SP, Kim KM, Angerhofer A, Johnson RJ, Henderson GN. Inactivation of nitric oxide by uric acid. Nucleosides Nucleotides Nucleic Acids. 2008;27(8):967-78.

56. Maxwell AJ, Bruinsma KA. Uric acid is closely linked to vascular nitric oxide activity: Evidence for mechanism of association with cardiovascular disease. J Am Coll Cardiol. 2001;38(7):1850-8.
57. Han HJ, Lim MJ, Lee YJ, Lee JH, Yang IS, Taub M. Uric acid inhibits renal proximal tubule cell proliferation via at least two signaling pathways involving PKC, MAPK, cPLA2, and NF-κB. Am J Physiol Renal Physiol. 2007;292(1):F373-F81.
58. Kanellis J, Watanabe S, Li JH, Kang DH, Li P, Nakagawa T, et al. Uric acid stimulates monocyte chemoattractant protein-1 production in vascular smooth muscle cells via mitogen-activated protein kinase and cyclooxygenase-2. Hypertension. 2003;41(6):1287-93.
59. Netea MG, Kullberg BJ, Blok WL, Netea RT, Van der Meer JWM. The role of hyperuricemia in the increased cytokine production after lipopolysaccharide challenge in neutropenic mice. Blood. 1997;89(2):577-82.
60. Roncal CA, Mu W, Croker B, Reungjui S, Ouyang X, Tabah-Fisch I, et al. Effect of elevated serum uric acid on cisplatin-induced acute renal failure. Am J Physiol Renal Physiol. 2007;292(1):F116-F22.
61. Patetsios P, Song M, Shutze WP, Pappas C, Rodino W, Ramirez JA, et al. Identification of uric acid and xanthine oxidase in atherosclerotic plaque. Am J Cardiol. 2001;88(2):188-91.
62. Marsch E, Sluimer JC, Daemen MJAP. Hypoxia in atherosclerosis and inflammation. Curr Opin Lipidol. 2013;24(5):393-400.
63. Suzuki T. Nitrosation of uric acid induced by nitric oxide under aerobic conditions. Nitric oxide. 2007;16(2):266-73.
64. Laroux FS, Pavlick KP, Hines IN, Kawachi S, Harada H, Bharwani S, et al. Role of nitric oxide in inflammation. Acta Physiol Scand. 2001;173(1):113-8.
65. Tripathi P, Tripathi P, Kashyap L, Singh V. The role of nitric oxide in inflammatory reactions. FEMS Immunol Med Microbiol. 2007;51(3):443-52.
66. Korhonen R, Lahti A, Kankaanranta H, Moilanen E. Nitric oxide production and signaling in inflammation. Curr Drug Targets Inflamm Allergy. 2005;4(4):471-9.
67. Halliwell B, Gutteridge JM. Free radicals in biology and medicine: Oxford university press Oxford; 1999.
68. Charo IF, Taubman MB. Chemokines in the pathogenesis of vascular disease. Circ Res. 2004;95(9):858-66.
69. Howell RR, Wyngaarden JB. On the mechanism of peroxidation of uric acids by hemoproteins. J Biol Chem. 1960;235:3544-50.
70. Halliwell B, Gutteridge JMC. Biologically relevant metal ion-dependent hydroxyl radical generation An update. FEBS Lett. 1992;307(1):108-12.
71. Muraoka S, Miura T. Inhibition by uric acid of free radicals that damage biological molecules. Pharmacol Toxicol. 2003;93(6):284-9.
72. Regoli F, Winston GW. Quantification of total oxidant scavenging capacity of antioxidants for peroxynitrite, peroxyl radicals, and hydroxyl radicals. Toxicol Appl Pharmacol. 1999;156(2):96-105.
73. Whiteman M, Ketsawatsakul U, Halliwell B. A reassessment of the peroxynitrite scavenging activity of uric acid. In: Chiueh CC, Hong JS, Leong SK, editors. Nitric Oxide: Novel Actions, Deleterious Effects and Clinical Potential. Annals of the New York Academy of Sciences. 962. New York: New York Acad Sciences; 2002. p. 242-59.
74. Kuzkaya N, Weissmann N, Harrison DG, Dikalov S. Interactions of peroxynitrite with uric acid in the presence of ascorbate and thiols: Implications for uncoupling endothelial nitric oxide synthase. Biochem Pharmacol. 2005;70(3):343-54.

75. Santos CXC, Anjos EI, Augusto O. Uric acid oxidation by peroxynitrite: multiple reactions, free radical formation, and amplification of lipid oxidation. Arch Biochem Biophys. 1999;372(2):285-94.
76. Davies KJA, Sevanian A, Muakkassahkelly SF, Hochstein P. Uric acid-iron ion complexes. A new aspect of the antioxidant functions of uric acid. Biochem J. 1986;235(3):747-54.
77. Clausen MR, Huvaere K, Skibsted LH, Stagsted J. Characterization of peroxides formed by riboflavin and light exposure of milk. Detection of urate hydroperoxide as a novel oxidation product. J Agric Food Chem. 2009;58(1):481-7.
78. Simic MG, Jovanovic SV. Antioxidation mechanisms of uric acid. J Am Chem Soc. 1989;111(15):5778-82.
79. Moawad MM. Complexation and thermal studies of uric acid with some divalent and trivalent metal ions of biological interest in the solid state. J Coord Chem. 2002;55(1):61-78.
80. Dubler E, Jameson GB, Kopajtić Z. Uric acid salts of magnesium: crystal and molecular structures and thermal analysis of two phases of Mg (C 5 H 3 N 4 O 3) 2· 8H 2 O. J Inorg Biochem. 1986;26(1):1-21.
81. Rouault TA. How mammals acquire and distribute iron needed for oxygen-based metabolism. PLoS Biol. 2003;1(3):e79.
82. Nanami M, Ookawara T, Otaki Y, Ito K, Moriguchi R, Miyagawa K, et al. Tumor Necrosis Factor-α–Induced Iron Sequestration and Oxidative Stress in Human Endothelial Cells. Arterioscler Thromb Vasc Biol. 2005;25(12):2495-501.
83. Decker A. Phenolics: prooxidants or antioxidants? Nutr Rev. 1997;55(11):396-8.
84. Stait S, Leake DS. The effects of ascorbate and dehydroascorbate on the oxidation of low-density lipoprotein. Biochem J. 1996;320:373-81.
85. Yamanaka N, Oda O, Nagao S. Prooxidant activity of caffeic acid, dietary non-flavonoid phenolic acid, on Cu 2+-induced low density lipoprotein oxidation. FEBS lett. 1997;405(2):186-90.
86. Abuja PM. Ascorbate prevents prooxidant effects of urate in oxidation of human low density lipoprotein. FEBS Lett. 1999;446(2):305-8.
87. Patterson RA, Horsley ETM, Leake DS. Prooxidant and antioxidant properties of human serum ultrafiltrates toward LDL important role of uric acid. J Lipid Res. 2003;44(3):512-21.
88. Chao H-H, Liu J-C, Lin J-W, Chen C-H, Wu C-H, Cheng T-H. Uric acid stimulates endothelin-1 gene expression associated with NADPH oxidase in human aortic smooth muscle cells. Acta Pharmacol Sin. 2008;29(11):1301-12.
89. Thomas MJ. Urate causes the human polymorphonuclear leukocyte to secrete superoxide. Free Radic Biol Med. 1992;12(1):89-91.
90. Kittridge KJ, Willson RL. Uric acid substantially enhances the free radical-induced inactivation of alcohol dehydrogenase. FEBS Lett. 1984;170(1):162-4.
91. Aruoma OI, Halliwell B. Inactivation of α1 -antiproteinase by hydroxyl radicals The effect of uric acid. FEBS Lett. 1989;244(1):76-80.
92. Jalal DI, Chonchol M, Chen W, Targher G. Uric acid as a target of therapy in CKD. Am J Kidney Dis. 2013;61(1):134-46.
93. Smith CA, Mitchinson MJ, Aruoma OI, Halliwell B. Stimulation of lipid peroxidation and hydroxyl-radical generation by the contents of human atherosclerotic lesions. Biochem J. 1992;286:901-5.

94. Swain J, Gutteridge JMC. Prooxidant iron and copper, with ferroxidase and xanthine oxidase activities in human atherosclerotic material. FEBS lett. 1995;368(3):513-5.
95. Steinbrecher UP, Zhang H, Lougheed M. Role of oxidatively modified LDL in atherosclerosis. Free Radic Biol Med. 1990;9(2):155-68.
96. Frostegård J. Autoimmunity, oxidized LDL and cardiovascular disease. Autoimmun Rev. 2002;1(4):233-7.
97. Kita T, Kume N, Minami M, Hayashida K, Murayama T, Sano H, et al. Role of oxidized LDL in atherosclerosis. Ann N Y Acad Sci. 2001;947(1):199-206.
98. Filipe P, Lanç V, Silva JN, Morlière P, Santus R, Fernandes A. Flavonoids and urate antioxidant interplay in plasma oxidative stress. Mol Cell Biochem. 2001;221(1-2):79-87.
99. Schlotte V, Sevanian A, Hochstein P, Weithmann KU. Effect of uric acid and chemical analogues on oxidation of human low density lipoprotein in vitro. Free Radic Biol Med. 1998;25(7):839-47.
100. Bedard K, Krause K, -H. The NOX family of ROS-generating NADPH oxidases: physiology and pathophysiology. Physiol Rev. 2007;87(1):245-313.
101. Baldwin W, McRae S, Marek G, Wymer D, Pannu V, Baylis C, et al. Hyperuricemia as a mediator of the proinflammatory endocrine imbalance in the adipose tissue in a murine model of the metabolic syndrome. Diabetes. 2011;60(4):1258-69.
102. Böhm F, Pernow J. The importance of endothelin-1 for vascular dysfunction in cardiovascular disease. Cardiovasc Res. 2007;76(1):8-18.
103. Lloyd-Mostyn RH, Lord PS, Glover R, West C, Gilliland IC. Uric acid metabolism in starvation. Ann Rheum Dis. 1970;29(5):553.
104. Men L, Wang Y. The oxidation of yeast alcohol dehydrogenase-1 by hydrogen peroxide in vitro. J Proteome Res. 2007;6(1):216-25.
105. Johnson D, Travis J. The oxidative inactivation of human alpha-1-proteinase inhibitor. Further evidence for methionine at the reactive center. J Biol Chem. 1979;254(10):4022-6.
106. Soehnlein O. Multiple roles for neutrophils in atherosclerosis. Circ Res. 2012;110(6):875-88.
107. Naruko T, Ueda M, Haze K, van der Wal AC, van der Loos CM, Itoh A, et al. Neutrophil infiltration of culprit lesions in acute coronary syndromes. Circulation. 2002;106(23):2894-900.
108. Hampton MB, Kettle AJ, Winterbourn CC. Inside the neutrophil phagosome: oxidants, myeloperoxidase, and bacterial killing. Blood. 1998;92(9):3007-17.
109. Santus R, Patterson LK, Filipe P, Morlière P, Hug GL, Fernandes A, et al. Redox reactions of the urate radical/urate couple with the superoxide radical anion, the tryptophan neutral radical and selected flavonoids in neutral aqueous solutions. Free Radic Res. 2001;35(2):129-36.
110. Repetto M, Boveris A, Semprine J. Lipid peroxidation: chemical mechanism, biological implications and analytical determination: INTECH Open Access Publisher; 2012.
111. Garrod AB. Observations on certain pathological conditions of the blood and urine, in gout, rheumatism, and Bright's disease. Med Chir Trans. 1848;31:83.
112. Conner EM, Grisham MB. Inflammation, free radicals, and antioxidants. Nutrition. 1996;12(4):274-7.
113. von Hohenheim PATB. Das Buch Paragranum / Septem Defensiones. 3rd ed. Peukert W-E, editor. Berlin: CreateSpace Independent Publishing Platform; 2013.

114. Tomaselli GF, Barth AS. Sudden cardio arrest: oxidative stress irritates the heart. Nat Med. 2010;16(6):648-9.
115. Cardoso DR, Franco DW, Olsen K, Andersen ML, Skibsted LH. Reactivity of bovine whey proteins, peptides, and amino acids toward triplet riboflavin as studied by laser flash photolysis. J Agric Food Chem. 2004;52(21):6602-6.
116. Cardoso DR, Homem-de-Mello P, Olsen K, da Silva AB, Franco DW, Skibsted LH. Deactivation of triplet-excited riboflavin by purine derivatives: Important role of uric acid in light-induced oxidation of milk sensitized by riboflavin. J Agric Food Chem. 2005;53(9):3679-84.
117. Noble RW, Gibson QH. The reaction of ferrous horseradish peroxidase with hydrogen peroxide. J Biol Chem. 1970;245(9):2409-13.
118. Hildebrandt AG, Roots I. Reduced nicotinamide adenine dinucleotide phosphate (NADPH)-dependent formation and breakdown of hydrogen peroxide during mixed function oxidation reactions in liver microsomes. Arch Biochem Biophys. 1975;171(2):385-97.
119. Zhou Y-L, Liao J-M, Chen J, Liang Y. Macromolecular crowding enhances the binding of superoxide dismutase to xanthine oxidase: implications for protein–protein interactions in intracellular environments. Int J Biochem Cell Biol. 2006;38(11):1986-94.
120. McCord JM, Fridovich I. The reduction of cytochrome c by milk xanthine oxidase. J Biol Chem. 1968;243(21):5753-60.
121. Banerjee D, Madhusoodanan UK, Sharanabasappa M, Ghosh S, Jacob J. Measurement of plasma hydroperoxide concentration by FOX-1 assay in conjunction with triphenylphosphine. Clin Chim Acta. 2003;337(1):147-52.
122. Townsend DM, Tew KD, Tapiero H. The importance of glutathione in human disease. Biomed Pharmacother. 2003;57(3):145-55.
123. White AC, Thannickal VJ, Fanburg BL. Glutathione deficiency in human disease. J Nutr Biochem. 1994;5(5):218-26.
124. Dröge W. Oxidative stress and ageing: is ageing a cysteine deficiency syndrome? Philos Trans R Soc Lond B Biol Sci. 2005;360(1464):2355-72.
125. Heafield MT, Fearn S, Steventon GB, Waring RH, Williams AC, Sturman SG. Plasma cysteine and sulphate levels in patients with motor neurone, Parkinson's and Alzheimer's disease. Neurosci Lett. 1990;110(1):216-20.
126. Dröge W, Breitkreutz R. Glutathione and immune function. Proc Nutr Soc. 2000;59(04):595-600.
127. Stipanuk MH, Dominy JE, Lee J-I, Coloso RM. Mammalian cysteine metabolism: new insights into regulation of cysteine metabolism. J Nutr. 2006;136(6):1652S-9S.
128. Barford D. The role of cysteine residues as redox-sensitive regulatory switches. Curr Opin Struct Biol. 2004;14(6):679-86.
129. Elias RJ, McClements DJ, Decker EA. Antioxidant activity of cysteine, tryptophan, and methionine residues in continuous phase β-lactoglobulin in oil-in-water emulsions. J Agric Food Chem. 2005;53(26):10248-53.
130. Taylor MJ, Richardson T. Antioxidant activity of cysteine and protein sulfhydryls in a linoleate emulsion oxidized by hemoglobin. J Food Sci. 1980;45(5):1223-7.
131. Bump EA, Brown JM. Role of glutathione in the radiation response of mammalian cells invitro and in vivo. Pharmacol Ther. 1990;47(1):117-36.
132. Younes M, Siegers C-P. Mechanistic aspects of enhanced lipid peroxidation following glutathione depletion in vivo. Chem Biol Interact. 1981;34(3):257-66.
133. Anundi I, Högberg J, Stead AH. Glutathione depletion in isolated hepatocytes: its relation to lipid peroxidation and cell damage. Acta Pharmacol Toxicol. 1979;45(1):45-51.

134. Bellomo G, Orrenius S. Altered thiol and calcium homeostasis in oxidative hepatocellular injury. Hepatology. 1985;5(5):876-82.
135. Higuchi Y. Glutathione depletion‐induced chromosomal DNA fragmentation associated with apoptosis and necrosis. J Cell Mol Med. 2004;8(4):455-64.
136. Kidd PM. Natural antioxidants—first line of defense. In: Kidd PM, Huber W, editors. Living with the AIDS Virus: A Strategy for Long-Term Survival. Albany, California: PMK Biomedical-Nutritional Consulting; 1991. p. 115-42.
137. Haddad JJ. Glutathione depletion is associated with augmenting a proinflammatory signal: evidence for an antioxidant/pro-oxidant mechanism regulating cytokines in the alveolar epithelium. Cytokines Cell Mol Ther. 2000;6(4):177-87.
138. Rahman I, MacNee W. Oxidative stress and regulation of glutathione in lung inflammation. Eur Clin Respir J. 2000;16(3):534-54.
139. Rahman I, MacNee W. Regulation of redox glutathione levels and gene transcription in lung inflammation: therapeutic approaches. Free Radic Biol Med. 2000;28(9):1405-20.
140. Marcinkiewicz J, Grabowska A, Bereta J, Stelmaszynska T. Taurine chloramine, a product of activated neutrophils, inhibits in vitro the generation of nitric oxide and other macrophage inflammatory mediators. J Leukoc Biol. 1995;58(6):667-74.
141. Klamt F, Shacter E. Taurine chloramine, an oxidant derived from neutrophils, induces apoptosis in human B lymphoma cells through mitochondrial damage. J Biol Chem. 2005;280(22):21346-52.
142. Peskin AV, Winterbourn CC. Kinetics of the reactions of hypochlorous acid and amino acid chloramines with thiols, methionine, and ascorbate. Free Radic Biol Med. 2001;30(5):572-9.
143. Peskin AV, Winterbourn CC. Taurine chloramine is more selective than hypochlorous acid at targeting critical cysteines and inactivating creatine kinase and glyceraldehyde-3-phosphate dehydrogenase. Free Radic Biol Med. 2006;40(1):45-53.
144. Ellman GL. Tissue sulfhydryl groups. Arch Biochem Biophys. 1959;82(1):70-7.
145. Dypbukt JM, Bishop C, Brooks WM, Thong B, Eriksson H, Kettle AJ. A sensitive and selective assay for chloramine production by myeloperoxidase. Free Radic Biol Med. 2005;39(11):1468-77.
146. Reszka KJ, Matuszak Z, Chignell CF, Dillon J. Oxidation of biological electron donors and antioxidants by a reactive lactoperoxidase metabolite from nitrite (NO 2−): an EPR and spin trapping study. Free Radic Biol Med. 1999;26(5):669-78.
147. Mason RP, Rao DN. Thiyl free radical metabolites of thiol drugs, glutathione, and proteins. Methods Enzymol. 1990;186:318.
148. Svensson BE, Gräslund A, Ström G, Moldeus P. Thiols as peroxidase substrates. Free Radic Biol Med. 1993;14(2):167-75.
149. Pommier J, Cahnmann HJ. Interaction of lactoperoxidase with thiols and diiodotyrosine. J Biol Chem. 1979;254(8):3006-10.
150. Munday R. Toxicity of thiols and disulphides: involvement of free-radical species. Free Radic Biol Med. 1989;7(6):659-73.
151. Mansoor MA, Svardal AM, Ueland PM. Determination of the in vivo redox status of cysteine, cysteinylglycine, homocysteine, and glutathione in human plasma. Anal Biochem. 1992;200(2):218-29.
152. Hwang CJSA, Sinskey AJ, Lodish HF. Oxidized redox state of glutathione in the endoplasmic reticulum. Science. 1992;257(5076):1496-502.
153. Brocklehurst K. Specific covalent modification of thiols: applications in the study of enzymes and other biomolecules. Int J Biochem. 1979;10(4):259-74.

154. Klomsiri C, Karplus PA, Poole LB. Cysteine-based redox switches in enzymes. Antioxid Redox Signal. 2011;14(6):1065-77.
155. Maret W, Jacob C, Vallee BL, Fischer EH. Inhibitory sites in enzymes: zinc removal and reactivation by thionein. Proc Natl Acad Sci. 1999;96(5):1936-40.
156. Mazzola JL, Sirover MA. Alteration of intracellular structure and function of glyceraldehyde-3-phosphate dehydrogenase: a common phenotype of neurodegenerative disorders? Neurotoxicology. 2002;23(4):603-9.
157. Arutyunova EI, Danshina PV, Domnina LV, Pleten AP, Muronetz VI. Oxidation of glyceraldehyde-3-phosphate dehydrogenase enhances its binding to nucleic acids. Biochem Biophys Res Commun. 2003;307(3):547-52.
158. Furfine CS, Velick SF. The acyl-enzyme intermediate and the kinetic mechanism of the glyceraldehyde 3-phosphate dehydrogenase reaction. J Biol Chem. 1965;240(2):844-55.
159. Segal HL, Boyer PD. The role of sulfhydryl groups in the activity of D-glyceraldehyde 3-phosphate dehydrogenase. J Biol Chem. 1953;204(1):265-81.
160. Velick SF, Hayes JE. Phosphate binding and the glyceraldehyde-3-phosphate dehydrogenase reaction. J Biol Chem. 1953;203(2):545-62.
161. Hill EJ, Chou TH, Shih MC, Park JH. Covalent binding of 3-pyridinealdehyde nicotinamide adenine dinucleotide and substrate to glyceraldehyde 3-phosphate dehydrogenase. J Biol Chem. 1975;250(5):1734-40.
162. Rodriguez CE, Fukuto JM, Taguchi K, Froines J, Cho AK. The interactions of 9, 10-phenanthrenequinone with glyceraldehyde-3-phosphate dehydrogenase (GAPDH), a potential site for toxic actions. Chem Biol Interact. 2005;155(1):97-110.
163. Danshina PV, Schmalhausen EV, Avetisyan AV, Muronetz VI. Mildly Oxidized Glyceraldehyde‐3‐Phosphate Dehydrogenase as a Possible Regulator of Glycolysis. IUBMB life. 2001;51(5):309-14.
164. Biteau B, Labarre J, Toledano MB. ATP-dependent reduction of cysteine–sulphinic acid by S. cerevisiae sulphiredoxin. Nature. 2003;425(6961):980-4.
165. Dietze EC, Schäfer A, Omichinski JG, Nelson SD. Inactivation of glyceraldehyde-3-phosphate dehydrogenase by a reactive metabolite of acetaminophen and mass spectral characterization of an arylated active site peptide. Chem Res Toxicol. 1997;10(10):1097-103.
166. Chen Y, He R, Liu Y, Xue Z. Effect of human neuronal tau on denaturation and reactivation of rabbit muscle D-glyceraldehyde-3-phosphate dehydrogenase. Biochem J. 2000;351:233-40.
167. Seidler NW. GAPDH and Intermediary Metabolism. GAPDH: Biological Properties and Diversity: Biological Properties and Diversity. 985. Kansas City, MO, USA: Springer Science & Business Media; 2012. p. 38-56.
168. Hald E, Lehmann P, Ziegenhorn J. Molar Absorptivities of β-NADH and β-NAD at 260 nm. Clin chem. 1975;21(7):884-7.
169. Laemmli UK. Cleavage of structural proteins during the assembly of the head of bacteriophage T4. Nature. 1970;227(5259):680-5.
170. Schägger H. Tricine–SDS-PAGE. Nat Protoc. 2006;1:16-22.
171. Mann M, Hendrickson RC, Pandey A. Analysis of proteins and proteomes by mass spectrometry. Annu Rev Biochem. 2001;70(1):437-73.
172. Birkett DJ. Mechanism of inactivation of rabbit muscle glyceraldehyde 3-phosphate dehydrogenase by ethacrynic acid. Mol Pharmacol. 1973;9(2):209-18.
173. Bode J, Blumenstein M, Raftery MA. Nonidentical alkylation sites in rabbit muscle glyceraldehyde-3-phosphate dehydrogenase. Biochemistry. 1975;14(6):1146-52.

174. Keele BB, McCord JM, Fridovich I. Further characterization of bovine superoxide dismutase and its isolation from bovine heart. J Biol Chem. 1971;246(9):2875-80.
175. Schroeder WA, Shelton JR, Shelton JB, Robberson B, Apell G. The amino acid sequence of bovine liver catalase: a preliminary report. Arch Biochem Biophys. 1969;131(2):653-5.
176. Rombauts WA, Schroeder WA, Morrison M. Bovine Lactoperoxidase. Partial Characterization of the Further Purified Protein*. Biochemistry. 1967;6(10):2965-77.
177. Waud WR, Brady FO, Wiley RD, Rajagopalan KV. A new purification procedure for bovine milk xanthine oxidase: effect of proteolysis on the subunit structure. Arch Biochem Biophys. 1975;169(2):695-701.
178. Kolarich D, Weber A, Turecek PL, Schwarz HP, Altmann F. Comprehensive glyco‐proteomic analysis of human α1‐antitrypsin and its charge isoforms. Proteomics. 2006;6(11):3369-80.
179. Price KL, Sautin YY, Long DA, Zhang L, Miyazaki H, Mu W, et al. Human vascular smooth muscle cells express a urate transporter. Journal of the American Society of Nephrology. 2006;17(7):1791-5.

Appendix 1: Supplementary Figures

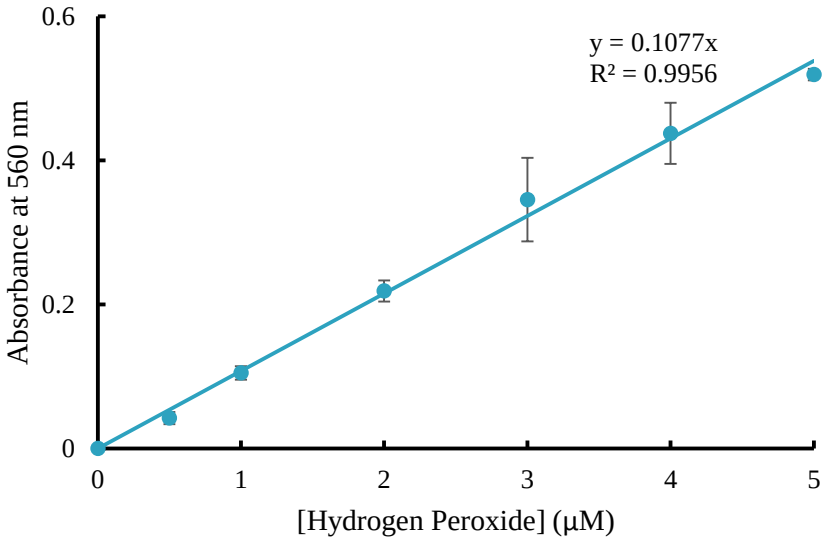

Figure 32: Standard curve for the FOX assay based on H_2O_2 absorbance at 560 nm. The absorbance of hydrogen peroxide was linear at 560 nm. This standard curve was used to determine the concentration of urate hydroperoxide with the FOX assay. The assumption must be made that urate hydroperoxide oxidized Fe^{2+} at the same stoichiometry as hydrogen peroxide. This graph was the mean of three experiments. The error bars represented the standard deviation of three experiments.

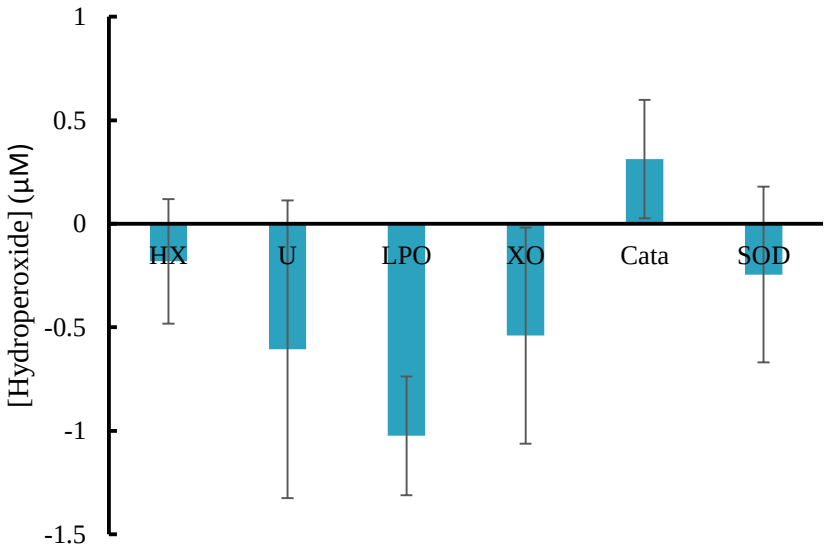

Figure 33: FOX assay of each substance required to form urate hydroperoxide. The final concentration of substances were: 100 µM hypoxanthine, 100 µM urate, 200 nM lactoperoxidase 0.9 µM xanthine oxidase, 100 µg/mL catalase and 10 µg/mL superoxide dismutase. None of the substances produced a significant concentration of hydroperoxide compared to the phosphate buffer control. This graph was the mean of two experiments. The error bars represented the standard deviation for the two experiments. One-way ANOVA followed by Holm-Sidak multiple comparison was performed on the mean of two experiments to identify samples that were significantly different from phosphate buffer (* $p < 0.05$).

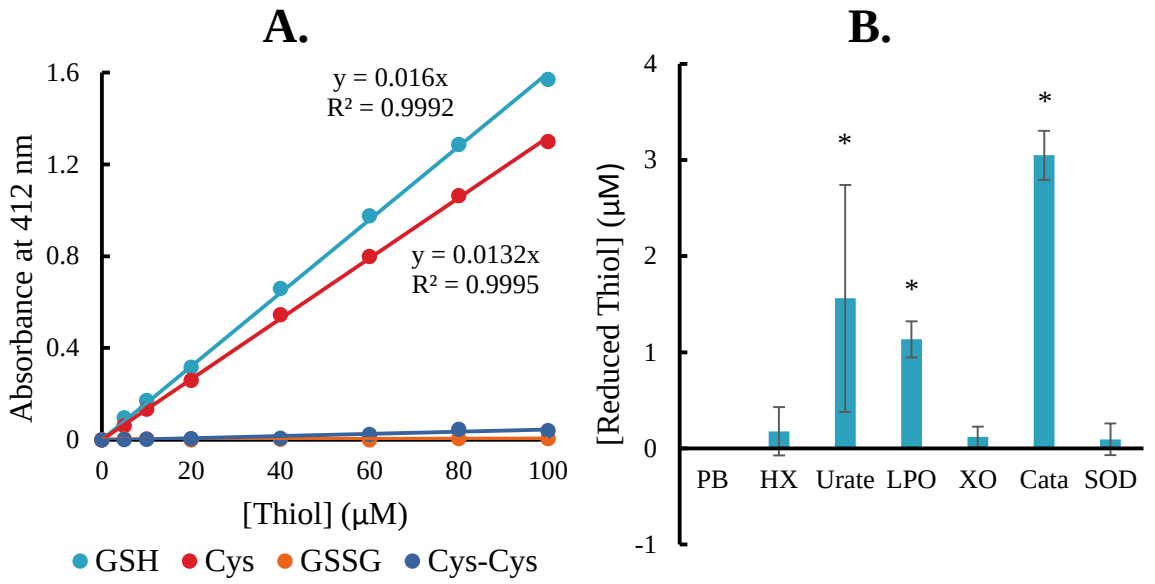

Figure 34: Thiol standard curve and xanthine oxidase/lactoperoxidase system controls with the DTNB assay. **A.** Standard curve for DTNB absorbance at 412 nm vs. concentration of cysteine, glutathione, cystine and glutathione disulfide. Cysteine and glutathione produce linear absorbance at 415 nm. The absorbance for cystine and glutathione was negligible. **B.** DTNB assay of all substances of the xanthine oxidase/lactoperoxidase system: 50 mM phosphate buffer, 78 µM hypoxanthine, 195 µM urate, 156 nM lactoperoxidase, 1.4 µM xanthine oxidase, 78 µg/mL catalase and 7.8 µg/mL superoxide dismutase. The absorbance of hypoxanthine, xanthine oxidase and superoxide were negligible. The absorbance for urate, lactoperoxidase and catalase were small but significant. These graphs represented one experiment. The error bars represented the standard deviation for triplicate readings. One-way ANOVA followed by Holm-Sidak multiple comparison on triplicate readings was used to identify samples that were significantly different from phosphate buffer (* $p < 0.05$).

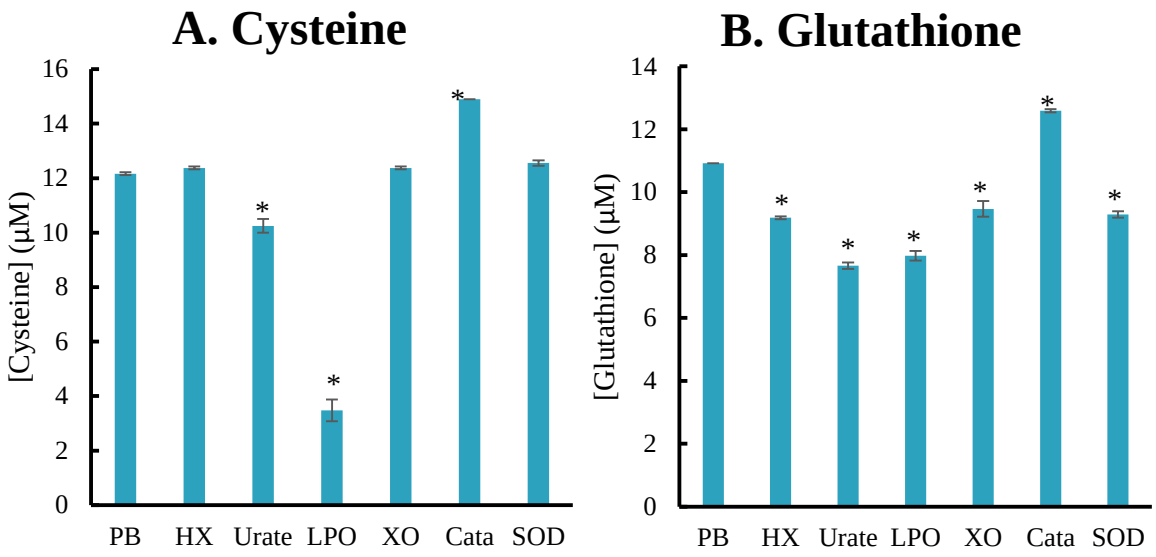

Figure 35: Depletion of free thiols by urate hydroperoxide controls. **A.** DTNB assay of depletion of cysteine by the substances of the xanthine oxidase/lactoperoxidase system. Hypoxanthine, xanthine oxidase and superoxide dismutase did not significantly affect the cysteine concentration. However, lactoperoxidase depleted three quarters of cysteine. Catalase caused a 1 µM increase in reduced thiol concentration due to its interaction with DTNB. **B.** DTNB assay of depletion of glutathione by the substances used of the xanthine oxidase/lactoperoxidase system. Catalase caused a 1 µM increase in reduced thiol concentration, whereas all other substances caused a 1 µM loss. These graphs were representative of two experiments. Error bars were based standard deviation for triplicate readings. One-way ANOVA followed by Holm-Sidak multiple comparison on triplicate readings was used to identify samples that were significantly different from thiols in phosphate buffer (* $p < 0.05$).

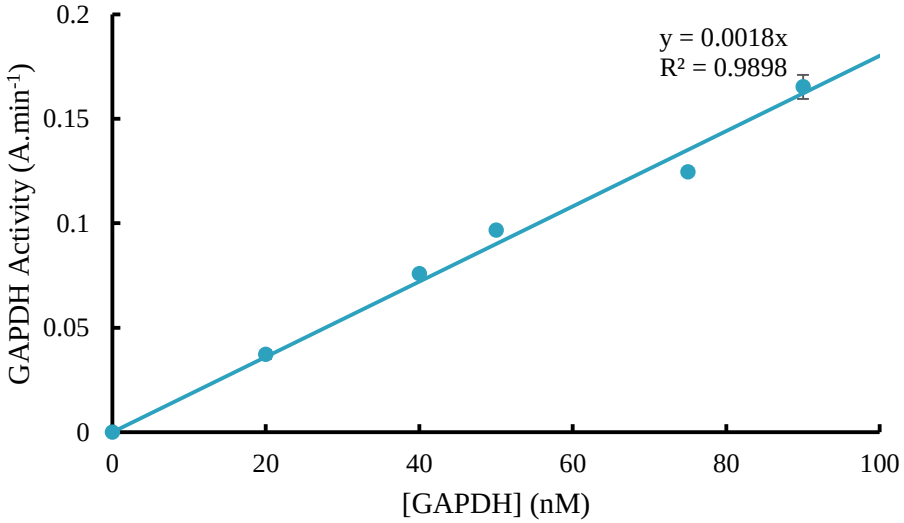

Figure 36: Standard curve for GAPDH concentration vs. initial activity. The assay cuvette contained 2 mM DTT. Initial GAPDH activity increased linearly with enzyme concentration. The concentration of GAPDH used for proceeding assays were > 60 nM. This graph represented one experiment. The error bars represented the standard deviation for triplicate readings.

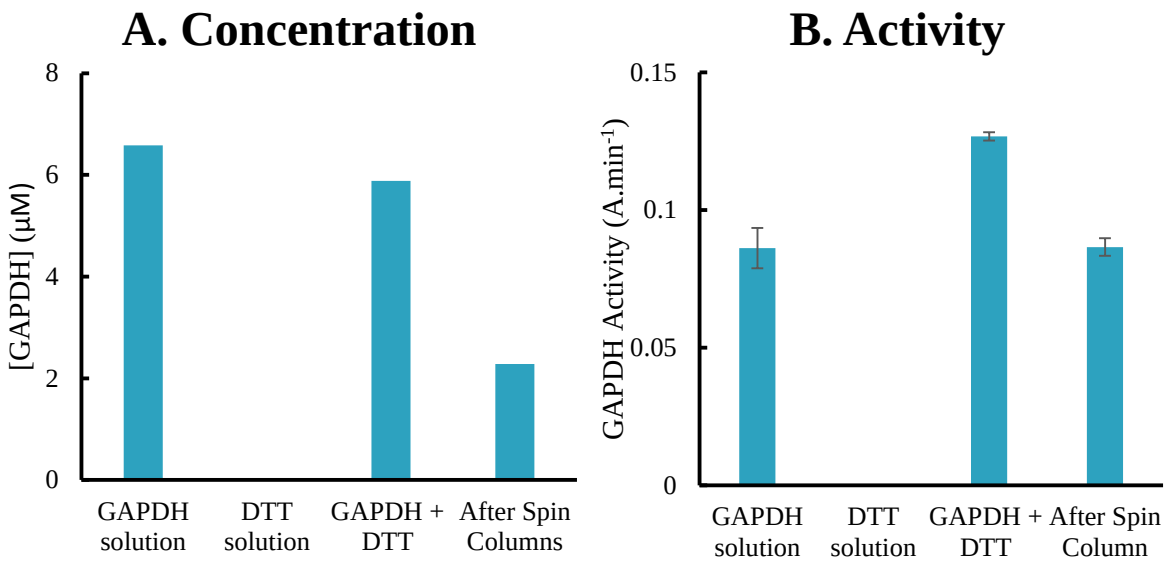

Figure *37*: GAPDH concentration and activity during spin column preparation. **A.** GAPDH concentration during spin column preparation. A small dilution was seen with DTT treatment. Two thirds of GAPDH was lost when the protein was isolated with spin columns. **B.** GAPDH activity during spin column preparation. GAPDH activity increased significantly when the enzyme was treated with DTT. Following isolation with spin columns, the GAPDH activity dropped due to the loss of protein. Reduction of GAPDH with DTT was necessary to achieve a measurable activity, even though a significant amount of protein was lost. These graphs represented one experiment. The error bars represented the standard deviation for triplicate readings.

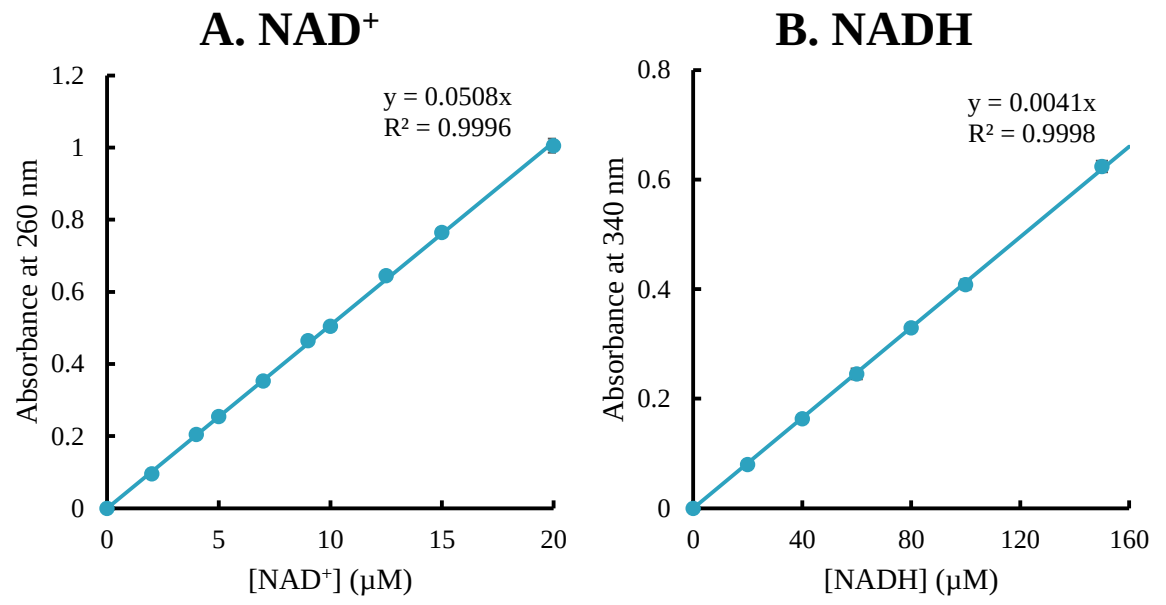

Figure 38: NAD standard curves for absorbance at 260 and 340 nm. A. NAD^+ standard curve at 260 nm. NAD^+ absorbance was linear with extinction coefficient 50,800 M^{-1} cm^{-1}, absorbance at 340 nm was negligible**. B.** NADH standard curve at 340 nm. NADH absorbance was linear with the extinction coefficient 4,100 M^{-1} cm^{-1}. Absorbance at 340 nm was exclusive to NADH, hence it can be used to show the loss or formation of this oxidation state. These graphs represented one experiment and error bars represented standard deviation for triplicate readings.

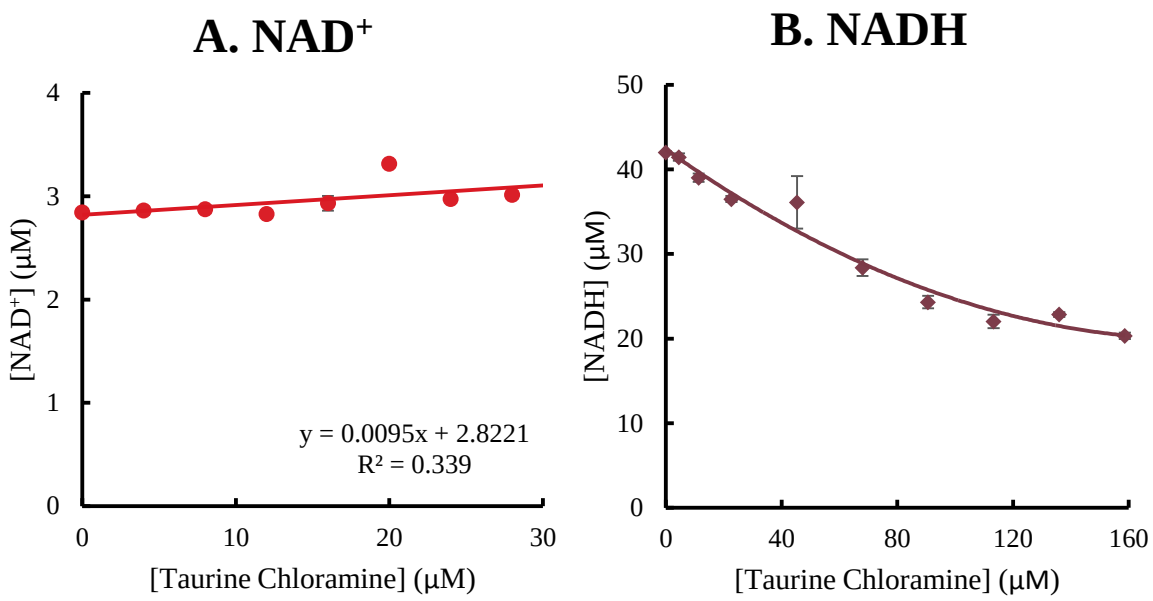

Figure 39: Dose-dependent exposure of NAD to taurine chloramine. **A.** Treatment of NAD^+ to taurine chloramine at 260 nm. Taurine chloramine did not significantly change the absorbance at 260 or 340 nm, hence taurine chloramine does not reduce this cofactor. **B.** Treatment of NADH to taurine chloramine at 340 nm. Taurine chloramine caused a loss of absorbance for NADH which plateaued at half of the initial absorbance. The initial ratio of depletion for NADH to taurine chloramine was 1:2. High concentrations (> 80 μM) were required to deplete half of NADH. The interaction of taurine chloramine with NAD would not significantly affect the GAPDH assay since the concentrations of these substances were low. These graphs represented one experiment and the error bars are standard deviation for triplicate readings.

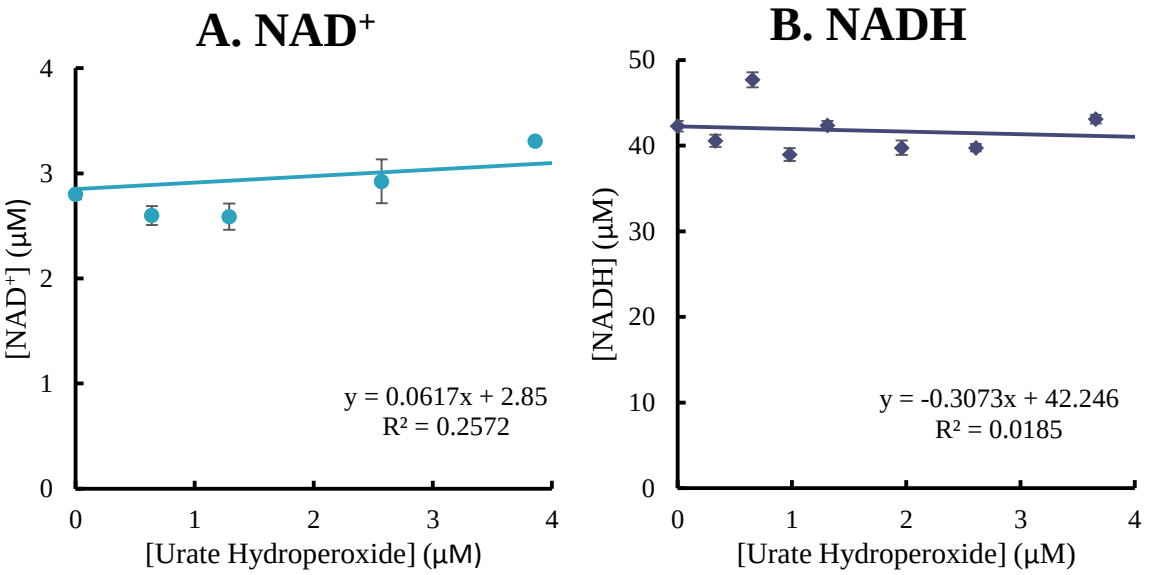

Figure 40: Dose-dependent exposure of NAD to urate hydroperoxide. **A.** Dose-dependent treatment of NAD^+ with urate hydroperoxide and measurement of absorbance at 260 nm. **B.**: Dose-dependent treatment of NADH with urate hydroperoxide and measurement of absorbance at 340 nm. Urate hydroperoxide did not significantly change the absorbance at 260 or 340 nm for either oxidative states. Urate hydroperoxide does not seem to oxidatively interact with either of these molecules at concentrations that could be formed during exposure of GAPDH to urate hydroperoxide. These graphs represented one experiment. The error bars represented the standard deviation for triplicate readings.

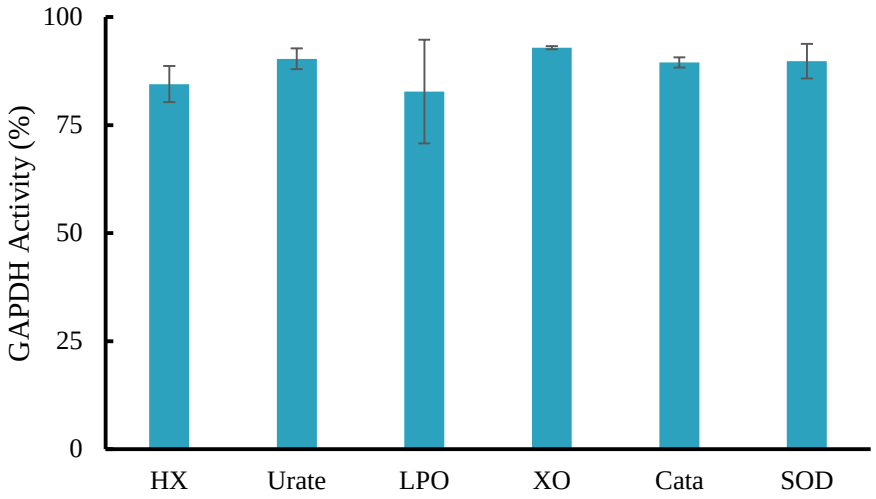

Figure 41: GAPDH activity following exposure to the substances of the xanthine oxidase/lactoperoxidase system. GAPDH in phosphate buffer represented 100% activity. The concentration of substances was the same as later experiments where GAPDH was treated with urate hydroperoxide: 90 µM hypoxanthine, 360 µM urate, 190 nM lactoperoxidase, 1.6 µM xanthine oxidase. All substances had > 80% activity compared with the phosphate buffer control. This graphs represented one experiment. The error bars represented the standard deviation for triplicate readings. One-way ANOVA followed by Holm-Sidak multiple comparison on triplicate readings was used to identify samples that were significantly different from the phosphate buffer control (* p <0.05).

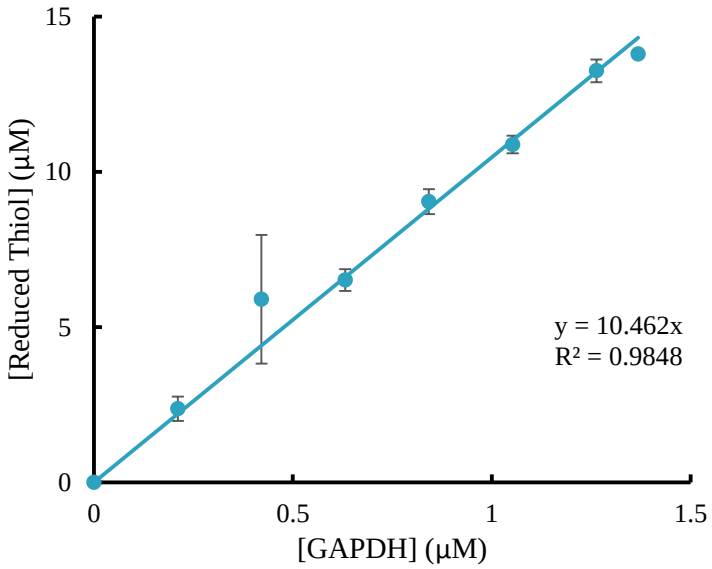

Figure 42: Standard curve of GAPDH concentration vs. reduced thiol concentration during the DTNB assay in a quartz cuvette. Approximately 12 thiols per micromolar GAPDH were measured. This equated to 12 cysteine residues per GAPDH tetramer. GAPDH has four cysteine residues per subunit, hence four thiols per GAPDH tetramer did not react with DTNB under these conditions. These graphs represented one experiment. The error bars represented the standard deviation for triplicate readings.

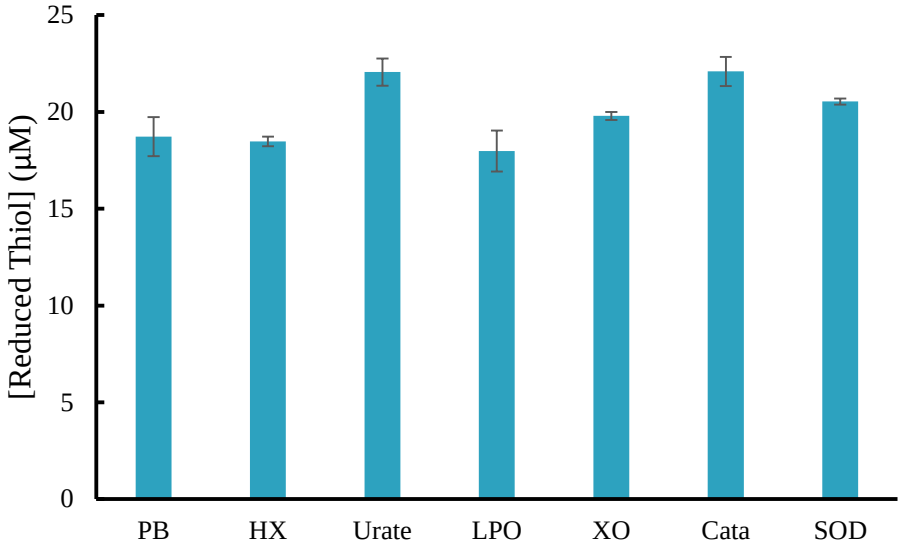

Figure 43: Depletion of cysteine residues on GAPDH by the xanthine oxidase/lactoperoxidase system. GAPDH (3 µM) was incubated with 50 mM phosphate buffer, 90 µM hypoxanthine, 360 µM urate, 190 nM lactoperoxidase, 1.7 µM xanthine oxidase, 95 µg/mL catalase and 9.5 µg/mL superoxide dismutase. The DTNB assay was performed in quartz cuvettes. Compared with phosphate buffer, hypoxanthine and lactoperoxidase had no effect on the reduced thiol concentration. Urate, xanthine oxidase, catalase and superoxide dismutase increased the reduced thiol concentration. One-way ANOVA followed by Holm-Sidak multiple comparison on triplicate readings was used to identify samples that were significantly different from GAPDH in phosphate buffer (* $p < 0.05$).

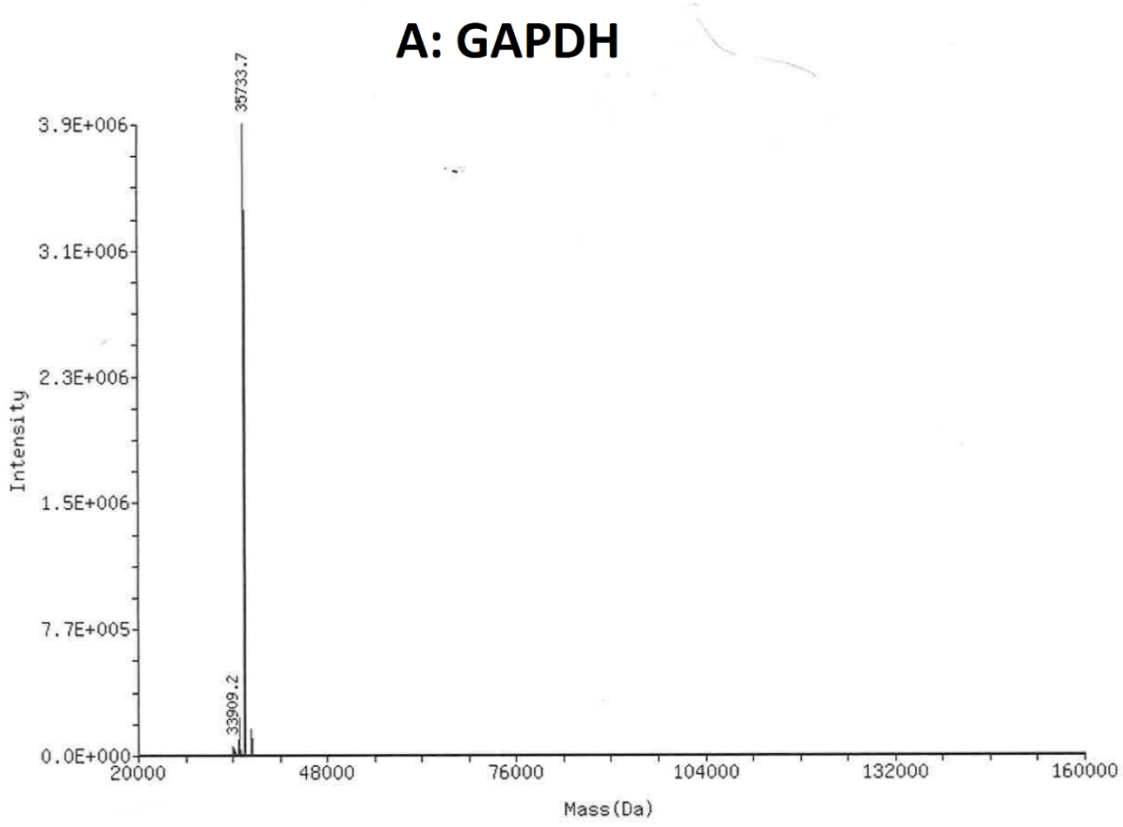

B: GAPDH + DTT

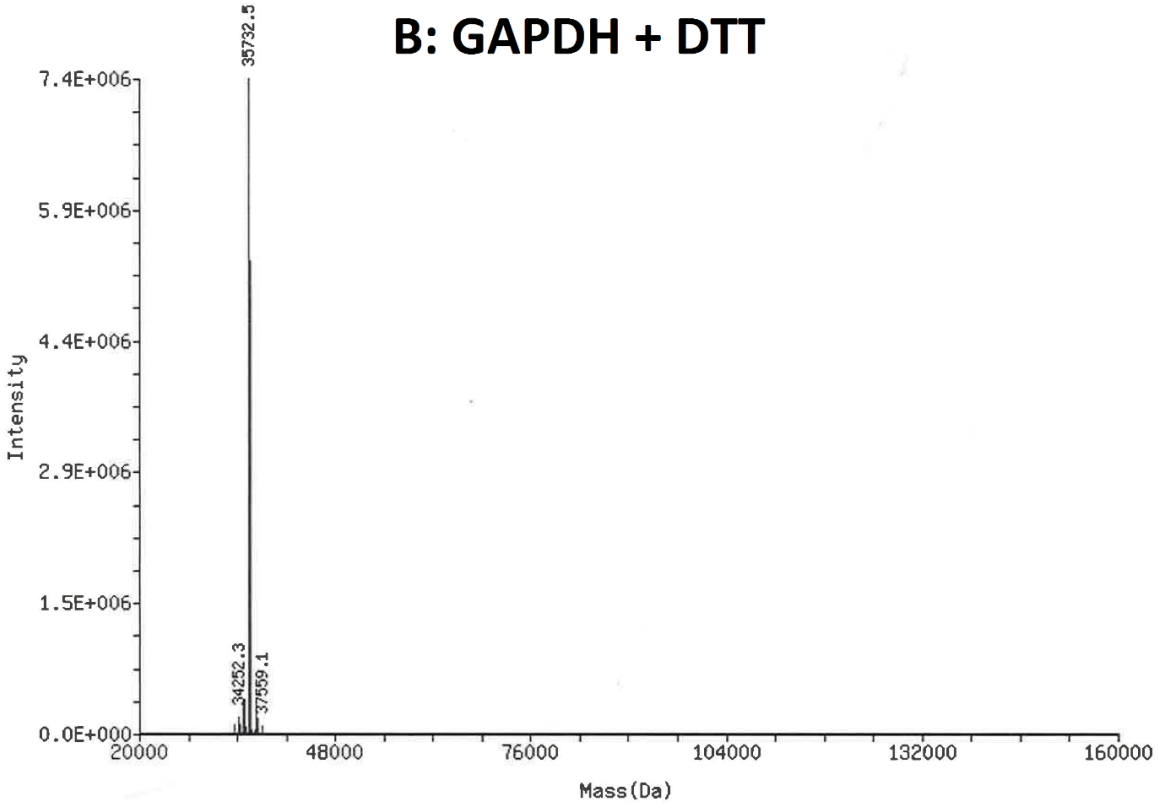

C: GAPDH + Urate Hydroperoxide

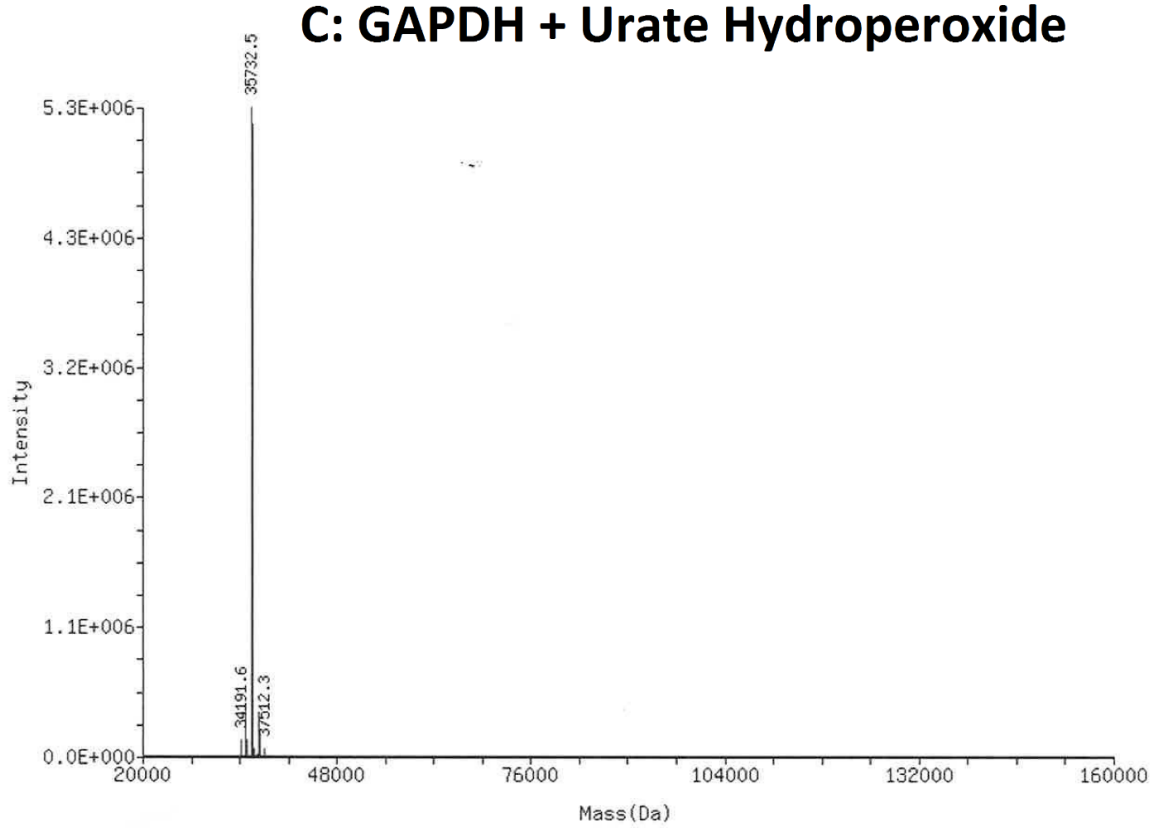

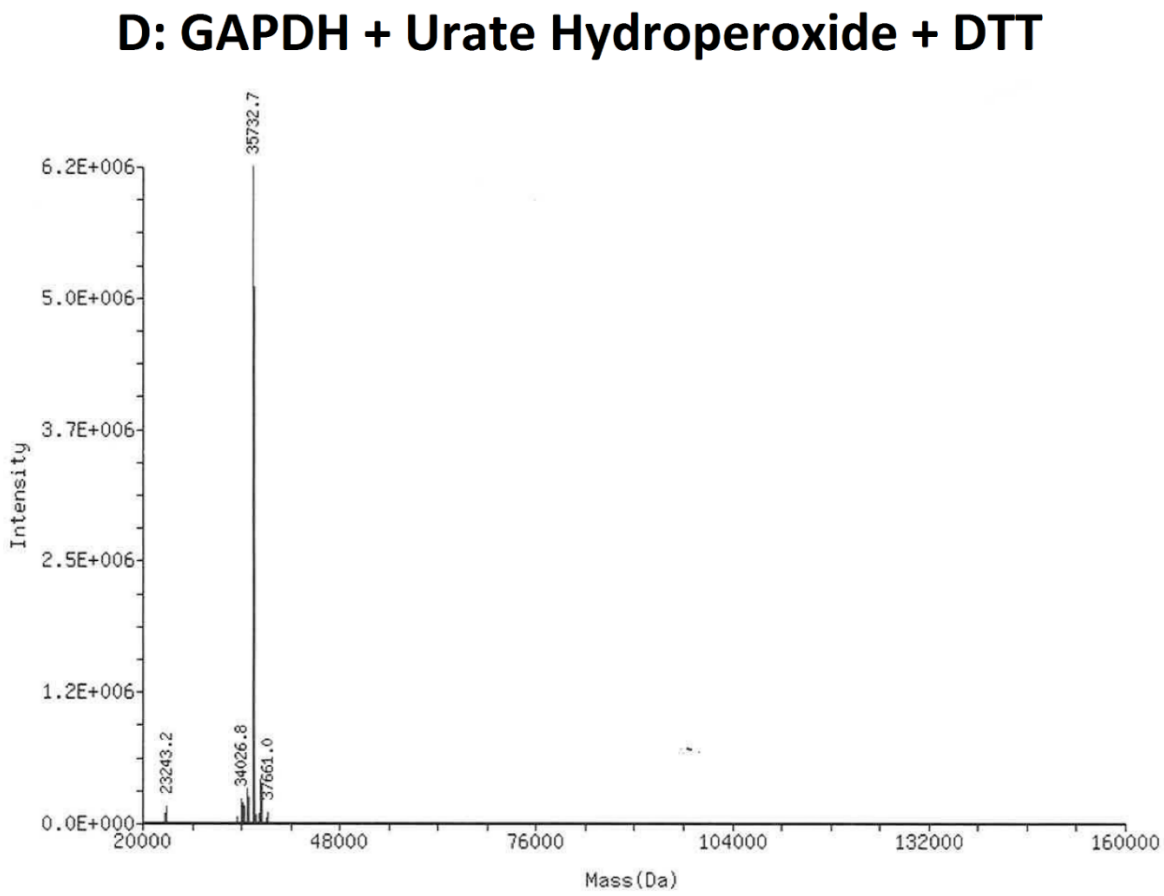

Figure 44: Mass Spectrum for the GAPDH and urate hydroperoxide experiment treated with urate hydroperoxide (1:1 ratio). A: GAPDH isolated with spin columns. **B:** GAPDH reduced DTT. **C:** GAPDH exposed to urate hydroperoxide. **D:** GAPDH exposed to urate hydroperoxide and reduced with DTT. These graphs represented one experiment.

Appendix 2: Supplementary Methods and Materials

5.1 Chapter 2

Table 6*:* Volumes of substances used for the FOX assay of urate hydroperoxide formation. Each sample represented the full system, removal of a substance or addition of superoxide dismutase. When urate hydroperoxide formation was complete the FOX reagent was added.

		Substance Used	A: **Without HX**	B: **Without Urate**	C: **Without LPO**	D: **Without XO**	E: **Full System**	F: **With SOD**
Volumes of Substances used (µL)	Reaction System. Final vol. 300 µL	10 mM HX	-	3	3	3	3	3
		1 mM Urate	30	-	30	30	30	30
		5.7 µM LPO	17	17	-	17	17	17
		90 µM XO	3	3	3	-	3	3
		50 mM PB	250	250	277	264	247	244
		0.2 mg/mL SOD	-	-	-	-	-	3
	Stop Reaction. Vol. 306 µL	2 mg/mL Cata	3	3	3	3	3	3
		0.2 mg/mL SOD	3	3	3	3	3	3
	FOX assay. Vol. 408 µL	FOX Reagent	102	102	102	102	102	102

5.2 Chapter 3

Table 7: Samples made for the xanthine oxidase/lactoperoxidase system which was subsequently used to treat 70 µM cysteine or 30 µM glutathione. Samples A-G represented the full system or controls where each substance was removed or quencher added. After 10 min incubation the reaction was stopped with catalase and superoxide dismutase. Samples (780 µL) were transferred into plastic cuvettes with cysteine or glutathione.

		Xanthine Oxidase/Lactoperoxidase System Samples							
		Substance Used	A: **Without HX**	B: **Without Urate**	C: **Without LPO**	D: **Without XO**	E: **Full System**	F: **With SOD**	G: **With Cata**
Vol. used (µL)	Reaction System. Final vol. 3,300µL	10 mM HX	-	33	33	33	33	33	33
		1 mM Urate	825	-	825	825	825	825	825
		5.7 µM LPO	115.8	115.8	-	115.8	115.8	115.8	115.8
		90 µM XO	66	66	66	-	66	66	66
		50 mM PB	2293.2	3085.2	2376	2326.2	2260.2	2095.2	2095.2
		0.2 mg/mL SOD	-	-	-	-	-	165	-
		2 mg/mL Cata	-	-	-	-	-	-	165
	Stop Reaction.	2 mg/mL Cata	165	165	165	165	165	165	165
	Final vol. 3,630 µL	0.2 mg/mL SOD	165	165	165	165	165	165	165

Table 8: Samples made for dose-dependent treatment of cysteine and glutathione with taurine chloramine. Taurine chloramine (20 µM) was mixed at an increasing volume to 25 µM cysteine or 15 µM glutathione. The volume of each sample was equalled with phosphate buffer. After10 min the DTNB assay was performed.

		Final Concentrations (µM)		Volumes in Plastic Cuvettes (µL)			
Taurine Chloramine Depletion of Cysteine	**Sample**	**[Tau-Cl]**	**[Cys]**	**125 µM Cys**	**20 µM Tau-Cl**	**50 mM PB**	**10 mM DTNB**
	Blank	0	0	0	0	980	20
	PB Control	0	25	200	0	780	20
	Tau-Cl Control	15.6	0	0	780	0	20
	1	2	25	200	100	680	20
	2	4	25	200	200	580	20
	3	6	25	200	300	480	20
	4	8	25	200	400	380	20
	5	10	25	200	500	280	20
	6	12	25	200	600	180	20
	7	15.6	25	200	780	0	20
Taurine Chloramine Depletion of Glutathione	**Sample**	**[Tau-Cl]**	**[GSH]**	**75 µM GSH**	**20 µM Tau-Cl**	**50 mM PB**	**10 mM DTNB**
	PB Control	0	15	200	0	780	20
	8	2	15	200	100	680	20
	9	4	15	200	200	580	20
	10	6	15	200	300	480	20
	11	8	15	200	400	380	20
	12	10	15	200	500	280	20
	13	12	15	200	600	180	20
	14	15.6	15	200	780	0	20

Table 9: Samples made for dose-dependent exposure of glutathione to urate hydroperoxide. An increasing volume of urate hydroperoxide was added to 30 µM glutathione. The volume was equalled with phosphate buffer. Control samples, with the xanthine oxidase/lactoperoxidase system without hypoxanthine, were made to match urate hydroperoxide samples. After 10 min incubation the DTNB assay was performed.

Samples		**Final Concentrations (µM)**		**Volumes in Plastic Cuvettes (µL)**				
		[UHP]	**[GSH]**	**150 µM GSH**	**UHP solution**	**UHP Control Solution (w/o HX)**	**PB**	**10 mM DTNB**
Control Samples	Blank	0	0	0	0	-	980	20
	PB Control	0	30	200	0	-	780	20
	1	0	30	200	-	100	680	20
	2	0	30	200	-	200	580	20
	3	0	30	200	-	300	480	20
	4	0	30	200	-	400	380	20
	5	0	30	200	-	500	280	20
	6	0	30	200	-	600	180	20
	7	0	30	200	-	780	0	20
UHP Samples	UHP Control	9.1	0	200	780	-	0	20
	8	1.2	30	200	100	-	680	20
	9	2.3	30	200	200	-	580	20
	10	3.5	30	200	300	-	480	20
	11	4.7	30	200	400	-	380	20
	12	5.9	30	200	500	-	280	20
	13	7	30	200	600	-	180	20
	14	9.1	30	200	780	-	0	20

5.3 Chapter 4

Table 10: Xanthine oxidase/lactoperoxidase system in the quartz cuvette during continuous inactivation of GAPDH. These substances were accompanied by the substances for the GAPDH assay. The two initiators, xanthine oxidase and GAPDH, were added last to start both systems.

		Quartz Cuvette Samples							
	Substance Used	1: **TEA**	2: **Without HX**	3: **Without Urate**	4: **Without LPO**	5: **Without XO**	6: **Full System**	7: **With SOD**	8: **With Cata**
Vol. used (µL)	50 mM TEA Buffer	830	525	765	550	353	515	465	465
	10 mM HX	-	-	10	10	10	10	10	10
	1 mM Urate	-	250	-	250	250	250	250	250
	5.7 µM LPO	-	35	35	-	35	35	35	35
	90 µM XO	-	20	20	20	-	20	20	20
	0.2 mg/mL SOD	-	-	-	-	-	-	50	-
	2 mg/mL Cata	-	-	-	-	-	-	-	50

Table 11: Xanthine oxidase/lactoperoxidase system samples used to treat GAPDH. Samples A-G represented the xanthine oxidase/lactoperoxidase system with controls where each substance removed or quenchers were added. After 20 min incubation the formation of urate hydroperoxide was stopped with catalase and superoxide dismutase.

		Xanthine Oxidase/Lactoperoxidase System Samples						
	Substance Used	A: **Without HX**	B: **Without Urate**	C: **Without LPO**	D: **Without XO**	E: **Full System**	F: **With SOD**	G: **With Cata**
Reaction System final vol. 300µL	10 mM HX	-	3	3	3	3	3	3
	1 mM Urate	120	-	120	120	120	120	120
	5 µM LPO	12	12	-	12	12	12	12
	90 µM XO	6	6	6	-	6	6	6
	50 mM PB	279	159	171	165	159	144	144
	0.2 mg/mL SOD	-	-	-	-	-	15	-
	2 mg/mL Cata	-	-	-	-	-	-	15
Stop Reaction	2 mg/mL Cata	14	14	14	14	14	14	14
Final vol. 328 µL	0.2 mg/mL SOD	14	14	14	14	14	14	14

Table 12: Sample composition for GAPDH reactivation experiment following inactivation by taurine chloramine. This experiment involved two sets of samples to represent before and after DTT treatment. The concentration of taurine chloramine was varied by adding different volumes of a 20 µM solution and equalling the volume with catalase-treated phosphate buffer.

` Samples		**Final Concentration of Substances (µM)**			**Volume of Substances used (µL)**			
		[Tau-Cl]	[GAPDH]	[DTT]	10 µM GAPDH	20 µM Tau-Cl	50 mM Cata-treated PB	0.1 M DTT
GAPDH Inactivation Controls	Tau-Cl Control	18	0	0	0	180	4	0
	1	3	1	0	20	30	154	0
	2	6	1	0	20	60	124	0
	3	9	1	0	20	90	94	0
	4	12	1	0	20	120	64	0
	5	15	1	0	20	150	34	0
	6	18	1	0	20	180	4	
DTT Treated	Tau-Cl Control	18	0	0	0	180	0	4
	PB Control	0	1	200	20	0	180	4
	7	3	1	200	20	30	150	4
	8	6	1	200	20	60	120	4
	9	9	1	200	20	90	90	4
	10	12	1	200	20	120	60	4
	11	15	1	200	20	150	30	4
	12	18	1	200	20	180	0	4

Table 13: Sample composition for the GAPDH reactivation experiment following inactivation by urate hydroperoxide. This experiment involved two sets of samples to represent before and after DTT treatment. The concentration of urate hydroperoxide was varied by adding different volumes of a 7 µM solution and equalling the volume with catalase-treated phosphate buffer.

` Samples		Final Concentration of Substances (µM)			Volume of Substances used (µL)			
		[UHP]	[GAPDH]	[DTT]	10 µM GAPDH	7 µM UHP	50 mM Cata-treated PB	0.1 M DTT
GAPDH Inactivation Controls	UHP Control	5.7	0	0	0	180	4	0
	1	0.9	1	0	20	30	154	0
	2	1.9	1	0	20	60	124	0
	3	2.8	1	0	20	90	94	0
	4	3.8	1	0	20	120	64	0
	5	4.7	1	0	20	150	34	0
	6	5.7	1	0	20	180	4	
DTT Treated	UHP Control	5.7	0	0	0	180	0	4
	PB Control	0	1	200	20	0	180	4
	7	0.9	1	200	20	30	150	4
	8	1.9	1	200	20	60	120	4
	9	2.8	1	200	20	90	90	4
	10	3.8	1	200	20	120	60	4
	11	4.7	1	200	20	150	30	4
	12	5.7	1	200	20	180	0	4

5.3.1 Mass Spectrometry

GAPDH samples (0.5 µg) were injected onto an Accucore-150-C4 (50 x 2.1 mm, 2.6 µM, Thermo Scientific) column using a Dionex Ultimate 3000 HPLC system (Thermo Scientific). Proteins were eluted from the column (60˚C) with an acetonitrile gradient from 9:1 of solvent A:B (table 4) to 2:8 over 4.6 mins. The flow rate of the mobile phase was 400 µL/min. The eluted protein was passed to a Velos Pro mass spectrometer. Mass spectral data was taken between m/z 400 and 2000 on positive ion mode. Proteins peaks were averaged and deconvoluted using ProMass for Xcalibur (version 2.8). The tune file was set to capillary temperature of 275°C and spray voltage of 4 kV. Three microscans were averaged, the maximum inject time was 10 ms and automatic gain control target settings were 3×10^4 in full mass spectrometry and 1×10^4 in multi-stage mass spectrometry.